

## PDF hosted at the Radboud Repository of the Radboud University Nijmegen

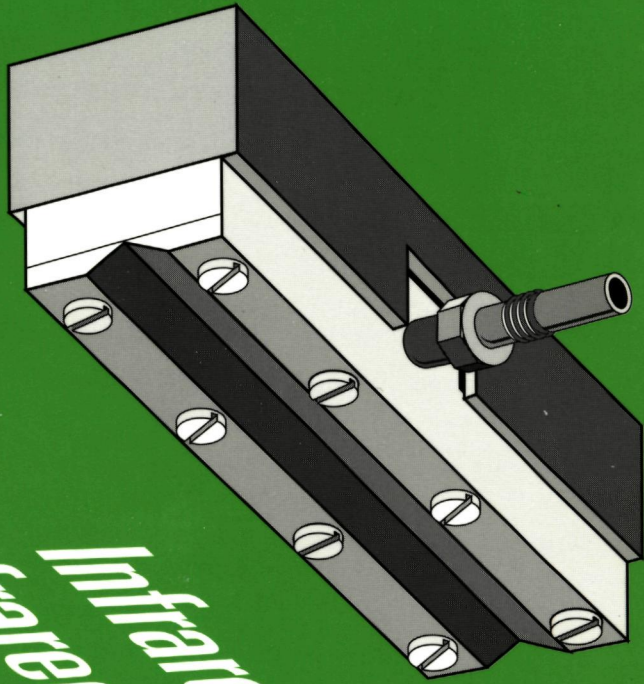
The following full text is a publisher's version.

For additional information about this publication click this link.

<http://hdl.handle.net/2066/145800>

Please be advised that this information was generated on 2017-03-14 and may be subject to change.

4825



**Far infrared and  
Infrared spectroscopy  
On Transient Molecules**

Harold Linnartz



**INFRARED AND FAR INFRARED SPECTROSCOPY  
ON TRANSIENT MOLECULES**

Linnartz, Harold

Infrared and far infrared spectroscopy on transient  
molecules / Harold Linnartz. - [S.l. : s.n.]. - Ill.

Proefschrift Nijmegen. - Met lit. opg. - Met samenvatting  
in het Nederlands.

ISBN 90-9007209-8

Trefw.: moleculaire spectroscopie.

# INFRARED AND FAR INFRARED SPECTROSCOPY ON TRANSIENT MOLECULES

EEN WETENSCHAPPELIJKE PROEVE OP HET GEBIED VAN  
DE NATUURWETENSCHAPPEN

## PROEFSCHRIFT

TER VERKRIJGING VAN DE GRAAD VAN DOCTOR  
AAN DE KATHOLIEKE UNIVERSITEIT NIJMEGEN,  
VOLGENS BESLUIT VAN HET COLLEGE VAN DECANEN  
IN HET OPENBAAR TE VERDEDIGEN  
OP WOENSDAG 29 JUNI 1994,  
DES NAMIDDAGS TE 1.30 UUR PRECIES

door

**HAROLD HENRICUS VINCENTIUS JOZEF LINNARTZ**

geboren op 16 oktober 1965  
te Heerlen

**Promotor** : Prof. Dr. J. Reuss

**Co-Promotores** : Dr. M. Havenith  
Institut für Angewandte Physik der Universität Bonn

Dr. W.L. Meerts  
Dr. J.J. ter Meulen

---

Part of this work has been made possible by financial support from the European Community within the scope of the network "Structure and Dynamics of Molecular Ions" (EC 892 001 59/OP1).

*Zeg trouwens nooit van iets dat het vanzelf spreekt. Laten wij liever tegen elkaar zeggen: 'Jongens, denk erom, het is niet zo,' zoals de geleerden wel doen in de spaarzame ogenblikken dat zij zich zelf van hun onmacht bewust zijn. 'Het is niet zo', dat moest je eigenlijk schrijven op de titelpagina van ieder boek, je moest het beitelen aan de gevel van iedere school, je moest geen voordracht houden zonder deze woorden als waarschuwing vooraf en als correctie daarna. 'Het is niet zo', dat moest het leidende motief zijn van iedere wetenschap. 'Het is niet zo, het is niet zo', dat is het beginsel van alle wijsheid.*

*'Waar of niet?' vroeg Salomon aan Zeitscheck.*

*'Het is niet zo', antwoordde deze.*

*Uit 'Drie rode rozen' van A. J. Herzberg*

*Ter nagedachtenis aan  
mijn vader*





## Voorwoord

Een voorwoord komt voor de schrijver meestal te laat. Het is het nawoord, dat als introductie dient voor het werk, dat dan eigenlijk al gereed is. In zoverre heeft de schrijver altijd het laatste woord, ook al is dat op de eerste pagina. Een voorwoord is een nawoord dat op de verkeerde plaats terecht is gekomen. Maar toch, zo is het niet.

Een voorwoord is vooral ook een woord vóór; een woord van dank voor het werk van zovelen, die een bijdrage hebben geleverd en in zoverre kan er geen betere plaats voor worden gevonden dan die eerste pagina.

Graag wil ik op deze plaats mijn dank uitspreken aan iedereen die op directe of indirecte wijze heeft meegeholpen aan de totstandkoming van dit boekje. In het bijzonder wil ik bedanken;

- *Jean Schleipen, 'dei mig as sjtudent hat injeweit' in de wereld die Molecuul en Laserfysica heet.*
- *Professor Buck, Reinhard Krohne und Andreas Rudolph für die sehr schöne und lehrreiche Zeit am Max Planck Institut in Göttingen. Es ist Schade, daß es in Nimwegen kein Gänseliesel gibt.*
- *Erik Zwart, die mij de nukken en kuren van de ver infrarood opstelling heeft getoond en wiens werk een prima basis vormde om op voort te bouwen.*
- *Annemieke Kips, die haar afstudeerwerk liet samenvallen met mijn promotie onderzoek, schitterende metingen aan het dimeer verrichtte, dubbelresonanties maar niets vond en nu met vier lasers gelijktijdig de moleculen de stuipen op het lijf jaagt.*
- *Het tetrsteam Giel Berden en Genie Stoffels, de flightsimulator expert Michel Versluis en princefanaat Marcel Drabbels, voor de ronduit chaotische, maar altijd inspirerende sfeer op het uiteinde van de gang.*
- *Mijn directe begeleiders, Leo Meerts en Hans ter Meulen, die beide een belangrijke bijdrage hebben geleverd aan het welslagen van het onderzoek.*
- *Promotor, Dr. Vater en afdelingsgoeroe Jörg Reuss, voor de begeleiding en het op de juiste tijden 'ok' en 'niet-ok' zeggen.*
- *Dave Parker voor de vele corrections in my manuscripts.*
- *Ad van der Avoird, Paul Wormer, John van Bladel en Edgar Olthof voor hun theoretische bijdrage aan dit proefschrift. Zonder wisselwerking tussen experiment en theorie zouden we bijlange na niet het punt hebben bereikt waar we nu zijn. Ik hoop dat we de prettige samenwerking in de toekomst kunnen voortzetten.*
- *Eugène van Leeuwen, Frans van Rijn, Cor Sikkens en John Holtkamp, de technische staf, zonder wiens hulp de opstelling nooit draaiende gehouden had kunnen worden. Eugène, ik hoop dat we de magneet nooit meer nodig hebben.*

Alle andere medewerkers en studenten van de afdeling Molecuul en Laser Fysica voor de schadeloze reeks vlaai- en koffiepauzes, zeilweekenden, vrijdagmiddag 'vergaderingen', bowling en, en, en.

De ondersteunende afdelingen van de Faculteit der Natuurwetenschappen voor de snelle en accu- te dienstverlening. De medewerkers van de Instrumentmakerij, de Quick-service, de Glasblazer afdeling Illustratie en Fotografie en Ferry Derksen van de 'Ferry' service hebben allen een on- verspreide bijdrage geleverd aan de inhoud van dit boekje.

Prof. Kuijpers van de afdeling Sterrenkunde en de leden van de Astronomische Kring Nijme- ge voor de prettige samenwerking in de afgelopen jaren.

Die viele Besuchen an Bonn waren unvergeßlich und dann nicht nur die Privatbesuchen.... Ich danke mich ganz herzlich bedanken bei Professor Urban und seiner Gruppe für die Gastfreun- dschaft und die schöne Zeit die ich als Sommergast am Institut für Angewandte Physik hatte. Beson- deren moechte ich mich bei Martina Havenith bedanken. Ihr Beitrag an den gemeinsam durchgeführten Experimenten in Bonn war sehr wichtig, an den Experimenten in Nimwegen unentbehrlich. Ich hoffe, daß die Zusammenarbeit demnächst für längere Zeit ist.

The cooperation within the EC Network 'Structure and Dynamics of Molecular Ions' was excellent as 'neutralized ions' turned out to be very interesting too. I want to thank all the members of the participating groups and I hope that the good contacts between the groups will survive. So, perhaps, on the next ECUS.

ker niet op de laatste plaats wil ik hier de mensen bedanken die buiten het lab een belangrij- ge rol speelden.

Zes jaar gang 139 en bijna vier jaar lang gang 133, een onuitputtelijk magazijn voor het opdo- nen van mensenkennis, inspiratiebron voor van alles en nog wat, maar vooral voor het openhouden van het blikveld.

Ich möchte hier meine Helga bedanken, für das Geduld und die Unterstützung, vor allem in den letzten Jahren. Ich hoffe, daß unser Leben schnell, ganz schnell was weniger hektisch wird.

Enslotte wil ik mijn ouders bedanken. Voor de hulp, de ondersteuning, de interesse en nog zoveel meer. Ik vind het ontzettend erg, dat mijn vader mijn promotie niet meer kan meemaken. Hij zou het er zo op verheugd hebben. Aan hem draag ik dit proefschrift op.

# Contents

<b>1</b>	<b>Introduction</b>	<b>13</b>
1.1	General	13
1.2	The tunable far infrared sideband spectrometer	14
1.3	The present investigation	17
	References	19
<b>2</b>	<b>The Ammonia Dimer: Complex Dynamics with a Dynamical Complex</b>	<b>21</b>
2.1	Introduction	22
2.2	Group theory	25
	<b>An infrared-far infrared double resonance study on <math>(\text{NH}_3)_2</math> in a Jet</b>	<b>29</b>
2.3	Introduction	30
2.4	Experimental details	31
2.5	Double resonance results and analysis	33
2.6	Assignment of the far infrared transitions	38
2.7	Conclusion	41
	Acknowledgement	41
	<b>The electric dipole moment of <math>(\text{NH}_3)_2</math> for <math>G: K =1</math></b>	<b>43</b>
2.8	Introduction	44
2.9	Experiment	45
2.10	Theory	46
2.11	Results and discussion	48
2.12	Structural implications	49
	Acknowledgement	51
	<b>The ammonia dimer; new infrared-far infrared double resonance results</b>	<b>53</b>
2.13	Introduction	54
2.14	Experiment	56
2.15	Results	56
	2.15.1 Splitting between $979$ and $1004\text{ cm}^{-1}$	57
	2.15.2 Splittings within the $979\text{ cm}^{-1}$ peak	58
2.16	Discussion and conclusions	62
	Acknowledgement	64
	References	65

<b>3</b>	<b>Infrared Photodissociation of Small Size-selected Neutral Clusters</b>	<b>67</b>
3.1	Introduction . . . . .	68
3.2	Experimental method . . . . .	68
3.2.1	Size-selection . . . . .	68
3.2.2	Infrared photodissociation . . . . .	70
3.2.3	Experimental setup . . . . .	71
	<b>Infrared photodissociation of size-selected methylamine clusters</b> . . . . .	<b>73</b>
3.3	Introduction . . . . .	74
3.4	Experiment . . . . .	74
3.4.1	Molecular beam apparatus . . . . .	74
3.4.2	Laser system . . . . .	75
3.5	Results . . . . .	75
3.5.1	Size-selection . . . . .	75
3.5.2	Photodissociation . . . . .	78
3.6	Discussion . . . . .	81
3.6.1	Line shifts and structural implications . . . . .	81
3.6.2	Linewidth . . . . .	84
3.6.3	Cross sections . . . . .	84
	Acknowledgement . . . . .	85
	<b>Infrared photodissociation of size-selected carbonyl sulphide clusters</b> . . . . .	<b>87</b>
3.7	Introduction . . . . .	88
3.8	Experimental . . . . .	88
3.9	Results and discussion . . . . .	90
3.9.1	Structural implications . . . . .	90
3.9.2	Linewidths . . . . .	92
	References . . . . .	94
<b>4</b>	<b>The Electric Dipole Moment of <math>\text{KrH}^+</math></b>	<b>97</b>
4.1	Introduction . . . . .	98
4.2	Experimental . . . . .	99
4.3	Results . . . . .	100
4.4	Theory . . . . .	101
4.5	Summary . . . . .	106
	Acknowledgement . . . . .	106
	References . . . . .	106
<b>5</b>	<b>IR and FIR Direct Absorption Spectroscopy of Molecular Ions in a Supersonic Jet Expansion</b>	<b>109</b>
5.1	Introduction . . . . .	110
5.2	Experimental . . . . .	111
5.3	Results and discussion . . . . .	114
5.3.1	$\text{NO}^+$ . . . . .	114
5.3.2	$\text{N}_2\text{H}^+$ . . . . .	115
5.4	Conclusions . . . . .	115
	Acknowledgement . . . . .	116
	References . . . . .	116

<b>Summary</b>	<b>1</b>
<b>Samenvatting</b>	<b>1</b>
<b>Curriculum Vitae</b>	<b>1</b>
<b>Publications</b>	<b>1</b>



## Introduction

### 1.1 General

Spectroscopy of molecules in the gas phase is a very powerful tool for the investigation of molecular properties. With the use of a large variety of techniques, covering the whole frequency range from microwave to extreme ultraviolet, it is possible to record and investigate the spectrum of a molecule. This spectrum is unique, it is the spectroscopic fingerprint of a molecule and reflects the world of matter at the very fundamental level of molecular motions. From this fingerprint many properties can be extracted and it is possible to gain insight both in molecular structure and in intramolecular motions or intermolecular interactions. It also functions as a guide for further research. Once the spectrum is known, it can be used for the search of molecules in areas as air pollution, combustion processes and interstellar or atmospheric chemistry. And once the spectrum is fully understood it may serve to characterize processes quantitatively or to manipulate molecules, for example in steering chemical reactions.

In this thesis the frequency range is limited to the infrared and far infrared part of the electromagnetic spectrum and consequently low energetic motions such as rotations and vibrations will be topic of the discussion. The investigated molecules are weakly bound molecular complexes and molecular ions. These molecules are transient; under normal conditions their existence is very short due to reactive or dissociative molecular collisions and consequently they have to be produced during the experiments. To do so, point and slit nozzle expansions (complexes) and hollow cathode or magnetically extended negative glow discharges (ions) are used. These techniques are described in the chapters 2 to 4. In chapter 5 a new technique for the production of ions - a high voltage high pressure corona excited slit nozzle discharge - is presented. The applied technique for detection is direct absorption of tunable (narrowband) radiation.

The major part of this thesis describes measurements on molecular complexes. Such a complex consists of two or more molecules (atoms) that are weakly bound together. High resolution spectroscopy is an excellent way to study this weak bond and it offers the opportunity to learn more about the forces that act between molecules. The scientific interest in this field is very strong



and it surely is still growing, both from an experimental [1, 2] and theoretical [3] point of view. In all frequency regions complex studies are progressing, however, the far infrared is of special interest. The energy differences associated with rotations of complexes and vibrations between the constituents of the complex typically correspond to this part of the electromagnetic spectrum. Far infrared spectroscopy therefore directly reflects the inter- and intramolecular dynamics, taking place in the complex and in that way it is complementary to the information that can be obtained from scattering experiments which also provide information on the repulsive part of the intermolecular potential [4]. High resolution spectroscopy is normally restricted to small complexes, consisting of two, at the most three components. Due to the high degree of freedom in larger clusters high resolution spectra become congested or too difficult to analyze. This is a pity. Clusters have unique properties falling between those of isolated molecules and bulk condensed matter. A good comprehension of clusters therefore should improve the understanding of the transition from molecular physics to solid state physics with all its implications, such as the development of the continuous band structure of a solid out of the discrete spectrum of molecules. But this is a twilight zone where the real work still has to be performed.

Another way to look at clusters is to detect the infrared dissociation pattern. In these experiments a vibrational mode of one of the molecular components is excited by infrared photons and in case that the transferred energy is larger than the binding energy dissociation will be induced [5, 6, 7, 8]. These medium resolution experiments provide structural information, also on clusters larger than dimers and trimers, as will be illustrated in chapter 3. The same is true for the combination of infrared and far infrared radiation in a double resonance experiment. This will be shown in chapter 2.

The second part of this thesis deals with ion spectroscopy. Molecular ions, i.e. charged molecules, play an important role in the chemistry of interstellar space. Actually, ion spectroscopy was initiated by astrophysicists. The first ion signals were found in the Orion nebula in 1973 and two years later assigned as arising from  $\text{HCO}^+$ . The subsequent development of several types of discharge plasma, generating sufficiently high densities of ions to permit high resolution absorption measurements, had an enormous impact and as a consequence the field of molecular ion spectroscopy has literally exploded [9].

Most of the experiments described in this thesis are performed with the tunable far infrared sideband spectrometer at the Department of Molecular and Laser Physics at the University of Nijmegen. This spectrometer will be discussed in more detail in the next paragraph. The other experiments are based on measurements performed during a ten month stay at the Max Planck Institut für Strömungsforschung in Göttingen, and on measurements performed during several stays at the Institut für Angewandte Physik in Bonn. The employed techniques - infrared photodissociation of size-selected neutral clusters (Göttingen) and tunable infrared diode laser spectroscopy of ions in a jet expansion (Bonn) - will be discussed in the appropriate chapters.

### 1.2 The tunable far infrared sideband spectrometer

The far infrared spectrometer of our laboratory is the result of nearly three decades of submillimeter research in Nijmegen. In initial experiments in 1965 klystron driven harmonic generators provided submillimeter radiation up to 300 GHz [10]. In the years thereafter this range was extended up to 700 GHz [11]. The introduction of the HCN laser [12] and the simultaneous progress on sideband generation of HCN laser and klystron radiation in Schottky barrier diodes [13] and

the effective coupling of the laser radiation onto the diodes [14] extended the possibilities of the spectrometer considerably. However, the HCN laser is only lasing on a few lines around 900 GHz and a further expansion of the frequency range of the spectrometer became necessary. This was realized by the construction of a CO<sub>2</sub> laser pumped far infrared laser that can be operated at numerous frequencies in the submillimeter region. Consequently sideband generation yields tunable far infrared radiation in a very large frequency range [15]. In the last five years the spectrometer has been improved in making its operation more feasible and extending its use to jet absorption spectroscopy [1]. An important improvement was the introduction of a completely battery driven bias voltage supply which extended the average lifetime of a Schottky contact from several weeks to several months. Furthermore the scanning procedures became more comfortable by a computer controlled synthesizer output.

The sideband spectrometer in Nijmegen can be operated nearly continuously in the frequency range from 180 to 3000 GHz (6-100 cm<sup>-1</sup>). These frequencies are generated either by higher harmonic generation of microwave radiation in a Schottky barrier diode (180-600 GHz) or by non-linear mixing of an optically pumped fixed far infrared laser and tunable microwave radiation, again in a Schottky barrier diode (550-3000 GHz). Figure 1.1 shows the present setup.

The far infrared laser is a 3.85 m long home-built low pressure waveguide laser with an inner diameter of 32 mm. It can be operated both sealed-off and in flow for different kinds of gases. The laser is pumped by a line tunable CO<sub>2</sub> laser (Apollo Lasers Inc., model 150) with a typical single line power output of 100 W. The induced vibrational excitation and subsequent rotational relaxation of the molecules in the waveguide laser form the population inversion mechanism. Depending on the gas and the infrared pumping frequency several thousands of far infrared frequencies can be generated. However, for the purpose of this setup it is sufficient to use five different gases (HCOOH, CH<sub>3</sub>I, CH<sub>3</sub>F, CH<sub>2</sub>F<sub>2</sub> and CH<sub>3</sub>OH), from which about 30 strong far infrared laser oscillations can be obtained with a typical output power of 50 mW.

The far infrared radiation ( $f_i$ ) propagates through free space, passing a polarizing interferometer and in the mixer (see fig. 1.1) it is focussed on a small antenna (1.5-3 mm) that is positioned on top of a non-linear element, a Schottky barrier diode. The coupling efficiency is increased by the use of a corner reflector which consists of two highly polished gold coated plates at right angles to each other. In the experiments described here, we have used diodes (type 1i7) from the Semiconductor Device Laboratory of the University of Virginia. The diode is soldered on a gold pin which passes through a rectangular waveguide. The pin acts as an antenna for the incoming microwaves ( $f_m$ ). This radiation is supplied by a set of Oki and Varian klystrons in the 18 to 24 and 45 to 114 GHz range. Some of these klystrons are older than the author of this thesis and therefore recently four new powerful klystrons (200 to 500 mW) have been purchased in the 65 to 83 and 89 to 95 GHz range. The microwave frequencies are stabilized and controlled by a phase-lock system. For this a high frequency klystron (above 45 GHz) is locked to a low frequency klystron (18 to 24 GHz) which is locked to a HP 8660B frequency synthesizer ( $\leq 1$  GHz). The synthesizer in turn is locked to a Rb frequency standard. In this way a frequency accuracy well within the experimental requirements is assured. Furthermore, the synthesizer is externally controlled by a computer which indirectly provides a tuning of the klystrons via the phase-lock system.

The frequency mixing occurs via the non-linear response of the diode to both incoming electric fields. The outgoing sideband radiation,  $f_s = f_i \pm n.f_m$  (with  $n$  indicating the  $n^{\text{th}}$  sideband), is emitted along the same antenna pattern as the fundamental laser beam is coming in. However,

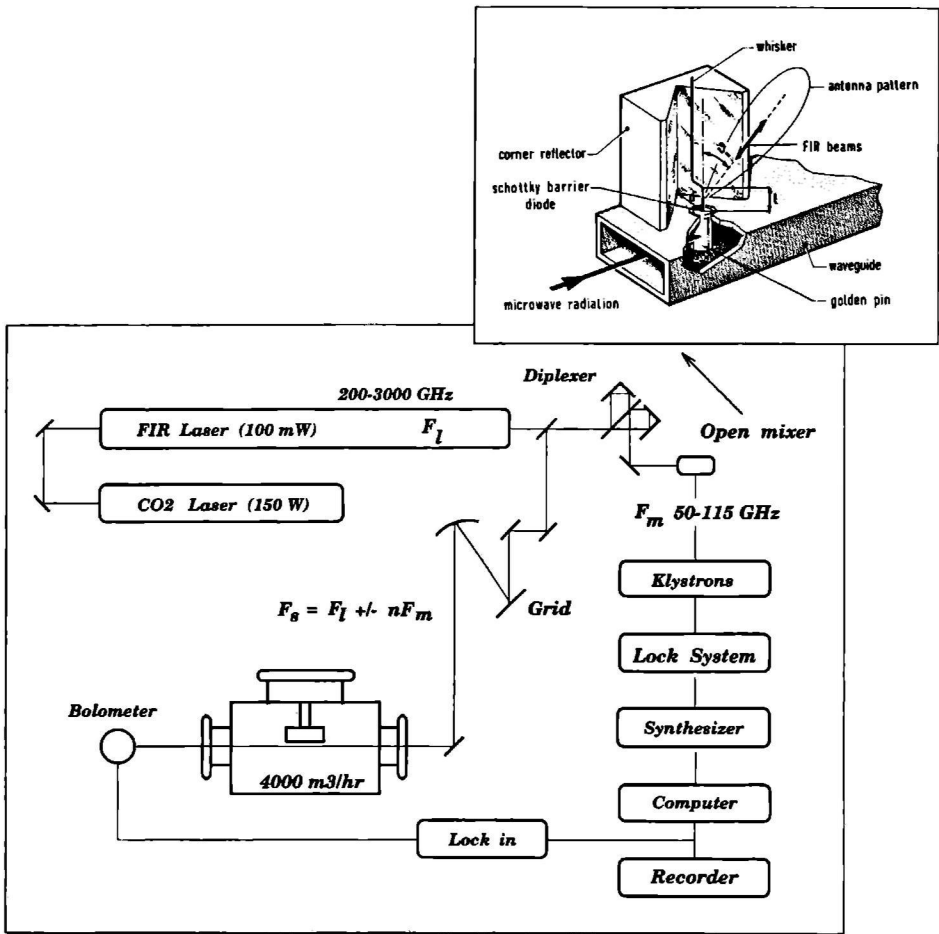


Figure 1.1: Schematic setup of the Nijmegen tunable far infrared sideband spectrometer. The enlarged part shows the open mixer.

the radiation emitted by the mixer antenna only partly consists of sideband radiation. By far most of the radiation is due to reflections of the fundamental laser frequency. For this reason the sidebands have to be separated from the laser radiation. This can be achieved by a Martin-Puplett polarizing diplexer, in which the sidebands are linearly polarized  $90^\circ$  with respect to the fundamental beam [1, 2] and a grating monochromator. The latter causes a loss of power of about 50 %, but it is very convenient in finding and selecting sidebands. Finally, the radiation is guided by a set of lenses and mirrors through an absorption chamber and is focussed onto a 4 K InSb hot-electron bolometer (Infrared Laboratories) which is sensitive enough to detect absorptions of the order of  $10^{-5}$ .

In the lower frequency range (180 to 650 GHz) radiation is generated using higher harmonics of klystron radiation,  $f_s = n.f_m$  (with  $n$  indicating the  $n^{\text{th}}$  harmonic). This is an old technique, developed in the fifties and sixties [16]. For our setup it is in principle the same as generating sideband radiation, but without actually using a fundamental far infrared laser frequency. The use of higher harmonics has the advantage of a higher accuracy; the frequency of the harmonics is precisely known since the klystrons are directly phase-locked to the frequency standard. The accuracy in frequency therefore is determined by the linewidth and is typically about 50 kHz. In case of sideband generation, the uncertainty is determined by the uncertainty of the far infrared laser frequency which amounts to about 1 MHz.

Another advantage of higher harmonic generation is the increase of the scanning range for a specific klystron. The higher the harmonic number, the larger the region that can be scanned. An disadvantage, of course, is the drop in power which determines the frequency below which harmonic generation and above which laser sideband generation yields better results. We estimate this to be somewhere between 550 and 600 GHz. The polarizing interferometer is not necessary in this setup, but it is useful to check the order of the harmonic. With the monochromator the desired harmonic can be selected which makes it possible to optimize the whole alignment for the given harmonic. In particular, the bias voltage that is applied to the diode via a BNC plug connected to the gold pin (that is insulated from the rest of the mixer) and the position of the corner reflector influence the harmonic power considerably. The harmonic is guided through the absorption chamber and detected by the InSb bolometer.

With exception of the ion measurements described in chapter 4, the absorption takes place in a vacuum tank, into which a molecular jet is expanded. In order to increase the absorption length a slit nozzle is used, similar to that described in [17]. To maintain the expansion from a 4 cm x 75  $\mu\text{m}$  nozzle, an Edwards roots blower pumping system is used, consisting of two mechanical booster pumps in series (3500 and 500  $\text{m}^3/\text{hr}$ ) and a rotary pump (80  $\text{m}^3/\text{hr}$ ). Typical operation conditions are 500 to 700 Torr backing pressure and 100 mTorr in the chamber during jet operation. In this thesis several techniques will be discussed, based upon the use of slit nozzles; double resonances, Stark measurements and corona excitation.

### 1.3 The present investigation

Six years ago the application of the far infrared spectrometer in our laboratory was extended from cell and discharge cell to jet absorption spectroscopy. From that moment on several weakly bound complexes, including  $(\text{H}_2\text{O})_2$ ,  $(\text{D}_2\text{O})_2$ , Ar- $\text{D}_2\text{O}$  and Ar- $\text{NH}_3$  [1] were studied. These complexes have well-defined equilibrium structures, but the potential barriers between two equivalent configurations is in general so low that tunneling splittings can occur. At the same time another

complex was studied,  $(\text{NH}_3)_2$ . The analysis of this complex turned out to be very complicated. Both the equilibrium structure and the vibration-rotation-tunneling analysis were questionable and "the ammonia dimer riddle" became a problem that attracted attention worldwide. In chapter 2 a detailed analysis of this problem is presented. It starts with an infrared-far infrared double resonance experiment, from which a complete picture of the tunneling motions can be derived, as it occurs within the complex. As a consequence the appropriate molecular symmetry group can be determined. Using this group Stark measurements are discussed, giving structural information on two of the tunneling states. The chapter concludes with additional infrared-far infrared double resonance results, from which the overall infrared spectrum of  $(\text{NH}_3)_2$  can be assigned.

One of the experimental problems in studying complexes larger than dimers or trimers is the size selection. To study free clusters, beam or jet expansions have to be used and normally a distribution among several cluster sizes will be obtained. Small clusters can be studied more or less size-selective by using diluted mixtures of the cluster gas in a seeding gas (typically 1-5 %). Higher concentrations will yield larger clusters but also a distribution over a larger range of cluster sizes. Size-selective investigations of neutral clusters therefore cannot be achieved directly in a beam. In chapter 3 a study on clusters is presented in which the size selection is achieved by excluding larger clusters kinematically as the result of the scattering of a cluster beam from a rare gas beam and by excluding smaller clusters by mass spectroscopy. The combination of this method with an infrared dissociation setup yields size-selected structural information. This will be illustrated for  $(\text{CH}_3\text{NH}_2)_n$  and  $(\text{OCS})_n$  clusters with  $n=2$  to 6.

As was mentioned before, spectroscopy of ions is partly motivated by its importance for interstellar chemistry. Furthermore, ions are interesting from a theoretical point of view [9]. Although the electric dipole moment of molecules is an elementary property that is calculated relative easily, until now only two electric dipole moments of ions were determined experimentally ( $\text{ArH}^+$  and  $\text{N}_2\text{H}^+$ ). This was achieved by studying the Zeeman effect of several isotopomers since Stark measurements, although more accurate, cannot be used; the electric field would accelerate the ions out of the absorption zone. This method, based on the Zeeman effect, was first applied to  $\text{ArH}^+$  [18] using the  $\text{H} \leftrightarrow \text{D}$  substitution, but due to experimental difficulties the value found had to be revised twice. The second ion,  $\text{N}_2\text{H}^+$ , was studied in Nijmegen [19]. The incorporation of a superconducting magnet and the isotope substitution of the heavier part ( $^{14}\text{N}^{14}\text{NH}^+$ ,  $^{14}\text{N}^{15}\text{NH}^+$  and  $^{15}\text{N}^{14}\text{NH}^+$ ) resulted in an accurate experimental value that agreed very well with the theoretical value. To study the effect of the  $\text{H} \leftrightarrow \text{D}$  substitution on this method, we decided to study the electric dipole moment of  $\text{KrH}^+$  by measuring the Zeeman effect for  $^{84}\text{KrH}^+$  and  $^{84}\text{KrD}^+$ . This will be discussed in chapter 4.

Chapter 5 is an attempt to link the chapters 2 to 4; complexes and ions. In this chapter a new technique for the investigations of molecular ions by direct absorption spectroscopy is presented; the high voltage high pressure corona excited slit nozzle discharge. In chapter 5 the setup is described and the first results on  $\text{NO}^+$  and  $\text{N}_2\text{H}^+$  are presented. The ultimate goal is to study molecular ion complexes, using the discharge for the generation of ions and the expansion for the generation of complexes. Since the complexes are expansion cooled and since the spectra are not Doppler limited, an analysis of this new class of molecules will become feasible.

## References

- [1] E. Zwart, Submillimeter spectroscopy of molecular complexes and ions, Ph.D. Thesis, University of Nijmegen (1991).
- [2] M. Havenith, Infrared spectroscopy of Van der Waals complexes and ions, Ph.D. Thesis, Institut für Angewandte Physik der Universität Bonn (1990).
- [3] J.W.I. van Bladel, Quantum mechanical treatment of non-rigid molecules and Van der Waals complexes, Ph.D. Thesis, University of Nijmegen (1992).
- [4] J. Schleipen, State-to-state cross sections for rotational excitation of  $(\text{NH}_3)_2$  and OH by collisions with He, Ar and  $\text{H}_2$ , Ph.D. Thesis, University of Nijmegen (1993).
- [5] M. Snels, Infrared excitation of molecules and clusters, Ph.D. Thesis, University of Nijmegen (1986).
- [6] B. Heijmen, Photo-excitation and dissociation of small molecular clusters, Ph.D. Thesis, University of Nijmegen (1988).
- [7] Ch. Lauenstein, Zerfallsprozesse stoßselektierter Molekülcluster, Ph.D. Thesis, MPI für Strömungsforschung, Göttingen (1989).
- [8] A. Rudolph, Infrarot-Photodissoziation von stoßselektierten  $\text{C}_2\text{H}_4$ - und  $\text{CH}_3\text{OH}$ -Clustern, Ph.D. Thesis, MPI für Strömungsforschung, Göttingen (1989).
- [9] J.P. Maier (ed), Ion and cluster ion spectroscopy and structure, Elsevier (1989).
- [10] C. Huiszoon, High resolution millimeter wave spectroscopy, Ph.D. Thesis, University of Nijmegen (1966).
- [11] F.A. van Dijk, High resolution submillimeter wave spectroscopy of HBr, DBr and HI, Ph.D. Thesis, University of Nijmegen (1971).
- [12] B. Zuidberg, Heterodyne detection in submillimeter wave spectroscopy, Ph.D. Thesis, University of Nijmegen (1977).
- [13] D. Bicanic, Generation of frequency tunable laser sidebands in the THz region, Ph.D. Thesis, University of Nijmegen (1978).
- [14] F.C. van den Heuvel, Far infrared spectroscopy with a tunable source of radiation, Ph.D. Thesis, University of Nijmegen (1982).
- [15] P. Verhoeve, Far infrared laser sideband spectroscopy of transient species, Ph.D. Thesis, University of Nijmegen (1989).
- [16] O.R. Gilliam, C.M. Johnson, W. Gordy, Phys. Rev. 78 (1950) 140.
- [17] K.L. Busarow, G.A. Blake, K.B. Laughlin, R.C. Cohen, Y.T. Lee, R.J. Saykally, J. Chem. Phys. 89 (1988) 1268.
- [18] K.B. Laughlin, G.A. Blake, R.C. Cohen, R.J. Saykally, J. Chem. Phys. 90 (1989) 1358.
- [19] M. Havenith, E. Zwart, W.L. Meerts, J.J. ter Meulen, J. Chem. Phys. 93 (1990) 8446.



## The Ammonia Dimer Complex Dynamics with a Dynamical Complex

1

### Abstract

Chemically weak bonds play an important role in many biological and chemical processes. For this reason numerous theoretical and experimental studies were carried out in recent years in order to gain a better insight in the complex dynamics of weak intermolecular interactions. In case of a rigid complex, with clearly defined potential minima, it is not a problem to speak of an equilibrium structure. But what to do with a floppy complex, in which a number of large amplitude motions between several local minima can take place more or less undisturbed? These complexes have their own inter- and intramolecular dynamics and as will be shown for the  $(\text{NH}_3)_2$ , this can result in a very interesting discussion.

This chapter starts with a historical overview and a short introduction in the principles of group theory, applied to  $(\text{NH}_3)_2$ . It continues with an infrared-far infrared double resonance experiment, from which the appropriate molecular symmetry group can be derived. Using this group Stark measurements are discussed which yield structural information. The chapter concludes with additional infrared-far infrared results, from which the overall infrared spectrum can be explained.

---

<sup>1</sup>This chapter is based on the articles:

- \* An infrared-far infrared double resonance study on  $(\text{NH}_3)_2$  in a jet; M. Havenith, H. Linnartz, E. Zwart, A. Kips, J.J. ter Meulen, W.L. Meerts, Chem. Phys. Lett. 193 (1992) 261.
- \* The electric dipole moment of  $(\text{NH}_3)_2$  for  $G:|K|=1$ ; H. Linnartz, A. Kips, W.L. Meerts, M. Havenith, J. Chem. Phys. 99 (1993) 2449.
- \*  $(\text{NH}_3)_2$ , complexe dynamica met een dynamisch complex; H. Linnartz, A. Kips, W.L. Meerts, M. Havenith, A&Q 5 (1993) 20.
- \* The ammonia dimer; complex dynamics with a dynamical complex; H. Linnartz, M. Havenith, CAMP, accepted
- \* The ammonia dimer, new infrared-far infrared double resonance results; H. Linnartz, W.L. Meerts, M. Havenith, Chem. Phys., submitted.
- \* The ammonia dimer; to be hydrogen bonded or not to be hydrogen bonded. M. Havenith, H. Linnartz, W.L. Meerts, E. Olthof, A. van der Avoird, P.E.S. Wormer, N. Heineking, W. Stahl, Science, in preparation.



## 2.1 Introduction

One of the most intriguing bonds in the world of weak intermolecular forces is the hydrogen bond. By hydrogen bond we mean a nearly linear D-H $\cdots$ A arrangement which is adopted by a donor bond (D-H) and a molecule (A) that acts as a proton acceptor. The origin of hydrogen bonding is now generally understood to be primarily electrostatic, but with significant contributions arising from short range charge transfer interactions. Here we will concentrate on hydrogen bonds and go into detail on what seems to be one of the simplest prototypes for it; the ammonia dimer.

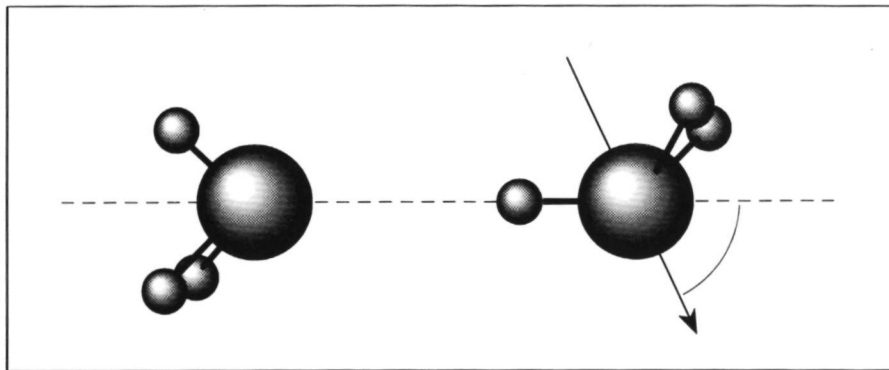
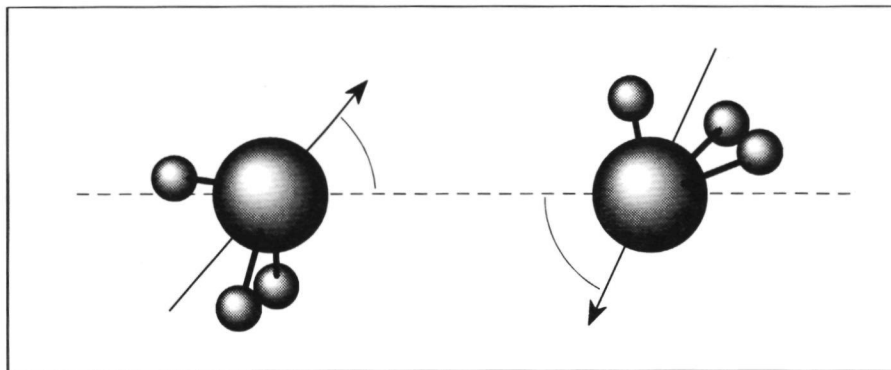


Figure 2.1: The ammonia dimer; the hydrogen bonded structure.

Ammonia, with its lone pair of electrons, is an excellent hydrogen bond acceptor. For a long time it was accepted within chemistry that ammonia can act as a hydrogen donor, too. For this reason the ammonia dimer was expected to have a linear hydrogen bonded structure (see fig. 2.1). In this arrangement one of the H-atoms of a  $\text{NH}_3$  monomer forms a linear bridge to the N-atom of the other monomer. However, in a series of papers [1, 2, 3] starting in 1985, Nelson, Fraser and Klemperer showed that  $(\text{NH}_3)_2$  has no hydrogen bonding for the G:K=0 state. From the measured rotational spectrum Nelson and coworkers could deduce the intermolecular distance between the two ammonia monomers, the projection of the electric dipole moment on the intermolecular axis (0.74 D) and the diagonal component of the quadrupole coupling tensor along the  $a$  inertial axis. Under the preassumption that  $(\text{NH}_3)_2$  can be considered as a rigid molecule, they calculated the structure from these values, yielding an equilibrium geometry in which both  $\text{NH}_3$  monomers are aligned nearly antiparallel, making polar angles with the intermolecular axis of  $49^\circ$  and  $65^\circ$  (see fig. 2.2). Since the dipole moment of free ammonia amounts to 1.47 D, the sum of the permanent dipoles of both monomers in a hydrogen bonded geometry, is estimated to be about 2.0 D. For this reason Nelson *et al* excluded the linear N-H $\cdots$ N bonding.

This conclusion was surprising in view of the fact that most *ab initio* calculations [4, 5, 6] predicted a nearly linear, hydrogen bonded structure. It also was against expectation at the background of theoretical and experimental studies on the  $(\text{HF})_2$  and  $(\text{H}_2\text{O})_2$  dimers that clearly gave evidence for a hydrogen bonded geometry (see e.g. [7, 8]). The only calculation that seemed to support a nearly cyclic structure [9] was shown later [10] to favor in fact a slightly bent hydrogen bonded structure.

In the ensuing debate the preassumption was questioned, whether  $(\text{NH}_3)_2$  is a rigid or a rather floppy molecule. It was argued that in case of large amplitude tunneling motions the structure deduced from the Nelson measurements only would reflect a vibrationally averaged structure which not necessarily has to coincide with a minimum in the intermolecular potential. However, from the fact that the relevant intermolecular bond angles hardly varied with isotopic substitution Nelson *et al* [2, 7] concluded that  $(\text{NH}_3)_2$  is a fairly rigid complex and consequently its equilibrium structure must be nearly cyclic. This conclusion was supported by the observation that the electric dipole moment for  $(\text{ND}_3)_2$  turned out to be 0.17 D smaller than the value that was found for  $(\text{NH}_3)_2$ . In case of vibrational averaging, this seems to be a contradiction, because the  $(\text{ND}_3)_2$  is expected to be less influenced by internal motions, i.e. to stay closer to equilibrium, and consequently it should have a larger electric dipole moment [2].



**Figure 2.2:** The ammonia dimer; the non-hydrogen bonded, so called cyclic or antiparallel structure.

In the following years the results of detailed infrared [11, 12, 13], far infrared [14, 15, 16, 17], infrared-far infrared [16], microwave [1] and infrared-microwave [18] studies became available. From these studies, especially from [16, 17], it became clear that the ammonia dimer is a very floppy molecule, exhibiting large amplitude motions; a result that was also found by a theoretical study by van Bladel *et al* [10]. In addition it became clear that the monomer umbrella inversion is only partly quenched in the complex. This was a rather unexpected result, since the umbrella inversion in most  $\text{NH}_3$  containing complexes is completely quenched. Only  $\text{Ar-NH}_3$  [19, 20] possesses a configuration in which the umbrella motion can take place nearly undisturbed. As a consequence the appropriate molecular symmetry group had to be extended and it turned out to be possible to assign all microwave and far infrared transitions known at that time within this new group. However, none of these studies could provide any structural information that could confirm or disprove the results found by Nelson *et al* and explain the discrepancy with the conclusions deduced from the  $(\text{ND}_3)_2$  measurements.

In 1993 dipole measurements by Linnartz *et al* [21] on the  $G:|K|=1$  state gave evidence that the antiparallel, so called cyclic structure is indeed more likely than the hydrogen bonded one, although one has to keep in mind that this structure is the consequence of vibrational averaging in a very floppy complex. "More likely" in this context means that the complex most of the time

will reflect an antiparallel configuration, as an intermediate between several tunneling motions. For this reason a comparison between experiment and theory is difficult. Whereas the electronic structure calculations focus mainly on finding the minimum of the intermolecular potential, the experiment yields a vibrational-rotation-tunneling averaged structure. Since the potential surface is very flat, it is quite a challenge to compute the averaged structure and to explain the results quantitatively. However, Olthof, Van der Avoird and Wormer [22] were able doing so, by solving the full six dimensional nuclear motion equation for a series of model potentials with different barriers for the interchange motion - which actually exchanges the role of both monomer units - and for the hindered rotations of the two ammonia monomers around their  $C_3$ -axes. In this study several measurable quantities were computed; electric dipole moments, energy splittings, nuclear quadrupole splittings and the amount of quenching of the monomer umbrella inversions. The potential that gave best agreement with the observed quantities has an equilibrium hydrogen bonded structure and a small barrier ( $24 \text{ cm}^{-1}$ ) for interchange tunneling, but a vibration-rotation-tunneling averaged ground state structure that is nearly cyclic. Furthermore van der Avoird *et al* were able to extend the use of this potential to  $(\text{ND}_3)_2$  [23]. From this it became clear that it is also possible to explain the decrease of the G:K=0 dipole moment, when going from  $(\text{NH}_3)_2$  (0.74 D) to  $(\text{ND}_3)_2$  (0.57 D), without explicitly demanding a rigid structure.

To understand this, one has to think in terms of localized wavefunctions. As one would expect (the "rigid structure" argument), the wavefunction of  $(\text{ND}_3)_2$  compared to  $(\text{NH}_3)_2$  has a larger amplitude near its equilibrium position. This results in an increase of the average dipole moment. However, there is a second phenomenon with an opposite effect. Due to the ortho-para difference the G state wavefunction is mainly localized on one side of the two (equivalent) minima. This effect will be less for  $(\text{ND}_3)_2$  than for  $(\text{NH}_3)_2$ , due to the smaller rotational constant. As a consequence the wavefunction of  $(\text{ND}_3)_2$  at the other minimum will be substantially larger, i.e. a decrease of the average dipole moment. Apparently, the second effect dominates the first which explains the decrease in dipole moment, without assuming a near-rigidity of the complex.

In the most recent study Olthof and coworkers use an even smaller barrier of  $7.5 \text{ cm}^{-1}$  for the interchange motion [29]. This is less than 1 % of the binding energy of the complex which is estimated to be about  $950 \text{ cm}^{-1}$  [11]. With this very small barrier height, nearly all experimental data can be reproduced and, especially, the accuracy in predicting the band origins is remarkably good (within  $0.5 \text{ cm}^{-1}$ ).

From a structural point of view the discussion whether ammonia is hydrogen bonded or not, both experimentally [7, 8, 24, 25, 30] and theoretically [23, 26, 27] comes to an end. The ammonia dimer seems to have a hydrogen bonded equilibrium structure, but this does not represent the actual structure. Due to the low barriers all measured quantities retain to an averaged structure that is nearly cyclic. Since the important features of a hydrogen bond - near linearity and strong directionality of the bond - are not met, it is not correct to speak of hydrogen bonding in  $(\text{NH}_3)_2$ .

In this chapter part of the history described above will be discussed in detail. It will be shown how infrared, far infrared and infrared-far infrared double resonance measurements can give important structural information on motions going on in a floppy complex. For this type of complexes it may be difficult to classify the energy levels according to vibrational and rotational quantum numbers. As a matter of fact the distinction between vibrational and rotational motion might even become impossible. In such a case group theory turns out to be a powerful tool.

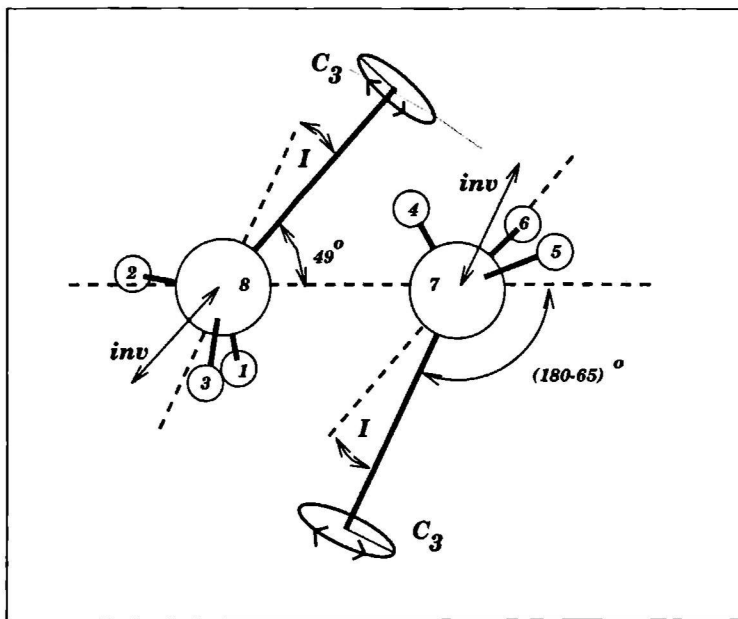


Figure 2.3: Feasible motions (rotation around  $C_3$ -axes, interchange of both monomers ( $I$ ) and monomer inversion ( $inv$ )) between equivalent structures.

## 2.2 Group theory

With group theory it is possible to classify an energy level diagram, without explicitly solving the Schrödinger equation [28]. The idea is to look at all possible transitions between non-distinguishable minima in the potential function. For these transitions it is necessary to tunnel through a barrier which spectroscopically is observed as a splitting. In case that the minima are separated by an infinitely high barrier, the corresponding energy levels will be completely degenerate. This degeneracy is lifted in case of finite barriers and obviously the splitting will increase with decreasing barrier height. The group of all feasible motions, i.e. all motions that can be observed experimentally and consequently do not correspond to very unlikely motions (as breaking up internal bonds), is called the molecular symmetry group. Under the operations described by this group the Hamiltonian is invariant and each energy level can be labeled according to an irreducible representation of the symmetry group. Furthermore it is possible to determine selection rules and spin statistical weights.

In order to understand the spectrum of  $(\text{NH}_3)_2$  it is necessary to get a qualitative idea of the tunneling motions that are expected. If we exclude any element which corresponds to unfeasible motions, such as any motion which involves the breaking of the N-H bonds, motions which involve a change of the handedness of the  $\text{NH}_3$  monomers (including the umbrella inversion) only 36 permutation-inversion motions are left (see fig. 2.3). First the permutation of the hydrogen nuclei

on each (NH<sub>3</sub>) subunit [(123) or (456)]. Depending on how much this motion is hindered by the presence of the intermolecular potential, it can be considered as a free, hindered or rigid rotation. In the latter case vibration would be an appropriate name too. Furthermore the interchange of all nuclei on one subunit with those on the other subunit [(14)(25)(36)(78)] which actually exchanges the role of both monomers. And finally the inversion of all particle coordinates in the center of mass followed by permutations to preserve the handedness of the monomers [(23)(56)\*] and the products of all these motions with each other. This collection of motions forms the molecular symmetry group G<sub>36</sub>. Using group theory the analysis, in principle, is independent of the choice between free rotor and high barrier limit. It is also important to realize that this notation only describes the position of the atoms before and after they have undergone the tunneling motion. No statement is made about the actual pathway.

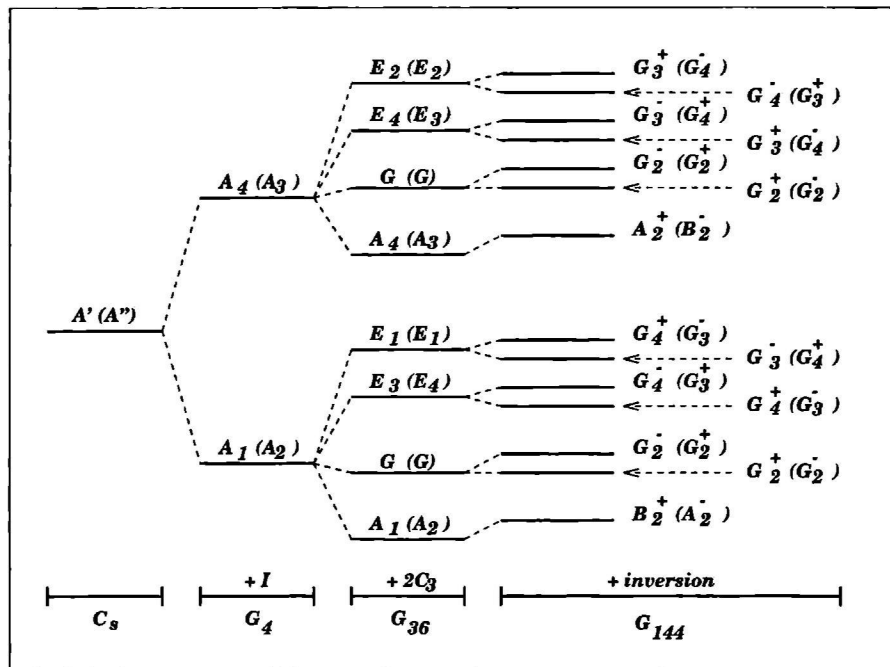


Figure 2.4: Correlation diagram for  $G_{144}$ . Subsequently the two  $C_3$ -rotations ( $2C_3$ ), the interchange ( $I$ ) and inversion are switched on group theoretically, starting from a classification in the point group  $C_s$  in the left-hand column for a rotational state in a rigid complex. The symmetry species of each state is indicated for even  $J$  and (odd  $J$ ).

Assuming a plane of symmetry, we expect from the character table of  $G_{36}$  each rotational level (NH<sub>3</sub>)<sub>2</sub> to be split in eight tunneling states; 2 A (ortho-ortho), 2 G (ortho-para/para-ortho) and 4 E (para-para NH<sub>3</sub>) states. In the free rotor limit these states correspond to different combinations of internally rotating monomers. Under the experimental conditions ( $T_{rot} < 10K$ ) only  $j=0$  and

$j=1$  will be populated. These cannot relax further, since they correspond to the lowest nuclear spin states with  $I=\frac{3}{2}$  and  $I=\frac{1}{2}$ , respectively. Consequently, for A-states both monomers have zero quanta of internal rotation, for G-states only one monomer is rotating and for E-states both monomers have  $j=1$ . The G-states are special in describing two monomers with different nuclear spin. For this reason interchange tunneling which would imply a para-ortho exchange, i.e. an exchange of different nuclear spins, is quenched. This is shown schematically in the first three columns of figure 2.4, where a correlation diagram for the motions in  $(\text{NH}_3)_2$  is drawn. From the left to the right the different motions are switched on group theoretically; starting from a rigid structure, in which all tunneling motions are freezed and consequently all tunneling levels are degenerate, the complex can be classified according to the point group  $C_3$ . Considering the  $(I+2C_3)$  limit [1], where the interchange splitting (I) is assumed to be large compared to internal rotation splitting ( $C_3$ ), switching on the interchange will lead to a splitting of the rotational level into two levels  $A_1$  and  $A_3$ . These levels will each split into four states if both rotations ( $2C_3$ ) are activated. These eight tunneling states can be described in  $G_{36}$ .

The same eight tunneling states are obtained in the  $(2C_3+I)$  limit, although the relative level ordering is different. This limit, in which the interchange splitting is assumed to be smaller than the splittings arising from internal rotation, was thought [1, 14] to be the more appropriate one. However, as was mentioned before, the interchange splittings observed are typically of the order of  $20 \text{ cm}^{-1}$ , which is very large and consequently the  $(I+2C_3)$  limit reflects the dynamics in the complex better.

In case the monomer umbrella inversion is also included (see fig. 2.3), the number of possible permutation-inversion motions increases by a factor of four, resulting in more splittings which is described properly by the molecular symmetry group  $G_{144}$ . This is shown in figure 2.4 in the last column. The symmetry labeling for each rotation tunneling state is indicated in each column for even J and (odd J). The correlation diagram is not an energy level scheme, but it gives an overview of the possible states and as such we will use it.



---

# An Infrared - Far Infrared Double Resonance Study on the Ammonia Dimer in a Jet

*M. Havenith*

*Institut für Angewandte Physik, Wegelerstraße 8, D 53115, Bonn*

*H. Linnartz, E. Zwart, A. Kips, J.J. ter Meulen and W.L. Meerts*

*Department of Molecular and Laser Physics, University of Nijmegen,  
Toernooiveld, NL 6525 ED, Nijmegen*

## Abstract

An infrared-far infrared double resonance experiment on  $(\text{NH}_3)_2$  in a jet is described. From the results, the nature of the tunneling splitting detected in former infrared and far infrared studies is identified. It is found that the  $(\text{NH}_3)_2$  complex exhibits the following feasible motions:

- internal rotation of each monomer along the  $C_3$ -axis,
- interchange tunneling and
- (monomer umbrella) inversion tunneling.

The far infrared transitions reported so far and three new bands reported in this work, can be assigned within the group  $G_{144}$ . It is found that upon infrared excitation of the  $\nu_2$  umbrella motion the inversion splitting amounts to  $3.7 \text{ cm}^{-1}$ .



## 2.3 Introduction

The ammonia dimer has been subject of discussion in the literature for a long time. The results of Nelson, Fraser and Klemperer [1, 2, 3] which showed that  $(\text{NH}_3)_2$  has no hydrogen bonding for the G:K=0 ( $G_\alpha$ ,  $G_\beta$ ) state, were surprising in view of former *ab initio* calculations (see e.g. [4, 5]). Furthermore Nelson and coworkers managed to assign their transitions within the group  $G_{36}$  [3] which includes the internal rotation of each monomer along the  $C_3$ -axis ( $C_3$ ) and the interchange tunneling between the two non-equivalent  $\text{NH}_3$  monomers (I). The two monomers were found to make nearly complementary angles with the axis connecting them. It was further assumed that  $(\text{NH}_3)_2$  exhibits a plane of symmetry and that it does not show any inversion splitting which implies that the barrier for inversion tunneling is infinitely high. In a later far infrared study by Havenith *et al* [14] several vibration-rotation-tunneling transitions were detected. It was concluded that  $G_{36}$ , indeed, is the smallest group explaining the observed transitions. Furthermore, it was concluded that the  $(2C_3+I)$  limit is appropriate. Additional far infrared measurements by Zwart [15], however, did not match with these observations and showed the need for further experiments. Zwart found three bands that were rotationally assigned as K:0-0 and K:1-1 transitions (see table 2.1). The K:0-0 transition with band origin at 483 GHz shares the same ground state as the K:0-1 transition, assigned as A-states before [14]. Except for these two bands no other bands shared a common level. A relative ordering of the states therefore was not possible. For this reason we decided to apply a new method to the problem: an infrared - far infrared double resonance experiment. This should help to label each state and to gain insight into the nature of the tunneling splittings.

As an outcome of theoretical work [4] the ammonia dimer was not expected to dissociate upon excitation with a single 10  $\mu\text{m}$  photon. Experiments [11, 12, 13], however, showed that one 970  $\text{cm}^{-1}$  photon is sufficient to cause dissociation of the complex. Additional information was found by Buck and coworkers [32]. In a scattering experiment with a secondary He beam an average energy of 520  $\text{cm}^{-1}$  was transferred to ammonia dimers without causing dissociation. This gives the lower limit, whereas the upper limit can be estimated from the experiment of Snels *et al* [11] to be about 950  $\text{cm}^{-1}$ . Snels and coworkers measured the overall infrared spectrum of  $(\text{NH}_3)_2$  by bolometric detection. Combining the outcome of this experiment, the results of an infrared-microwave double resonance experiment performed by Fraser *et al* on the G:K=0 states [18], information from an infrared-infrared double resonance experiment performed by Heijmen *et al* [13] and all far infrared data known [14], we will try here to correlate the overall infrared information to the state resolved far infrared information, in that way introducing a labeling technique.

The infrared spectrum as measured by Snels shows main peaks at 979  $\text{cm}^{-1}$  and 1004  $\text{cm}^{-1}$  (fig. 2.6a - taken from [11]), which was explained in [11] as originating from the excitation of the two non-equivalent  $\text{NH}_3$  monomers. The band at 979  $\text{cm}^{-1}$  shows a substructure, with a small peak at the 10R12 and larger peaks at the 10R22 and 1028  $\text{CO}_2$  laser lines. The two main peaks at 977.2  $\text{cm}^{-1}$  (10R22) and 980.9  $\text{cm}^{-1}$  (10R28) were found to be correlated to the excitation of the  $G_\alpha$  and  $G_\beta$  states, respectively [18]. A further peak arising at 970.5  $\text{cm}^{-1}$  (10R12) was interpreted as arising from  $|K|=1$  states [11, 31]. In this chapter we conclude that the inversion tunneling is responsible for the splittings observed in the microwave experiments [1] and for the splittings observed in the 979  $\text{cm}^{-1}$  band. This is in contrast to previous studies [2, 11], in which the interchange tunneling was assumed to be responsible for these splittings. With this conclusion we are able to (re)assign the previous far infrared data [14] as well as the new data reported in this

A. K=0-0, $\nu_{BO} = 483$ GHz				B. $ K =1-1$ , $\nu_{BO} = 454$ GHz			
$J'$	$J''$	Frequency	Obs-Cal	$J'$	$J''$	Frequency	Obs-Cal
8	9	383425.35	0.00	5	6	394443.63	-0.01
7	8	395324.85	-0.01	4	5	404262.96	0.03
6	7	407030.22	0.03	3	4	414075.83	-0.04
5	6	418538.25	0.00	2	3	423900.65	-0.03
4	5	429846.17	-0.02	1	2	433754.32	0.03
3	4	440951.39	-0.01	1	1	453656.39	-0.01
2	3	451851.51	0.01	2	2	453764.64	0.03
1	2	462544.37	0.01	3	3	453913.37	0.03
0	1	473028.10	0.00	2	1	473666.66	-0.05
1	0	493361.85	-0.01	3	2	483777.31	0.04
2	1	503209.32	0.00	4	3	493924.97	-0.03
3	2	512842.51	0.00	5	4	504093.69	0.00
4	3	522260.77	0.00	6	5	514264.15	0.00

C. $ K =1-1$ , $\nu_{BO} = 487$ GHz.							
$J'_{K'_a, K'_c}$	$J''_{K''_a, K''_c}$	Frequency	Obs-Cal	$J'_{K'_a, K'_c}$	$J''_{K''_a, K''_c}$	Frequency	Obs-Cal
6 <sub>16</sub>	7 <sub>17</sub>	408864.25	0.20	1 <sub>10</sub>	1 <sub>11</sub>	486433.19	0.61
6 <sub>15</sub>	7 <sub>16</sub>	409242.96	0.00	1 <sub>11</sub>	1 <sub>10</sub>	486398.24	0.13
5 <sub>15</sub>	6 <sub>16</sub>	420725.76	-0.87	2 <sub>11</sub>	2 <sub>12</sub>	485843.64	-0.08
5 <sub>14</sub>	6 <sub>15</sub>	421031.29	-0.04	2 <sub>12</sub>	2 <sub>11</sub>	485744.75	-0.59
4 <sub>14</sub>	5 <sub>15</sub>	432388.56	0.84	3 <sub>12</sub>	3 <sub>13</sub>	484980.92	-0.06
4 <sub>13</sub>	5 <sub>14</sub>	432616.78	0.35	3 <sub>13</sub>	3 <sub>12</sub>	484798.12	0.03
3 <sub>13</sub>	4 <sub>14</sub>	443825.84	0.26	2 <sub>12</sub>	1 <sub>11</sub>	506248.68	-0.35
3 <sub>12</sub>	4 <sub>13</sub>	443976.91	-0.12	2 <sub>11</sub>	1 <sub>10</sub>	506339.61	0.07
2 <sub>12</sub>	3 <sub>13</sub>	455007.43	-0.65	3 <sub>13</sub>	2 <sub>12</sub>	515553.29	0.25
2 <sub>11</sub>	3 <sub>12</sub>	455088.46	-0.31	3 <sub>12</sub>	2 <sub>11</sub>	515718.21	-0.03
1 <sub>11</sub>	2 <sub>12</sub>	465902.24	-0.04	4 <sub>14</sub>	3 <sub>13</sub>	524592.01	0.20
1 <sub>10</sub>	2 <sub>11</sub>	465929.26	0.37	4 <sub>13</sub>	3 <sub>12</sub>	524838.03	-0.17

Table 2.1: The observed frequencies and residuals of the fit (in MHz) for three new bands of  $(\text{NH}_3)_2$ .

work (table 2.1)

## 2.4 Experimental details

The  $(\text{NH}_3)_2$  complexes are produced in a continuous two dimensional supersonic jet by expanding a mixture of about 2 %  $\text{NH}_3$  in argon through a 4 cm x 75  $\mu\text{m}$  slit nozzle into a vacuum chamber that is maintained at about 100 mTorr by an 4000  $\text{m}^3/\text{hr}$  roots blower pumping system. The expansion mixture is optimized by gas flow controllers. The radiation is generated with the Nijmegen tunable far infrared sideband spectrometer [33] by mixing an Apollo  $\text{CO}_2$  laser optically pumped fixed far infrared laser frequency with tunable microwave radiation generated by a klystron in a Schottky

barrier diode. For frequencies in the range beneath 550 GHz higher harmonics of klystron radiation is taken, without using a fundamental laser frequency. For the transitions listed in table 2.1 we mainly have used harmonics supplied by a 60 or 70 GHz klystron. Radiation generated in this way is focussed in the molecular beam and detected by an InSb hot electron bolometer.

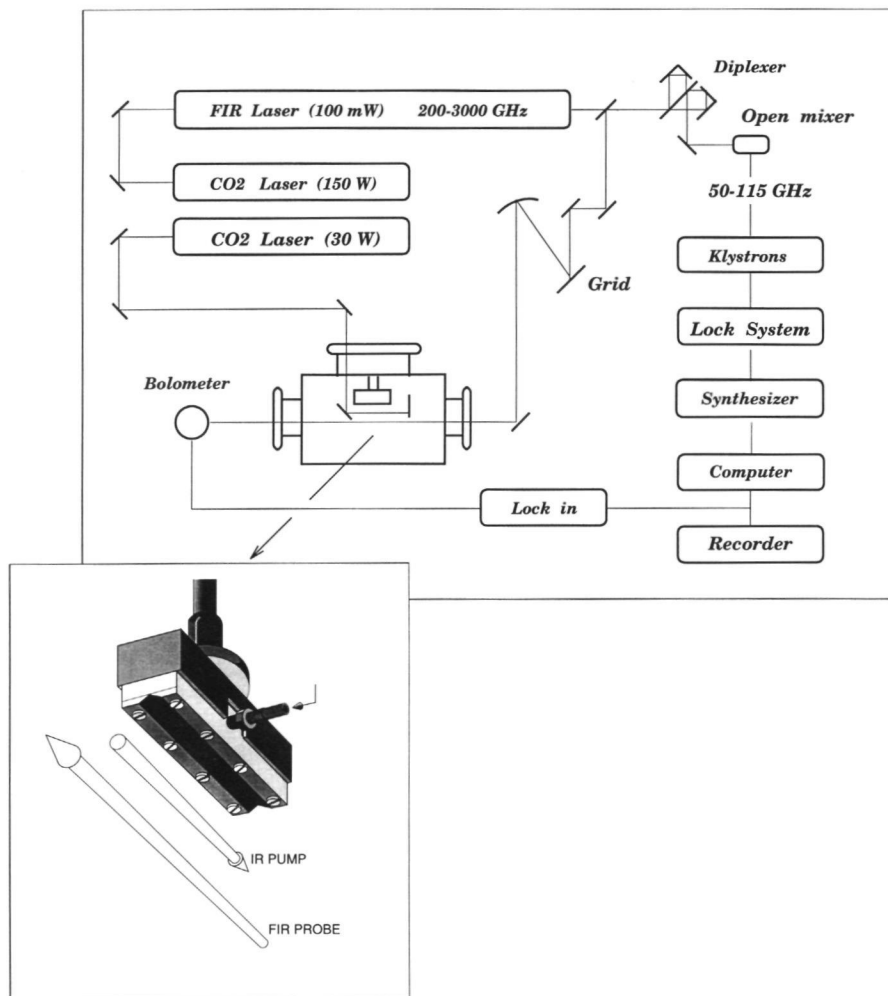


**Figure 2.5:** The infrared-far infrared double resonance setup in a molecular jet expansion. The enlarged part shows the jet setup.

For the double resonance experiments an infrared laserbeam, generated with a homebuilt CO<sub>2</sub> laser (typical single line output power of 25W) is guided antiparallel to the far infrared beam between

the nozzle and absorption zone (fig. 2.5). Because the infrared and far infrared beam have totally different optical properties, it is not possible to let them coincide.

The double resonance signal for a selected (and assigned) state is detected by observing the depletion in far infrared signal as function of the infrared frequency (10R8-10R32). To do so the CO<sub>2</sub> laser beam is chopper modulated (500 Hz) and consequently the bolometer signal, that is lock-in detected, directly reflects the loss in far infrared signal as result of the infrared pumping; this is the double resonance signal.

In the range of the 979 cm<sup>-1</sup> peak (see fig. 2.6a) we have studied the two G:K=0 states (G<sub>α</sub> and G<sub>β</sub> in [18]), band origin at 613 and 614 GHz, the A:K=0-1 state, band origin at 734 GHz and two of the E-states, band origin at 730 GHz [14, 34]. These bands cannot be investigated by harmonic generation, which gives rise to an additional experimental complication. The far infrared laser exhibits a thermal drift (about 1 MHz/hr) and in order to determine maximum depletion, the double resonance signals have to be recorded by scanning the far infrared frequency over the absorption line too. The linewidth of the double resonance signal consequently corresponds to the linewidth of the far infrared absorption line. By repeating this measurement for different CO<sub>2</sub> laser lines and correcting for fluctuations in both far infrared and infrared power, the double resonance spectra shown in figure 2.6b, c, f and g are obtained. These spectra are restricted to the 979 cm<sup>-1</sup> band, since no <sup>13</sup>CO<sub>2</sub> isotope laser was available with powers high enough to study double resonance spectra in the 1004 cm<sup>-1</sup> band too.

The cluster dissociation versus laser power has been measured for several CO<sub>2</sub> laser lines which showed a linear dependence. No saturation effects have been observed. The reproducibility of the observed spectra is better than 10 %.

## 2.5 Double resonance results and analysis

The results of the double resonance experiment are shown in figure 2.6. In order to test the method we first performed double resonance measurements on the G<sub>α</sub> and G<sub>β</sub> bands which were also observed by Fraser *et al* [18] in an infrared-microwave double resonance experiment. Whereas they found that either the 10R22 or 10R28 CO<sub>2</sub> laserfrequency is correlated with the G<sub>α</sub> or G<sub>β</sub> microwave transitions (fig. 2.6d and e), our measurements show a different result: as can be seen in figure 2.6b and c we find a correlation with both peaks for each of the G-states. That both peaks in fact are uncorrelated is proven by an infrared-infrared double resonance experiment, performed by Heijmen *et al* [13]. This implies that collisional relaxations in the jet expansion must be responsible for a redistribution of the population among the two levels. These relaxations are (nearly) absent in the beam experiments (as performed by Fraser, Snels and Heijmen) in which it is possible to work in the collisional free regime (roughly 40 nozzle diameters behind the nozzle). From the fact that the two infrared-far infrared double resonance spectra are the same within the experimental uncertainty, we conclude that the population is equally distributed among both states due to collisional relaxations. This result was quite unexpected and in fact also undesired. Since we wanted to have a labeling technique, correlating (unknown) far infrared transitions to specific parts of the overall infrared spectrum, collisional relaxations more or less resulted in a non state specific result again.

In figure 2.6f the double resonance spectrum of the A-state - as assigned in [14] - is displayed. We observe a spectrum which is clearly different from the spectra of the G-states: only one peak at 10R22 is obtained. This was, again, an unexpected result.

It is generally assumed that relaxation by collisions only can take place between levels with the same spin state [35]. We therefore conclude that in the state probed in figure 2.6f at least one of the two ( $\text{NH}_3$ ) monomers must have a spin which differs from the spins in the G-states. This still agrees with the assignment to an A-state; for A-states both monomers are in an ortho state, in G-states one monomer is in an ortho and the other one in a para state. However, if we assign the splitting between the two peaks at 10R22 and 10R28 to be due to the infrared excited interchange splitting, as was done before [11], we always would expect to see a second peak for the A-state caused by relaxation processes from the other interchange component of the A-state (see also fig. 2.4); in  $G_{36}$  we expect two A-states, split by interchange tunneling. This is in clear disagreement to our result. The only exception would be if for one state the two interchange components would be separated by a large energy gap, making relaxation from one interchange component to the other for this state less likely.

Since it was found before [35] that relaxation is very effective, we have to assume in order to explain our observation that the two A-states are separated by a large energy gap (of the order of  $100 \text{ cm}^{-1}$ ), whereas the G-states are close in energy, as was found here and in [14]. This implies that the interchange splitting is large for the A-states, whereas the two G-states should be close in energy. This is in disagreement, both to the  $(2C_3+I)$  limit - where the interchange splitting is assumed to be small - and the  $(I+2C_3)$  limit. The splitting of  $3.7 \text{ cm}^{-1}$  between the 10R22 and the 10R28  $\text{CO}_2$  laser lines therefore cannot be explained by interchange motion, but must be due to a different motion. Since the barrier for internal rotation is not influenced substantially by the umbrella vibration, the splittings for torsional states should not exceed a few GHz. The infrared splitting, however, is rather large and for this reason we exclude that the splitting is due to internal rotation. From these results we conclude that the splittings observed in the double resonance experiment must be due to an additional motion.

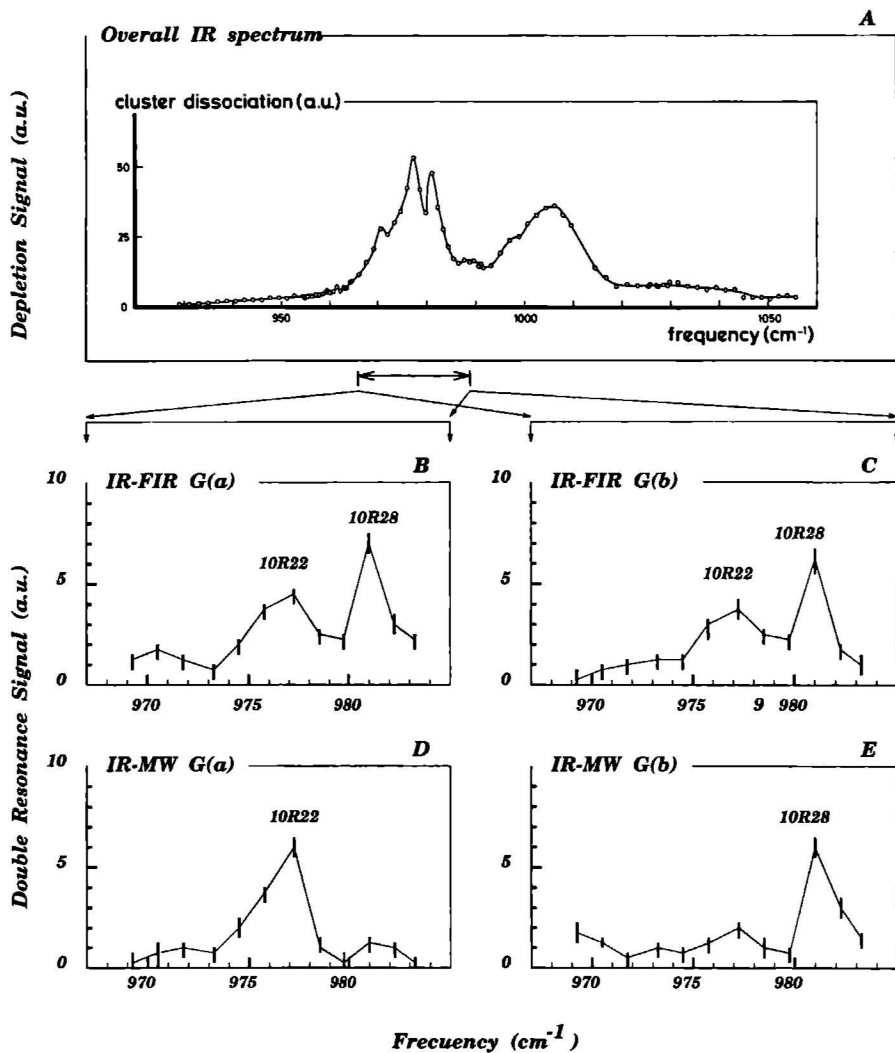
We therefore suggest that the splitting observed in the infrared-far infrared double resonance spectra is due to the partly quenched inversion of the  $\text{NH}_3$  monomer ( $3.7 \text{ cm}^{-1}$  versus approximately  $36 \text{ cm}^{-1}$  in free ammonia). This is consistent with the observation that the barrier varies with the excitation of the umbrella vibration. In the following we will verify this assumption. But first we will discuss the result of a group theoretical calculation which includes besides internal rotation along the monomer symmetry axes ( $C_3$ ) and interchange motion (I), also the monomer umbrella inversion. It is further assumed, as was done before [1, 14] that  $(\text{NH}_3)_2$  has a plane of symmetry.

The appropriate molecular symmetry group to classify all these motions is  $G_{144}$ . The character table including the spin statistical weights was given in [36]. Unfortunately some of the spin statistical weights turned out to be incorrect. The proper results are given in table 2.2 together with the decomposition of irreducible representations of  $G_{36}$  in those of  $G_{144}$ . From this table it can be seen that the G- and E-states will each be split in two states with a non-zero spin statistical weight, whereas A-states correlate to only one state with a non-zero spin statistical weight. In other words; for the two A-states only one inversion component is allowed and consequently no (collisional) relaxation between these states is possible, as it is for the G-states and as it would have been for the A-states, if the splitting would have been caused by interchange motion.

The symmetry species for the *rotational* part are  $A_1^+$  ( $K_c$  even) or  $B_1^-$  ( $K_c$  odd). The selection rules are  $+$   $\leftrightarrow$   $-$  (i.e.  $A_1^+ - A_1^-$ ).

The spectrum in figure 2.6f is assigned as originating from a  $B_2^+$  ground state. This explains the presence of only one peak in this figure (corresponding to only one inversion state). This

assignment is consistent with the set of parameters obtained in reference [14] which indicated a state lacking internal rotation. The two G-states ( $G_\alpha$  and  $G_\beta$ ) are assigned as the  $G_2^-$  and  $G_2^+$  states and the splitting of  $3.7\text{ cm}^{-1}$  to arise from the umbrella inversion in the  $\nu_2$  excited state. We can further test this assignment if we compare the intensities of the  $G_\alpha$  K:0-0 band to the  $B_2^+$  K:0-0 band. Intensity measurements yielded a ratio of 85:100 (error 30 %) [15]. Whereas this intensity ratio cannot be explained in the group  $G_{36}$  (the intensity ratio of any band compared to the G-state is smaller than 1:2) it fits very well with the new assignment, in which a ratio of 78:72 or 66:72 is expected. This confirms our initial assumption.



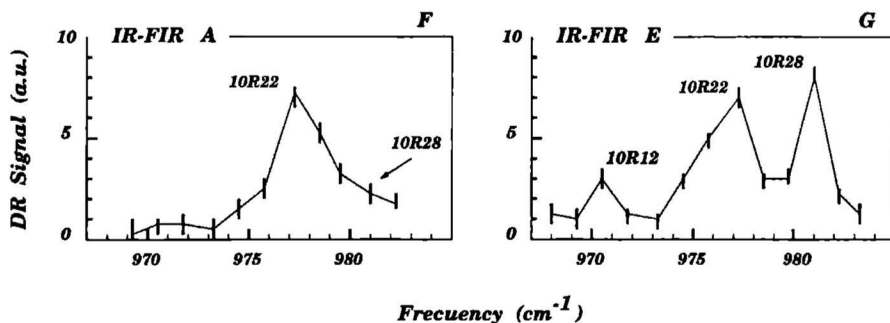


**Figure 2.6:** The IR, IR-FIR and IR-MW double resonance signals of  $(\text{NH}_3)_2$  as function of the  $\text{CO}_2$  laser frequency. Figure a gives the overall IR spectrum as measured by Snels *et al* (*Chem. Phys.* 115 (1987) 79). The double resonance spectra are restricted to the  $979\text{ cm}^{-1}$  peak. Figure b and c show the IR-FIR and figure d and e the corresponding IR-MW double resonance signals for the  $G_\alpha$  and  $G_\beta$  state as measured by Fraser *et al* (*J. Chem. Phys.* 82 (1985) 535), respectively. Figure f shows the results for the A-state and figure g for one of the E-states.

Within the group  $G_{144}$ ,  $G_2^+$  and  $G_2^-$  are the only states for which pure rotational transitions are allowed. In order to explain the presence of only two pure rotational transitions in the study of Nelson and Klemperer [1] no further precondition is required, whereas they had to demand that the internal rotation and interchange motion can be separated and that the  $(2C_3+I)$  limit is valid [3]. From our data we cannot decide, whether we observe the sum or the difference of the inversion splitting in the ground and the excited state. By an inspection of the experimental splittings it can easily be seen that the splittings between these bands can be described by a constant plus a J-dependent part. This leads to the assumption that we observe the sum of the inversion splittings as indicated in figure 2.7, which yields a splitting of approximately 450 MHz in both states. This increases to  $3.7\text{ cm}^{-1}$  under excitation of the umbrella vibration. In the absence of any other  $K:0-0$ ,  $G_2^+ - G_2^-$  transitions we assign this far infrared transition as a transition between the two interchange tunneling states  $G_2^+ - G_2^-$ ,  $G_2^- - G_2^+$ . The interchange splitting is rather large (about  $20\text{ cm}^{-1}$ ) compared to what was expected before [1, 11]. This implies that the barrier for interchange is rather small which implies in turn that the  $(2C_3+I)$  limit is not valid and consequently the molecule can *not* be characterized as rigid.

So far we have demonstrated that based on our double resonance experiment we can conclude that the inversion of the  $\text{NH}_3$  monomer, the interchange and the  $C_3$ -rotation are feasible motions. In the following we want to make a (re)assignment of the other bands reported in this work and in [14], based on the previous conclusions.

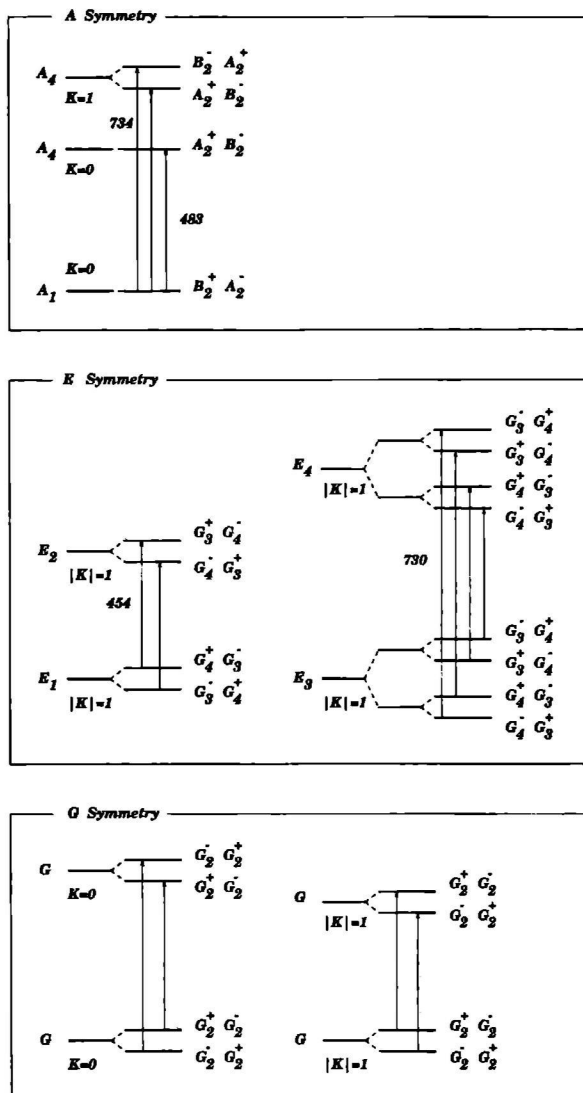


Figure 2.7: Energy diagram of the FIR transitions as assigned in this paper. The vertical axes are not on scale. The relative positions of the levels are also not experimentally determined. The indicated labeling on the left hand sides is in  $G_{36}$  that on the right hand side in  $G_{144}$  for  $J_{\text{even}}$  and  $J_{\text{odd}}$ , respectively.



$G_{36}$	$G_{144}$
$A_1 (66)$	$= B_2^+ (66) \oplus A_1^+ (0) \oplus E^- (0)$
$A_2 (78)$	$= A_2^- (78) \oplus B_1^- (0) \oplus E^+ (0)$
$A_3 (66)$	$= B_2^- (66) \oplus A_1^- (0) \oplus E^+ (0)$
$A_4 (78)$	$= A_2^+ (78) \oplus B_1^+ (0) \oplus E^- (0)$
$E_1 (36)$	$= G_3^- (21) \oplus G_4^+ (15)$
$E_2 (36)$	$= G_3^+ (21) \oplus G_4^- (15)$
$E_3 (30)$	$= G_4^+ (15) \oplus G_4^- (15)$
$E_4 (42)$	$= G_3^+ (21) \oplus G_3^- (21)$
$G (144)$	$= G_1^+ (0) \oplus G_1^- (0) \oplus G_2^+ (72) \oplus G_2^- (72)$

**Table 2.2:** Decomposition of irreducible representation of  $G_{36}$  in irreducible representations of  $G_{144}$ . In parentheses the spin statistical weights for  $(NH_3)_2$  are given.

## 2.6 Assignment of the far infrared transitions

### Band 1A - b.o. 483 GHz, (table 2.1)

Using combination differences we assign this band as the  $B_2^- - B_2^+$  transition (see fig. 2.7). We therefore obtain an interchange splitting for the A-state of 483 GHz.

### Band 1B - b.o. 454 GHz, (table 2.1)

This band was assigned as K:1-1, based on the absence of R(0) and P(1) lines. For high J values a small splitting in two lines with different intensities was seen but not fully resolved. Based on the former discussion we expect the splitting to be due to K-type splitting or inversion splitting. Since the splitting is much smaller than what is expected for a K-type doubling, we assign the band as one of the two K-type components, with an inversion splitting smaller than 2 MHz. It was found before in other  $NH_3$  containing complexes that for states with at least one active rotor - i.e. G and E-states in  $G_{36}$  - the K-type splitting is extremely large [37, 38]. This splitting increases from the high barrier to the free rotor limit for the ammonia rotation to e.g. several  $cm^{-1}$ . Since no other K-type doublet component is found, we conclude that for  $(NH_3)_2$  the high barrier limit is invalid. The differences in spin statistical weights between the two components lead to the assignment of a  $G_3^+ - G_3^-$ ,  $G_4^- - G_4^+$  transition, which correlates to the  $E_1 - E_2$  transition in  $G_{36}$  (see fig 2.7). The expected intensity ratio between the two components is 21:15, which is in perfect agreement with our observations (11:7).

### Bands E and F - b.o. 730 GHz, [14]

The double resonance experiment performed for these bands shows two peaks at 10R22 and 10R28 (not shown in fig. 2.6) which implies that they must possess a G symmetry in the group  $G_{144}$ . In addition a third peak was observed at 10R12. Snels *et al* [11] found that this peak becomes

stronger with increasing beam temperature and it therefore was assigned to originate from  $K=1$ . This was confirmed by Heijmen *et al* [13]. We assign the two bands to arise from the two corresponding inversion components. According to the discussion above the  $K$ -type doubling is again expected to be large. Therefore the doubling observed in [14], interpreted as  $K$ -type doubling must have a different physical meaning. In our model the only possible splitting which remains, is the interchange splitting. Whereas for the  $A$ -states the interchange splitting is found to be quite large (480 GHz) in this case the two interchange components are nearly degenerate. If the rotation of the ammonia monomer is described in terms of a nearly free rotation, the  $|K|=1$   $E$ -states in  $G_{36}$  can be visualized by the picture that the  $C_3$ -axis of each ammonia processes around the  $a$ -axis of the complex. The  $E_1$  and  $E_2$  states correspond to an anti-gearred motion of the two monomers, while the  $E_3$  and  $E_4$  states correspond to a geared motion. This is in agreement with the actual wavefunctions of the complex as derived by van Bladel *et al* [10]. In case of a geared motion of the two ammonia monomers, there should be no potential barrier for the interchange. Therefore the  $|K|=1$  states of  $E_3$  and  $E_4$  are expected to be nearly degenerate, whereas the  $|K|=1$   $E_1$  and  $E_2$  states will be considerably split. We therefore assign the bands  $E$  and  $F$  in [14] as  $G_4^+ - G_4^-$  or  $G_3^+ - G_3^-$  transitions as is displayed in figure 2.7. This explains the observed 1:1 intensity ratio between identical  $J_{K_a K_c}$  lines of the two inversion components [14] in a much more consistent way as was possible before; the states which are only distinguished by  $+$  and  $-$  have the same spin statistical weight (e.g.  $G_4^+$  and  $G_4^-$ ). The far infrared transition of 730 GHz corresponds then either to interchange or "K-type" splitting. This latter notation does not make sense anymore in the low/intermediate barrier limit. Based on theoretical calculations [10] it is most likely the first splitting.

In order to explain why the inversion splitting is smaller for the band 1B than for the bands  $E$  and  $F$ , we assume that for one band the sum between the inversion splittings was observed, while for the other band it is the difference. It is also likely that inversion is quenched more in the case of an anti-gearred rotation than it is in the case of a geared rotation. Assuming that the ground state and excited state exhibit nearly the same inversion splitting, the inversion splitting in each  $E_{3,4}$  state is estimated to be 19 MHz. (The band origins are separated by 38 MHz [14].)

### Band 1C - b.o. 487 GHz, (table 2.1)

The band at 487 GHz shows a resolvable splitting, which is assumed to be the inversion splitting. In order to fit the data the following expression was used:

$$E = E_0 + BJ(J+1) - DJ^2(J+1)^2 + HJ^3(J+1)^3 \quad (2.1)$$

$$\pm [aJ(J+1) - dJ^2(J+1)^2 + hJ^3(J+1)^3]$$

The fact that so many parameters are required, indicates perturbations by Coriolis interaction.  $a$ ,  $d$  and  $h$  describe the Coriolis interaction and distortion effects herein. The results of the fit for all three bands, reported in this work, are given in table 2.3. The ratio between the intensities of the two inversion components are found to be 1:1. This means that the band must originate from states correlating to  $G$  or  $E_{3,4}$  states in  $G_{36}$ . We therefore assign them as the  $G_2^+ - G_2^-$  transitions as indicated in figure 2.6. Comparing the intensity ratio of the 1C band ( $G_2^+$ ) with the 1B band ( $G_4^+$  and  $G_3^-$ ) a ratio of 59:30 was found [15]. Based on our assumption a ratio of 72:(21+15) = 72:36 (since the two lines were not resolved) is expected. This is in perfect agreement. The far infrared transition is either a transition to the other "K-type" component or to the other interchange component. Like for the  $E$  and  $F$  bands the latter case is most likely.

	$K=0-0$	$ K =1-1$	$ K =1-1$ <sup>a)</sup>
$\nu_{BO}$	483301.067(54)	453599.485(96)	486731.35(35)
$B''$	5136.601(13)	4974.023(24)	5125.409(53)
$D''$	58.53(34)	-191.7(1.3)	58.8(1.5)
$H''$		-605(20)	
$a''$			0.491(12)
$B'$	5030.494(13)	5002.952(12)	4966.441(95)
$D'$	48.47(50)	46.71(24)	-428.2(5.2)
$H'$			-2498(73)
$a'$			8.345(35)
$d'$			111.7(3.1)
$h'$			857(53)
$\sigma$	0.01	0.03	0.38

<sup>a)</sup>  $\nu_{BO}$  is the band origin;  $\sigma$  is the standard deviation of the fit. All constants are in MHz, except  $D$  and  $d$  in kHz and  $H$  and  $h$  in Hz. Between parentheses we list either the errors, calculated from the estimated 0.10 MHz frequency uncertainties (first two columns) or the standard deviations (last column), whichever is larger.

**Table 2.3:** Constants for the bands listed in table 2.1 as obtained from the fit.

A possible candidate responsible for the observed perturbation in the upper state can be the upper state of the  $K:0-0$ ,  $G_2^+ - G_2^-$  band. It should be mentioned at this point that the B-values found for the upper interchange component of the  $G_2^-$ ,  $K=0$  state are too large compared to e.g. the unperturbed A-states (and all other states). One might speculate whether this is a consequence of the interaction between these states.

### Band D - b.o. 747 GHz, [14]

The double resonance spectrum of this state is shown in figure 2.6g. From the presence of two peaks we conclude that the band is of G symmetry. The small splitting which was attributed to K-type splitting in [14] is assigned here as an inversion splitting. Since the two components were found to have identical spin statistical weights, they will be due to states correlating with  $E_{3,4}$  or G-states in  $G_{36}$ . In a check of the combination differences we were not able to find any coincidences with bands assigned so far. Therefore the band must originate from an upper  $G_2^{+,-}$  level or the assignment as a  $K:1-1$  transition has to be checked. Since for example the R(0) line is very close to a water absorption it is possible that lines were missed. On the other hand the double resonance signal at 10R12 suggests that a higher K level is involved. At the moment no definite assignment of this band can be given.

## 2.7 Conclusion

We have demonstrated that infrared-far infrared double resonance experiments are a powerful tool in order to reveal the nature of the tunneling splittings observed in the far infrared spectrum. We were able to prove that the ammonia dimer exhibits an inversion motion which was assumed to be quenched in former papers. It was possible to assign the bands published so far within the group  $G_{144}$ . It was also shown that the ammonia rotation cannot be described within the high barrier limit. The interchange splitting was found to be large, giving evidence for a floppy structure. Similar conclusions are also drawn from a very recent theoretical [10] and experimental study [17]. Whereas further far infrared measurements will provide additional information on energy spacing, the splitting due to the internal rotation can only be provided by *ab initio* calculations, since transitions between different internal rotor states are not allowed.

Further experiments to label the bands detected around 500 GHz are in progress. For that purpose we will install a second Apollo high power CO<sub>2</sub> laser as infrared pump laser. Since no saturation effect from the CO<sub>2</sub> laserpower could be found so far, an increase in power by a factor of five should allow a probing of even weak lines. Since the infrared absorption frequencies of ammonia trimer differ by ca. 50 cm<sup>-1</sup> from those of the dimer [11, 12], this method also allows to distinguish between dimer and trimer transitions.

## Acknowledgment

We want to thank Prof. J. Reuss, Prof. A. van der Avoird, Dr. J. van Bladel and Dr. P. Wormer for many stimulating discussions. Frans van Rijn is thanked for technical assistance. This work was supported by the European Community under grant (EC 892 001 59/OP1).



---

## The Electric Dipole Moment of the Ammonia Dimer for $G:|K|=1$

*H. Linnartz, A. Kips and W.L. Meerts*  
*Department of Molecular and Laser Physics, University of Nijmegen,*  
*Toernooiveld, NL 6525 ED, Nijmegen*

*M. Havenith*  
*Institut für Angewandte Physik, Wegelerstraße 8, D 53115, Bonn*

### Abstract

From the results of Stark measurements on the ammonia dimer, generated in a molecular jet expansion, it was possible to determine the electric dipole moment for the  $G:|K|=1$  state (bandorigin 486 GHz). The partly quenched monomer inversion in the complex gives rise to quadratic Stark effect. We find an electric dipole moment of  $|\mu| = (0.10 \pm 0.01)$  D in the ground state and an upper limit of 0.09 D for the dipole moment in the excited state. These small values give evidence that for the  $G:|K|=1-1$  states the "antiparallel" (cyclic) structure is more likely than the hydrogen bonded one.

## 2.8 Introduction

In the past ten years the ammonia dimer has turned out to be a very interesting van der Waals complex. The results of Nelson, Fraser and Klempner [1, 2] in 1985, which showed that  $(\text{NH}_3)_2$  has no hydrogen bonding for the G:K=0 state, were surprising in view of former *ab initio* calculations (see e.g. [4, 39]) that predicted a linear hydrogen bonded structure. Nelson and coworkers measured the intermolecular distance, the electric dipole moment (0.74(2) D) and the quadrupole coupling constants, from which they calculated the structure for the G:K=0 state, yielding an equilibrium structure in which both  $\text{NH}_3$  monomers are aligned antiparallel, making polar angles with the intermolecular axis of  $49^\circ$  and  $65^\circ$ . They excluded the linear H-N...H bonding, for which a much larger dipole moment (about 2 D) is expected. Nelson *et al* also managed to assign the measured microwave transitions within the group  $G_{36}$  [3] which includes the internal rotation of each monomer along the  $C_3$ -axis and the interchange tunneling between the two non-equivalent monomer units and in which the umbrella inversion is assumed to be totally quenched.

In 1985 Fraser *et al* performed an infrared-microwave double resonance experiment which showed a clear correlation between the infrared spectra and the G-states,  $G_\alpha$  and  $G_\beta$  [18], within the complex. The total infrared spectrum for  $(\text{NH}_3)_n$  clusters was measured at the same time in Nijmegen by Snels *et al* [11] and later extended by an infrared-infrared double resonance experiment on the ammonia dimer by Heijmen *et al* [13], who found the same correlations as were found in the infrared-microwave double resonance experiment [18]. A similar experiment to that of Snels was performed in 1987 by Huisken and Pertsch [12] with size-selected ammonia clusters, using the scattering of a  $(\text{NH}_3)_n$  beam by a rare gas beam to produce a well defined cluster size in the dissociation zone (see also chapter 3). Their results were in general agreement with the measurements of Snels.

In 1988 Havenith *et al* [14] started a far infrared study on several vibration-rotation-tunneling (VRT) transitions. Their work supported the conclusions drawn by Nelson [2]. However, additional far infrared measurements by Zwart *et al* [15, 16] on absorption bands in the 380-520 GHz range did not fit into the  $G_{36}$  approach and showed the need for further experiments. In 1992 three papers on the ammonia dimer were published (an infrared-far infrared double resonance study on  $(\text{NH}_3)_2$  in a molecular jet expansion [16]; a far infrared study on the complex [17]; and a theoretical study on the six dimensional VRT dynamics of the dimer [10]) which came to surprising conclusions:

- \* The umbrella inversion is only partly quenched within the complex, therefore the appropriate symmetry group is  $G_{144}$  [10, 16, 17].
- \* The interchange splitting is rather large ( $\approx 20 \text{ cm}^{-1}$ ), which implies that the intramolecular barrier for interchange is quite small. Therefore the molecule is not any longer supposed to exhibit a rigid behaviour as was stated in the approach of Nelson *et al* [16, 17].
- \* The K-type splitting turns out to be very large, which also excludes the high barrier limit [16].

Concluding that  $\text{NH}_3$  exhibits small barriers for internal motion, it is difficult to determine a structure for the molecule, since only vibrationally averaged structures are obtained experimentally. One of the most important measurable quantities is the electric dipole moment. The discussion

whether  $(\text{NH}_3)_2$  is hydrogen bonded or not is so far based upon the measurements of Nelson *et al* on the dipole moment of  $(\text{NH}_3)_2$  in one tunneling state; the  $G:K=0$  ground state. Since these measurements only yield information on a very specific part of a flat potential surface - with small barriers for internal motions - there is clearly need for more data. We will present here new Stark measurements on the  $G:|K|=1$  states.

## 2.9 Experiment

The ammonia dimer complexes are formed in a continuous two-dimensional ( $4\text{cm} \times 75\ \mu\text{m}$ ) supersonic jet expansion of 2 %  $\text{NH}_3$  in Ar. The spectra are recorded with the tunable far infrared

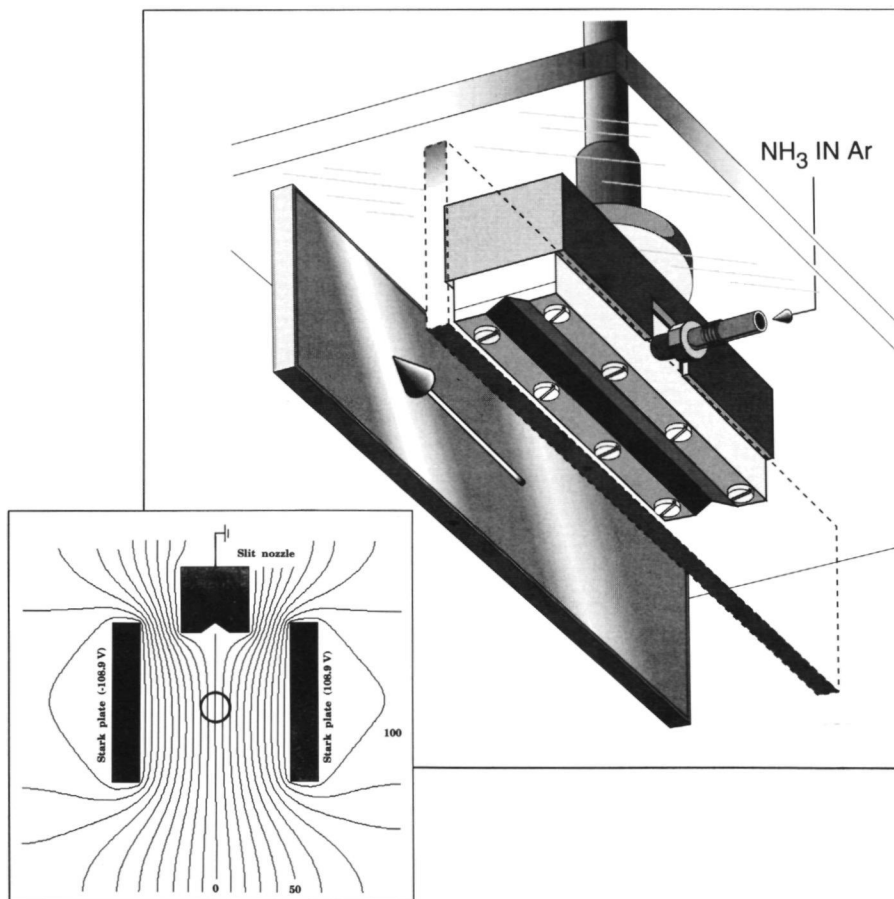


**Figure 2.8:** Setup for Stark measurements in a jet. The electric field simulation is drawn in the enlargement. In the absorption zone the electric field is nearly homogeneous.



spectrometer in Nijmegen [33]. The radiation used for the dipole measurements is generated with the seventh harmonic of a 70 GHz klystron and the eight harmonic of a 55 GHz klystron in a Schottky barrier diode and selected using a 0.8 grooves/mm grating. The radiation passes the molecular beam and is focussed onto an InSb hot-electron bolometer. The radiation is frequency modulated at 5 kHz and the detector output is monitored at twice this frequency.

For the Stark field two metal plates (15 x 5.4 x 1 cm) are used. These are positioned on both sides of the nozzle parallel to the slit, 5 cm apart. The electric field is applied by a stabilized (Fluke 332A) power supply. Due to the relatively large background pressure during jet operation (100 mTorr) the highest applicable field, without getting break-downs, amounts to 43.56 V/cm. It is important to know how much the homogeneity of the electric field is disturbed by the presence of the aluminum nozzle and by the finite dimensions of the Stark plates. Therefore we simulated the setup with "Simion" [40] (fig. 2.8). From this we concluded that inhomogeneities play only a minor role in the absorption zone which lies 2.5 cm under the slit. This can also be concluded from the fact that we see no line broadening effects in the electric field. For an applied field of 43.56 V/cm we calculate an electric field in the absorption zone of  $(40 \pm 1)$  V/cm.

The polarization of the far infrared radiation is parallel to the electric field.

## 2.10 Theory

In the  $G_{36}$  approach, in which inversion is assumed to be totally quenched, it was shown [10] that the degenerate G and  $E_3/E_4$  ( $|K|=1$ ) states will exhibit a first order Stark effect. We will explain this result and extend these considerations to the group  $G_{144}$  (fig. 2.4) which is applicable here.

A first order Stark effect will occur if two energetically degenerate states  $\phi_1$  and  $\phi_2$  have a non-vanishing Stark matrix element;  $\langle \phi_1 | \mu E | \phi_2 \rangle$ . Since the dipole moment operator in  $G_{36}$  is of symmetry  $A_3$  [1], first order Stark effects are only expected in two cases, both are  $K=1$  states:

1. If the two K-type doubling components for  $K=1$  G-states are expected to be energetically degenerate we would obtain a first order Stark splitting, since  $\langle G | A_3 | G \rangle \neq 0$  holds. However, since a large K-type splitting for  $|K|=1$  G-states was found [17], in  $G_{36}$  no observable Stark splitting will be expected.
2. As was discussed in [10, 16] the  $|K|=1$   $E_3/E_4$ -states are nearly degenerate, since they represent both geared motions of the  $NH_3$  monomer. The  $E_3/E_4$ -states should be split by interchange tunneling which is quite large for other symmetry states. But, since for geared motion no potential barrier for the interchange motion is expected, the two states are degenerate and only split by Coriolis interaction. If the K-type doublet components are also assumed to be energetically degenerate, one can obtain again non-vanishing matrix elements between degenerate states:  $\langle E_3 | A_3 | E_3 \rangle \neq 0$ . But, following the assignment as given in [16] and the energies as given in [17] the K-type doublet components are separated by 730 GHz. Therefore, no first order Stark effect is expected in  $G_{36}$  for these states.

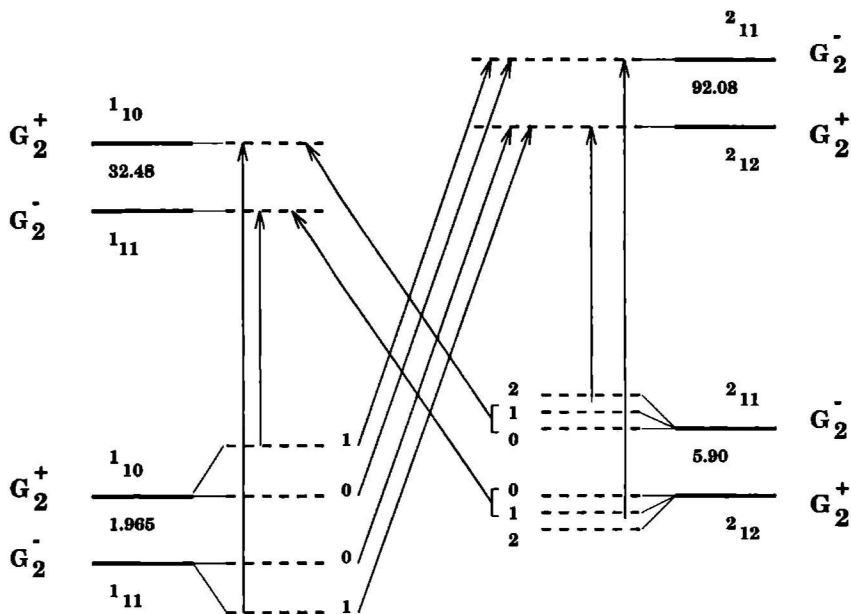


**Figure 2.9:** The energy level scheme for the  $G:|K|=1-1$  states for  $J=1$  and  $2$  for  $(\text{NH}_3)_2$ . The small splittings are due to inversion; the large splittings are due to interchange motion. The dotted lines indicate the  $M$  components in the presence of an electric field. The arrows show the observed transitions.

However, due to the inversion of the monomer units, each rotational level for these states will split into two components with different symmetry in  $G_{144}$ . The symmetry of the dipole moment operator in  $G_{144}$  is  $A_1^-$ . This means that non-vanishing matrix elements are obtained between the two inversion components of the  $G$ -states ( $\langle G_2^+ | A_1^- | G_2^- \rangle \neq 0$ ) and the two inversion components of the former  $E_3$ -states ( $E_3 = G_4^+ + G_4^-$ ) and the  $E_4$ -states ( $E_4 = G_3^+ + G_3^-$ ). If the zero field splitting is large compared to the term describing the Stark interaction between these levels, applying an electric field will yield a quadratic Stark effect. A Stark splitting is now expected for all  $K$ -values, where the observed splitting will depend on the size of the inversion splitting, the  $J$ -level involved and the  $Q$ - or  $P$ - and  $R$ -character of the transition. Each  $J$ -level will split into  $J+1$ ,  $|M|$  components. Because the polarization direction is parallel to the electric field only  $\Delta M = 0$  transitions are allowed. For  $Q$ -transitions the intensities are proportional to  $(M^2)$ , for  $P$ - and  $R$ -transitions to  $(J^2 - M^2)$ .

In contrast to the  $E$ -states the hyperfine structure for the  $G$ -states cannot be resolved in our experiment. Therefore for  $G$ -states the electric dipole moment can be calculated by diagonalizing

$$\begin{pmatrix} E_{01} & -\frac{\mu\epsilon KM}{J(J+1)} \\ -\frac{\mu\epsilon KM}{J(J+1)} & E_{02} \end{pmatrix} \quad (2.2)$$

where  $\mu$  is the electric dipole moment,  $\epsilon$  the applied electric field and  $K=1$ . From [16] it can be concluded that the energy difference between two inversion levels  $\Delta E_{inv} = E_{01} - E_{02}$  is given by

$$\Delta E_{inv} = 2\left[\frac{1}{4}(B - C)J(J + 1) - dJ^2(J + 1)^2 + hJ^3(J + 1)^3\right] \quad (2.3)$$

with

	initial state	final state
B-C	1.965(46) MHz	33.38(14) MHz
d		111.7(3.1) kHz
h		857(53) kHz

For  $J = 1 \leftarrow 1$  transitions only the  $\Delta M=0$  for  $|M|=1$  are observable. In this case the shift ( $\delta$ ) in the presence of an electric field is directly correlated to the value of the electric dipole moment.

## 2.11 Results and discussion

In figure 2.9 the energy level scheme is drawn for  $J=1$  and  $J=2$  in the ground and excited states. The small splittings are due to the umbrella inversion in the complex, the large transitions due to interchange motion. The dotted lines indicate the observed shifts and splittings in the presence of an electric field.

We measured the line positions for the four Q-transitions and the two P- and R-transitions without electric field and with an electric field of  $(40 \pm 1)$  V/cm in the absorption zone. The results are listed in table 2.4. For the Q(1) transitions the measurement is repeated for  $(30 \pm 1)$  V/cm, which is almost a factor  $\sqrt{2}$  smaller. The shift turns out to be a factor two smaller, which proves that the Stark effect is indeed quadratic.

For the  $J = 1 \leftarrow 1$  transitions the only component that can be seen is the  $\Delta M = 0$  for  $|M| = 1$ . This component shifts  $420 \pm 30$  kHz. The observed Stark shifts of table 2.4 lead to the conclusion that the shift in the Q(1) transitions is completely determined by the energy shift in the ground state. This is supported by the following arguments.

1. For the R(1) transitions we see two components (fig. 2.10). One for  $M=0$  and one for  $|M| = 1$  with an intensity ratio of 4 to 3. The  $M=0$  transition coincides with the zero field transition. The shift of the  $|M| = 1$  component is equal to the shift measured for the  $|M| = 1$  component of the Q(1) transition.
2. We observe one component of the Q(2) transition, shifted by  $(70 \pm 30)$  kHz. We expect two components ( $|M|=1$  and  $|M|=2$ ) with an intensity ratio of 1 to 4. Taking into account the different values for  $J$  and  $\Delta E_{inv}$ , we calculate the expected shift of these components from the shift of the  $|M| = 1$  Q(1) transition. The Stark shifts for the  $|M| = 1$  and  $|M|=2$

$J''_{K''_a, K''_c} \leftarrow J''_{K''_a, K''_c}$	$\nu_0$ (MHz)	Observed shift (kHz) $\epsilon = (40 \pm 1)$ V/cm	$ M $	Experimental uncertainty (kHz)
$1_{10} \leftarrow 1_{11}$	486433.22	+ 420	1	30
$1_{11} \leftarrow 1_{10}$	486398.33	- 420	1	30
$2_{12} \leftarrow 1_{11}$	506248.67	- 20	0	30
		+ 430	1	30
$2_{11} \leftarrow 1_{10}$	506339.63	+ 10	0	30
$2_{11} \leftarrow 2_{12}$	485843.64	+ 70	1 + 2	30
$2_{12} \leftarrow 2_{11}$	485744.81	- 70	1 + 2	30
$1_{11} \leftarrow 2_{12}$	465902.29	+ 10	0 + 1	30
$1_{10} \leftarrow 2_{11}$	465929.30	0	0 + 1	30

$J''_{K''_a, K''_c} \leftarrow J''_{K''_a, K''_c}$	$\nu_0$ (MHz)	Observed shift (kHz) $\epsilon = (30 \pm 1)$ V/cm	$ M $	Experimental uncertainty (kHz)
$1_{10} \leftarrow 1_{11}$	486433.22	+ 200	1	40
$1_{11} \leftarrow 1_{10}$	486398.15	- 180	1	40

**Table 2.4:** Observed Stark shifts for  $G:|K|=1$  transitions in  $(\text{NH}_3)_2$  for 40 and 30 V/cm.

components are smaller by a factor 27 and 6.8, respectively, yielding 15 kHz and 60 kHz. Within the Doppler limited linewidth of 200 kHz a single transition shifted by 50 kHz is expected. This is consistent with our measurements.

- For the P(1) transitions we observe a single component that is not shifted. We expect a  $M=0$  component - that will not shift - and a  $|M|=1$  component that almost coincides (15 kHz shift) with intensity ratios of 4 to 3, which is again in agreement with the observation.

From the shift measured for the Q(1) transitions we calculate an (absolute value of the) electric dipole moment of  $(0.10 \pm 0.01)$  D for the ground state. For the excited state we only can determine an upper limit. Taking into account an inversion splitting that is about 16 times larger than in the ground state and assuming an uncertainty of 30 kHz in the measurements (a shift larger than this value can be resolved) we calculate an upper limit of approximately 0.09 D.

## 2.12 Structural implications

The dipole moment of the complex can be calculated according to [1]

$$\mu_a = \mu_a^{ind} + \mu^{NH_3} < \cos \theta_1 + \cos \theta_2 > \quad (2.4)$$

where  $\theta_1$  and  $\theta_2$  form the angles between the  $C_3$ -axis and the  $a$  inertial axis of the complex.

A dipole moment as small as 0.10 D implies that for the  $G:|K|=1$  state the projection of the  $C_3$ -axis of the ammonia monomers onto the  $a$ -axis will be of equal size but opposite in direction. This means that the angles  $\theta_1$  and  $\theta_2$  form nearly complementary angles. However, we cannot

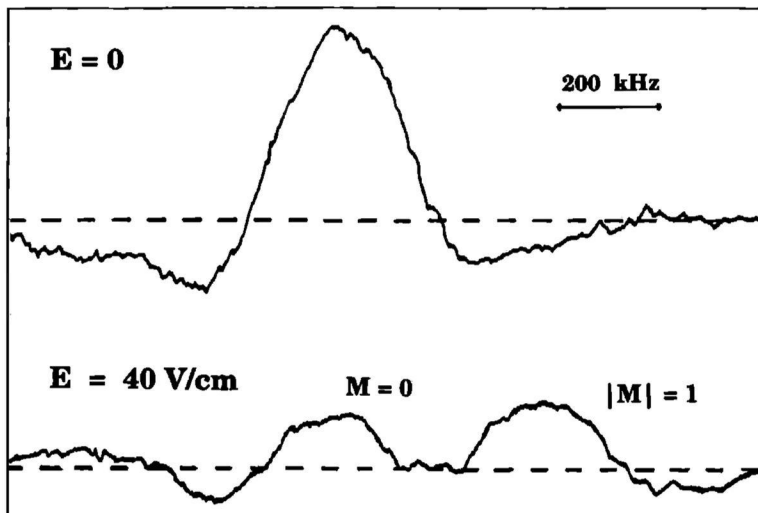


Figure 2.10: The  $G:K=1, I_{11} \leftarrow I_{10}$  transition in zero electric field and in a field of 40 V/cm.

determine the two angles independently without knowledge of the hyperfine splitting which is not resolved in our experiment. Moreover vibrational averaging effects, as discussed by van Bladel *et al* [10], might also be a principal problem when trying to deduce the structure.

In the following we will compare the measured dipole moment with the dipole moments as expected for the two structures discussed in literature: the classical hydrogen bonded structure and the cyclic (antiparallel) structure.

For the hydrogen bonded structure one of the ammonia monomers acts as a proton donor, whereas the other acts as proton acceptor. For this structure is  $\theta_1 = 0^\circ$  and  $\theta_2 = 68^\circ$ . For the cyclic structure, as was proposed by Nelson *et al* for the  $G:K=0$  ground state, these angles amount to  $48.6^\circ$  and  $115.5^\circ$  respectively (fig. 2.11).

The electric dipole moment of a hydrogen bonded structure is estimated by van Bladel *et al* [10] to be  $-1.6$  D. In this theoretical study vibrational averaging effects based on the potential calculated by Sagarik, Ahlrichs and Brode [9] were examined, but the electric dipole moment, measured by Nelson *et al* and especially the value obtained in this paper are too small to be explained as a vibrational averaging effect. Our measurements therefore support the conclusion that the  $(\text{NH}_3)_2$  is not a hydrogen bonding system.

Furthermore, our measurements confirm that the ammonia dimer van der Waals complex is a non-rigid molecule. A remarkable variation of  $\mu$  with  $K$  ( $K$  being the projection of the overall angular momentum, including internal rotation) is found. For  $K=0$ ,  $|\mu| = 0.74$  D and for  $|K|=1$ ,  $|\mu| = 0.10$  D. This gives evidence that the  $(\text{NH}_3)_2$  has a shallow potential, so that different  $K$ -levels probe different parts of the potential.

Further Stark measurements [41] and studies of the hyperfine structure in different tunneling levels

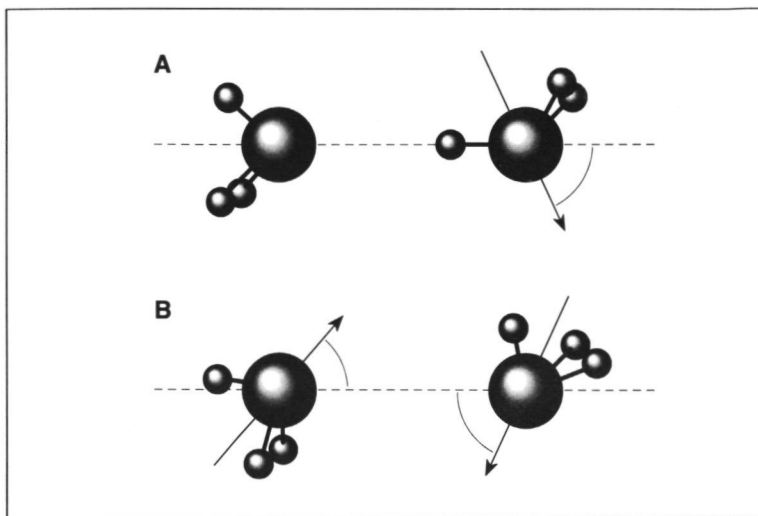


Figure 2.11: The classical hydrogen (a) and nearly antiparallel non-hydrogen (b) geometry of  $(\text{NH}_3)_2$ .

will be of great interest in clarifying the structure of this important molecule.

### Acknowledgement

We would like to thank Prof. Van der Avoird and Dr. Wormer for many helpful discussions. We also are grateful to Volker Wagener and Prof. Winnewisser for lending us a powerful 55 GHz klystron. This work was supported by the European Community (grant EC 892 001 59/OP1).



---

## The Ammonia Dimer New Infrared - Far Infrared Double Resonance Results

*H. Linnartz and W.L. Meerts*

*Department of Molecular and Laser Physics, University of Nijmegen,  
Toernooiveld, NL 6525 ED, Nijmegen*

*M. Havenith*

*Institut für Angewandte Physik, Wegelerstraße 8, D 53115, Bonn*

### Abstract

From the results of an infrared-far infrared double resonance experiment on  $(\text{NH}_3)_2$  complexes, generated in a supersonic slit nozzle expansion, it was possible to characterize the tunneling dynamics, occurring within the ammonia dimer (Havenith *et al*, Chem. Phys. Lett. 193 (1992) 261). In this chapter we present additional infrared-far infrared double resonance spectra which confirm the former analysis and from which it is possible to give a state specific explanation of the overall infrared spectrum of  $(\text{NH}_3)_2$  as measured by Snels *et al* (Chem. Phys. 115 (1987) 79) and Huisken *et al* (Chem. Phys. 126 (1988) 213).



## 2.13 Introduction

In the last years the ammonia dimer has turned out to be a very interesting complex. The results of Nelson *et al* in 1985 [1, 2, 3] which showed that  $(\text{NH}_3)_2$  has no hydrogen bonding for the  $G:K=0$  state, were surprising in view of former *ab initio* calculations (see e.g. [4, 5, 6]) that predicted a linear hydrogen bonded structure. From the measured rotational spectrum Nelson and his coworkers could deduce the intermolecular distance between the two ammonia monomers, the projection of the electric dipole moment on the dimer axis (0.74 D) and the diagonal component of the quadrupole coupling tensor along the  $a$  inertial axis. Under the preassumption that  $(\text{NH}_3)_2$  can be considered as a rigid molecule, they calculated the structure from these values, yielding an equilibrium geometry in which both  $\text{NH}_3$  monomers are aligned nearly antiparallel, making polar angles with the intermolecular axis of  $49^\circ$  and  $65^\circ$ . Since the dipole moment of free ammonia amounts to 1.47 D, the sum of the permanent dipoles of both monomers in a hydrogen bonded geometry is estimated to be about 2.0 D. For this reason Nelson *et al* excluded the linear  $\text{N-H}\cdots\text{N}$  bonding. The only calculation that seemed to support a nearly cyclic structure for  $(\text{NH}_3)_2$  [9] was shown later [10] to favor in fact a slightly bent hydrogen bonded structure.

In the ensuing debate the preassumption was questioned, whether  $(\text{NH}_3)_2$  is a rigid or a rather floppy molecule. In case of large amplitude tunneling motions the structure deduced from the Nelson measurements only reflects a vibrationally averaged structure which not necessarily has to coincide with a minimum in the intermolecular potential. However, from the fact that the relevant intermolecular bond angles hardly varied with isotopic substitution Nelson *et al* [2, 7] concluded that  $(\text{NH}_3)_2$  is a fairly rigid complex and consequently its equilibrium structure must be nearly cyclic. This conclusion was supported by the observation that the electric dipole moment for  $(\text{ND}_3)_2$  turned out to be 0.17 D smaller than the value that was found for  $(\text{NH}_3)_2$ . In case of vibrational averaging, this seems to be a contradiction, because the  $(\text{ND}_3)_2$  is expected to be less influenced by internal motions, i.e. to stay closer to equilibrium, and consequently it should have a larger electric dipole moment [2].

In the following years the results of detailed infrared [11, 12, 13], far infrared [14, 15, 16, 17], infrared-far infrared [16], microwave [1] and infrared-microwave [18] studies became available. From these studies, especially [16, 17], it was found that the ammonia dimer is a very floppy molecule, exhibiting large amplitude motions. A result that was also found by a theoretical study by van Bladel *et al* [10]. In addition it became clear that the monomer umbrella inversion is only partly quenched in the complex. This was a rather unexpected result, since the umbrella inversion in most  $\text{NH}_3$  containing complexes is completely quenched. Only  $\text{Ar-NH}_3$  [19, 20] possesses a configuration in which inversion can take place almost undisturbed. As a consequence the appropriate molecular symmetry group had to be extended to  $G_{144}$ . Using this group it turned out to be possible to assign all microwave and far infrared data known so far [16, 17]. However, none of these studies could provide any structural information that could confirm or disprove the results found by Nelson *et al* and explain the discrepancy with the conclusions deduced from the  $(\text{ND}_3)_2$  measurements.

In 1993 dipole measurements on  $G:|K|=1$  by Linnartz *et al* [21], explicitly using a Stark treatment in  $G_{144}$ , gave evidence that the antiparallel, so called cyclic structure is indeed more likely than the hydrogen bonded one, although one has to keep in mind that this structure is the consequence of vibrational averaging in a very floppy complex. "More likely" in this context means that the complex most of the time will reflect an antiparallel configuration, as an intermediate between

several tunneling motions. For this reason a comparison between experiment and theory is difficult. Whereas the electronic structure calculations focus mainly on finding the minimum of the intermolecular potential, the experiment yields a vibration-rotation-tunneling averaged structure. Since the potential surface is very flat, it is quite a challenge to compute the averaged structure and to explain the results quantitatively. Olthof, Van der Avoird and Wormer [42] were able doing so, by solving the full six dimensional nuclear motion equation for a series of model potentials with different barriers for the interchange motion and for the hindered rotations of the two ammonia monomers around their  $C_3$ -axes. In this study several measurable quantities were computed; electric dipole moments, energy splittings, nuclear quadrupole splittings and the amount of quenching of the monomer umbrella inversions. The potential that gave best agreement with the observed quantities has an equilibrium hydrogen bonded structure and a small barrier ( $24\text{ cm}^{-1}$ ) for interchange tunneling, but a vibration-rotation-tunneling averaged ground state that is nearly cyclic. Furthermore van der Avoird *et al* were able to extend the use of this potential to  $(\text{ND}_3)_2$  [23]. From this it became clear that in terms of localized wavefunctions it is also possible to explain the decrease of the G:K=0 electric dipole moment, when going from  $(\text{NH}_3)_2$  (0.74 D) to  $(\text{ND}_3)_2$  (0.57 D), without explicitly demanding a rigid structure. In the most recent study van der Avoird and coworkers use an even smaller barrier of  $7.5\text{ cm}^{-1}$  for the interchange motion [29]. This is less than 1 % of the binding energy of the complex, which is estimated to be about  $950\text{ cm}^{-1}$  [11]. With this very small barrier height, nearly all experimental data can be reproduced and, especially, the accuracy in predicting the band origins is remarkably good (within  $0.5\text{ cm}^{-1}$ ).

From a structural point of view the discussion whether ammonia is hydrogen bonded or not [7, 8, 24] comes to an end. The ammonia dimer seems to have an equilibrium hydrogen bonded structure, but this does not represent the actual structure. Due to the low barriers all measured quantities retain to an averaged structure that is nearly cyclic. Since the important features of a hydrogen bond - near linearity and strong directionality of the bond - are not met, it is not correct to speak of hydrogen bonding in  $(\text{NH}_3)_2$ .

However, there are still some unsolved problems. One of these is the infrared spectrum of  $(\text{NH}_3)_2$ . As an outcome of theoretical work [4] the complex was not expected to dissociate upon excitation with a single  $10\text{ }\mu\text{m}$  photon but experiments [11, 12, 13, 16, 43] showed that one  $970\text{ cm}^{-1}$  photon is sufficient to cause dissociation of the complex. Additional information was found by Buck and coworkers [32]. In a scattering experiment with a secondary He beam an average energy of  $520\text{ cm}^{-1}$  was transferred to ammonia dimers without causing dissociation. This gives the lower limit, whereas the upper limit can be estimated from the experiment of Snels *et al* [11] to be about  $950\text{ cm}^{-1}$ . Snels and coworkers measured the overall infrared spectrum of  $(\text{NH}_3)_2$  by bolometric detection. Combining the outcome of this experiment, information from the infrared-microwave double resonance experiment performed by Fraser *et al* [18], information from an infrared-infrared double resonance experiment performed by Heijmen *et al* [13], the photodissociation of size-selected ammonia clusters as performed by Huisken and Pertsch [12] and the results that are presented here, we are able to give a state specific interpretation of the infrared spectrum. For this we have studied several  $|K|=1$  states. We will present the infrared-far infrared double resonance results for the G (bandorigin 487 and 747 GHz) and  $E_{1/2}$  (b.o 454 GHz) states. These will be compared with the G:K=0 (b.o. 613/614 GHz) state as was published in [16]. Finally the K=0-1 and K=0-0 transitions for A symmetry (b.o. 483 and 734 GHz, resp.) are compared.

In this chapter we mostly use the  $G_{36}$  characters.  $G_{144}$  characters are put in parentheses. The far

infrared level numbering is taken as introduced by Loeser *et al* [17].

## 2.14 Experiment

The  $(\text{NH}_3)_2$  complexes are produced in a continuous two-dimensional supersonic jet by expanding a mixture of 2 %  $\text{NH}_3$  in argon through a 4 cm x 75  $\mu\text{m}$  slit nozzle into a vacuum chamber that is maintained at 50–100 mTorr by an 4000  $\text{m}^3/\text{hr}$  roots blower pumping system. The experimental mixture is optimized by gas flow controllers. The far infrared radiation is generated with the Nijmegen tunable far infrared sideband spectrometer [33] by mixing an Apollo  $\text{CO}_2$  laser optically pumped fixed far infrared laser frequency with tunable microwave radiation generated by a klystron, in a Schottky barrier diode. For the measurements in the 700–750 GHz range we used the sideband of the  $\text{CH}_3\text{I}$  670 463.0 MHz line or the  $\text{HCOOH}$  692 951.4 MHz line and a 60 or 70 GHz klystron. For frequencies in the 300–550 GHz range we used higher harmonics of klystrons (50–112 GHz), without a fundamental laser frequency.

The radiation passes the molecular beam and is focussed onto an InSb hot-electron bolometer. For the double resonance experiment an infrared beam, generated by a second Apollo  $\text{CO}_2$  laser (typical single line output power of 80 W) is guided antiparallel to the far infrared beam between the nozzle and absorption zone (fig. 2.5). The double resonance signal is detected by observing the depletion in the far infrared signal for a selected (and assigned) state as function of the infrared radiation (10R8–10R34). In order to achieve this the  $\text{CO}_2$  laser beam is chopper modulated with a frequency of 500 Hz. Consequently the bolometer signal that is lock-in detected, directly reflects the loss in far infrared signal as result of the infrared pumping; this is the double resonance signal. The cluster dissociation versus laser power has been measured for several  $\text{CO}_2$  laser lines. This showed a linear dependence. No saturation effects have been observed. The reproducibility of the observed spectra was better than 10 %, with exception of the  $E_{1,2}$  band, where the error is estimated to be smaller than 20 %.

## 2.15 Results

The infrared spectrum measured by Snels *et al* [11] shows main peaks at 979  $\text{cm}^{-1}$ , in the range of the  $^{12}\text{CO}_2$  laser and 1004  $\text{cm}^{-1}$ , in the range of the  $^{13}\text{CO}_2$  laser (see fig. 2.6a). The band at 979  $\text{cm}^{-1}$  shows a substructure, with peaks at the 10R12, 10R22 and 10R28  $\text{CO}_2$  laser line frequencies (fig. 2.6a). Since no isotope laser was available with powers high enough to perform a double resonance experiment, our measurements are restricted to the 979  $\text{cm}^{-1}$  peak. From an infrared-microwave double resonance experiment [18] the two main peaks of this substructure at 977.2 (10R22) and 980.9  $\text{cm}^{-1}$  (10R28) are found to be correlated to the excitation of the  $G_\alpha$  and  $G_\beta$  states ( $G_2^\pm$  in  $G_{144}$ ), respectively. An infrared-infrared double resonance experiment, performed by Heijmen *et al* [13] confirms that both peaks are mutually uncorrelated. Although the results of Snels were very important in providing the first complete infrared spectrum of  $(\text{NH}_3)_2$ , the experiment was not state specific. The infrared depletion signals are obtained from bolometric detection of the molecular beam. In this beam no state selection is possible and only partial size-selection is achieved. Consequently the measured infrared depletion spectrum shows the overall result of all populated states of the in the expansion formed  $(\text{NH}_3)_n$  clusters. Using diluted mixtures complex formation is restricted to  $n = 2$  and 3 [44], as can be seen in [11]. From the results of a scattering experiment of ammonia clusters from a rare gas beam in combination with infrared photodissociation techniques by Huisken and Pertsch [12], it can be concluded that

the peak at  $979\text{ cm}^{-1}$  completely originates from dimers and that the peak around  $1004\text{ cm}^{-1}$  is also partly due to trimers. Unfortunately, the dissociation signals for dimers in the scattering experiment are too low to fit the dissociation pattern for the  $979\text{ cm}^{-1}$  peak reliable and it still is not state specific.

For the reasons mentioned above, the analysis of the infrared spectrum turned out to be very hard, especially since the correct tunneling motions were not known at that time. However, from the fact that a cooling of the nozzle resulted in a narrowing of the observed bands, Snels and coworkers concluded that the widths of the dimer bands is determined by internal degrees of freedom that are depopulated in colder beams. This is confirmed in our experiment - the higher K-values are among others positioned at the wings of the bands - but our interpretation of the infrared spectrum is different. Snels *et al* explained the splitting between the  $979$  and  $1004\text{ cm}^{-1}$  peak as a consequence of the excitation of the umbrella modes in each of the two non-equivalent  $\text{NH}_3$  monomers, since they excluded the possibilities of resonant dipole-dipole interactions which was correct, and inversion which was wrong. As was discussed before the  $\nu_2$  umbrella motion is only partly quenched in the  $(\text{NH}_3)_2$  which is reflected in the infrared spectrum by the splitting between the 10R22 and 10R28  $\text{CO}_2$  laser line [16] for the G:K=0 states. This splitting was explained by Snels as the infrared excited interchange motion, but we will show here that the splitting due to interchange motion is much larger and corresponds to the splitting between the  $979$  and  $1004\text{ cm}^{-1}$  band.

In the infrared-far infrared double resonance experiment, the infrared spectrum can be labeled by selecting assigned far infrared transitions. This was demonstrated for the K:0 G and A transitions [16], from which it was concluded that the monomer umbrella inversion is not totally quenched within the ammonia dimer. Another important conclusion was that in contrast to the beam experiments performed by Nelson, Snels, Heijmen, Huisken and their coworkers collisional relaxations take place in the jet expansion which complicates the analysis.

Before presenting the different spectra, we first will discuss the splitting between the main peaks at  $979$  and  $1004\text{ cm}^{-1}$ , followed by a discussion on the substructure of the  $979\text{ cm}^{-1}$  peak.

### 2.15.1 Splitting between $979$ and $1004\text{ cm}^{-1}$

For the A and E-states we have two identical monomers. For this reason the infrared active modes can be described as symmetric and antisymmetric combinations of the individual monomeric motions. The corresponding symmetries of these infrared transitions are  $A_1$  (symmetric) and  $A_4$  (antisymmetric).

Infrared transitions of  $A_1$  symmetry obey the same selection rules as observed in the far infrared region: for A and E-states no pure vibrational-rotational transitions will occur, but all transitions will go from the lower interchange tunneling component to the upper interchange tunneling component (fig. 2.12). For A and E-states infrared transitions of  $A_1$  symmetry are therefore expected to be hidden under the broad peak at  $1004\text{ cm}^{-1}$ , since interchange tunneling is involved. The transitions are expected at  $\nu_0 + \frac{1}{2}(\delta E'' + \delta E')$ , where  $\delta E''$  and  $\delta E'$  correspond to the interchange tunneling in the ground and excited state, respectively. However, infrared transitions of  $A_4$  symmetry are expected at  $\nu_0 + \frac{1}{2}(\delta E'' - \delta E') \approx \nu_0$  and will only be shifted by the difference between the interchange tunneling in ground and excited state which is small. Transitions of A and E-states of the antisymmetric combination are therefore expected around  $979\text{ cm}^{-1}$  and can be attributed to our measured double resonance signals.

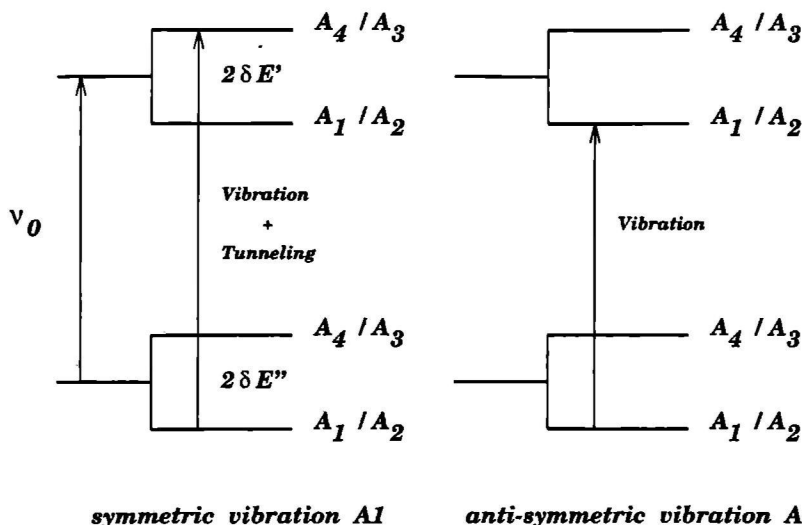


**Figure 2.12:** The splitting between the 979 and 1004  $\text{cm}^{-1}$  band is the result of the infrared excited interchange motion for all symmetries. As a consequence double resonance signals are expected for A, E and G-states in the 979  $\text{cm}^{-1}$  band. The splitting of 25  $\text{cm}^{-1}$  corresponds well to the value found in the ground state.

For the G-states both transitions to upper and lower tunneling states are allowed, for both symmetries. These states are special in being the only states where both pure rotational transitions and rotational interchange tunneling transitions are observable. We therefore expect to see two splittings in the infrared spectra; one small assigned as inversion splitting and one as vibrational interchange tunneling. The latter amounts to 25  $\text{cm}^{-1}$  which agrees well with the splitting found in the ground state. Since this splitting is rather large, we expect the upper level not to be populated in the expansion cooled complexes.

As a consequence we expect to find double resonance signals in the 979  $\text{cm}^{-1}$  peak for states with A, E and G symmetry.

### 2.15.2 Splittings within the 979 $\text{cm}^{-1}$ peak

$|K|=1$ , G ( $G_2^\pm$ ) b.o. 487 GHz and 747 GHz

In figure 2.13 the double resonance spectra are shown for G K:0-0 (fig. 2.13a) - b.o. at 613/614 GHz (see [16]) - for G K:1-1 (fig. 2.13b) - b.o. at 487 GHz - and for G K:1-1 (fig. 2.13c) - b.o. at 747 GHz.

As was discussed in [16] the two peaks at 10R22 and 10R28 in figure 2.13a can be attributed to transitions of the two inversion states in the vibrational excited  $\nu_2$  state. Compared to figure 2.13a additional depletion signals at the 10R12 and 10R32 can be seen in figure 2.13b. We will

first concentrate on the 10R12 signal. This signal is also found for another  $|K|=1-1$  transition

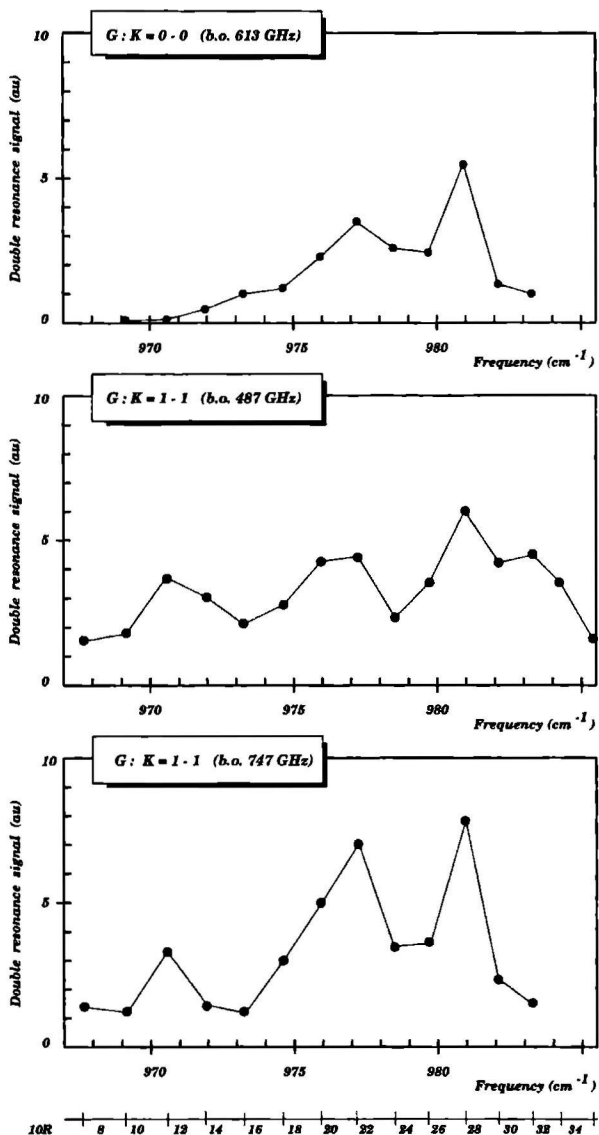


Figure 2.13: The double resonance spectra for the  $G:K=0-0$  (b.o. 613 GHz) (a),  $G:K=1-1$ ,  $G:K=1-1$  (b.o. 487 GHz) (b) and  $G:K=1-1$  (b.o. 747 GHz) (c). The estimated error is about 10 % of the depletion signal. The line under figure c gives the frequencies in CO<sub>2</sub> laser lines.

(fig. 2.13c), whereas it is not visible in the  $K=0-0$  band (fig. 2.13a). We will discuss now several possibilities for the observation of the 10R12 line, some of which can be excluded immediately.

1. One assumption for the presence of the peak at 10R12, which was also mentioned in [31], is that this signal is due to a  $b$ -type  $K:1 \rightarrow 0$  transition. But given the energy distance as found by Loeser *et al* [17] these peaks should be expected at

$$\begin{array}{ll} 10R28 - 3.8 \text{ cm}^{-1}, & 10R22 - 3.8 \text{ cm}^{-1} \text{ (levels 3,4 - 1)} \quad \text{for } K:1-1 \text{ (b.o. at 486 GHz)} \\ 10R22 - 7.7 \text{ cm}^{-1}, & 10R28 - 7.7 \text{ cm}^{-1} \text{ (levels 5,6 - 1)} \quad \text{for } K:1-1 \text{ (b.o. at 747 GHz)} \end{array}$$

But definitely no peak is observed at  $10R22 - 3.8 \text{ cm}^{-1} = 973.4 \text{ cm}^{-1}$  and no peak at  $10R28 - 7.7 \text{ cm}^{-1} = 973.1 \text{ cm}^{-1}$ . On the contrary a minimum in depletion signal was observed in both cases. We therefore exclude the possibility that  $b$ -type transitions are involved.

2. The second assumption is that all depletion signals can be explained by transitions between different  $K$ -levels - due to the fact that for  $K=1$  there are twice as many levels in upper and lower states as for  $K=0$  - explicitly excluding collisional relaxations. If we observe not only pure vibrational transitions around  $979 \text{ cm}^{-1}$  but also transitions from one  $K$ -type component to the other we will expect more lines. Assigning the transitions found in [17] for the  $G(G_2^\pm)$   $K=1$  ground state, we call the two states at 114 GHz (levels 3,4) one  $K$ -type component and the other at 232 GHz (levels 5,6) the second component. The energy difference between these states is  $3.9 \text{ cm}^{-1}$ . We therefore expect, when probing the 747 GHz band (levels 5,6 - 13,14) to observe all peaks that are also observed probing the 486 GHz transition (levels 3,4 - 9,10) minus the difference  $(232 - 114) \text{ GHz} = 118 \text{ GHz} \approx 3.9 \text{ cm}^{-1}$ . Therefore in figure 2.13c a peak at  $10R22 - 3.9 \text{ cm}^{-1} = 978.2 \text{ cm}^{-1}$  is expected which is obviously not the case. The presence of more than two peaks cannot be explained by transitions within  $K=1$ , exclusively.
3. We therefore assume that at least the occurrence of some of the peaks results from collisional relaxation within  $K=1$ . Collisional relaxation to  $K=0$  seems not likely, otherwise the peak at 10R12 should also be visible in figure 2.13a which is not the case. For each of the two  $G:K=1$  ground states, two inversion components are expected that do not have to coincide in frequency. Assuming a collisional relaxation only within  $K=1$  four peaks instead of two are expected when probing the ground state. Inspecting figure 2.13b we can distinguish three peaks with the 10R22 appearing broader than the other two. We therefore propose four peaks at the following frequencies: 10R12, between 10R18 and 10R20, 10R22 and 10R28. Furthermore we propose that the infrared transition from the ground state of the 747 GHz band splits into two inversion components observed at 10R22 and 10R28 and that the infrared transition sharing the same ground state as the 486 GHz far infrared transition splits into two inversion components observed at 10R12 and 10R18 as is shown in figure 2.14. By collisional relaxation depletion of one state gives rise to double resonance signal also in the spectrum of the other state, as was explained in detail in [16].

In order to explain the peak at 10R32 which is present in figure 2.13b but not in figure 2.13a we have to introduce in addition non-collisional transitions between different  $K$ -type components of  $K=1 G_2^\pm$  as was discussed in assumption (2). For the infrared-far infrared double resonance transitions for the 486 GHz band (levels 3,4 - 9,10) we expect to see two additional peaks at 10R22

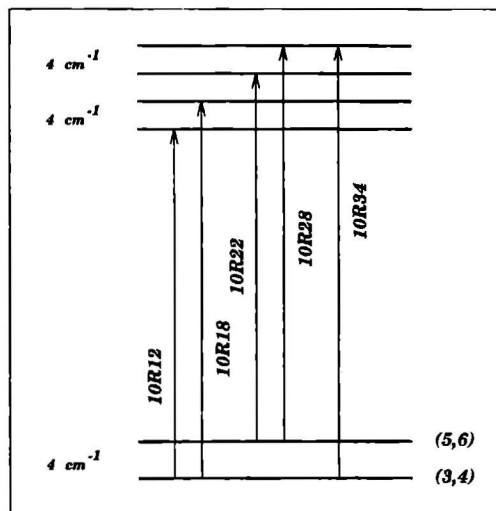


**Figure 2.14:** Energy level scheme for the infrared excitation of the 747 GHz (5,6) and 486 GHz (3,4) band. The lines 10R12-10R18/20 and 10R22-10R28 reflect the inversion components for both bands.

+ 3.9 cm<sup>-1</sup> ≈ 10R28 and 10R28 + 3.9 cm<sup>-1</sup> ≈ 10R34. The overlap of the stronger 10R28 and 10R34 gives the maximum at 10R32.

For the 747 GHz band (fig. 2.13c) we should see two more peaks, one at 10R12 - 3.9 cm<sup>-1</sup> (in the region where we did not scan) and one at 10R18 - 3.9 cm<sup>-1</sup> = 10R12, which will enhance the peak at 10R12, caused by population transfer. This is indeed the case. We can draw now a complete energy diagram for the vibrationally excited G ( $G_{\frac{1}{2}}^{\pm}$ ) states (fig. 2.15). Whereas the inversion splitting for the K=1 ground state is smaller than for K=0 (3.36 GHz) for the excited state the inversion splitting is 4 cm<sup>-1</sup> for each state and equal to the splitting found for K=0. The two  $G_{\frac{1}{2}}^{\pm}$  levels in the vibrationally excited state lie about 200 GHz apart. The features of the infrared-far infrared double resonance spectra, therefore can be explained by relaxation transitions between K-levels.

#### $|K|=1$ , $E_{1,2}$ ( $G_3^-/G_4^+$ ), b.o. 454 GHz

The infrared-far infrared double resonance spectra of the  $E_{1,2}$  at 454 GHz which are shown in figure 2.16. It turned out to be much more difficult to obtain reproducible depletion signals for this state, since the original far infrared transition was already a factor of two weaker than the G:K=1 transitions. We therefore show a typical result: two peaks at 10R30 and 10R18. Especially the peak at 10R18 seems to be broadened.

Based on assumption (1) we exclude the possibility of *b*-type transitions for radiation and collisional relaxation. Similar as in assumption (2) we can take the energy levels given by Loeser *et al* [17] and assign them to different K-type components 12 cm<sup>-1</sup> apart (5,6 - 11,12). Probing the far



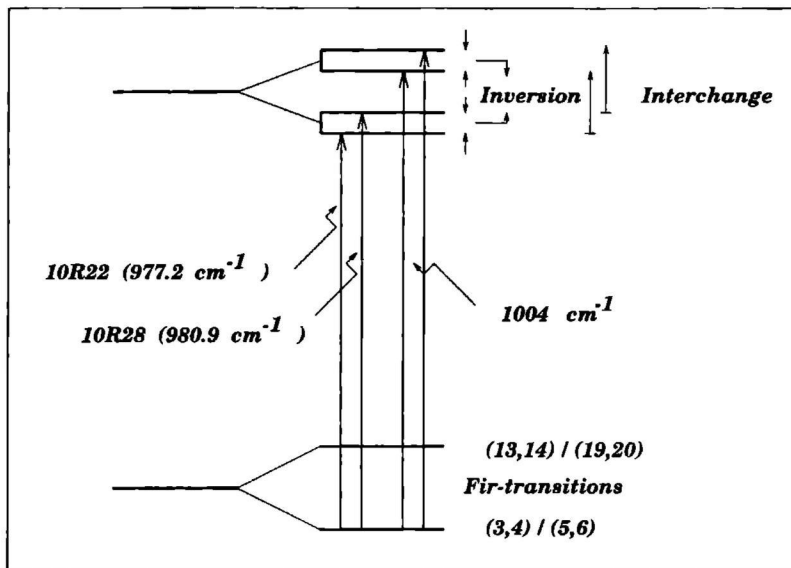


Figure 2.15: Energy level diagram for the vibrational excited  $G(G^\pm)$  states.

infrared transition at 454 GHz which starts from the lower component one should get additional peaks at the infrared frequencies of the second ground state +  $12 \text{ cm}^{-1}$ . We expect this to be outside the region which was scanned. Therefore the occurrence of two peaks at 10R30 and 10R18 must be attributed to the transition of the two inversion components. The inversion splitting in the excited vibrational state therefore would amount to about  $7 \text{ cm}^{-1}$ , whereas in the ground state the inversion splitting was found to be smaller than 2 MHz.

### $K=0$ , A ( $B_2^+/A_2^-$ ), b.o. 483 GHz

In figure 2.17 the infrared-far infrared double resonance signal for the A  $K=0-0$  transition with b.o. at 483 GHz is shown. This has the same features as the  $K=0-1$  transition with b.o. at 734 GHz [16], as is expected for transitions sharing the same starting level. The absence of other peaks is explained in [16].

## 2.16 Discussion and conclusions

Using an infrared-far infrared double resonance technique in a jet expansion it is possible to give a state resolved explanation of the infrared spectrum as measured by Snels *et al* [11]. The splitting between the two peaks at 979 and  $1004 \text{ cm}^{-1}$  reflects the infrared excited interchange, both for states with A, E and G symmetry. Part of the  $1004 \text{ cm}^{-1}$  peak, as measured by Snels, is due to dissociation of clusters larger than dimers.

The peak around  $979 \text{ cm}^{-1}$  clearly shows a substructure in the overall infrared spectrum which can be analyzed as arising from states with different K values and different symmetry. The splitting

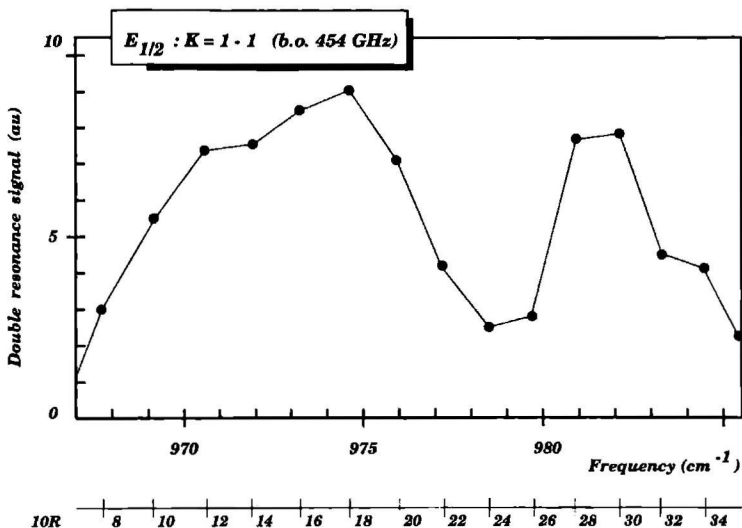


Figure 2.16: The double resonance spectrum for the  $E_{1/2}:K=1-1$  (b.o. 454 GHz). The error is estimated to be smaller than 20 % of the depletion signal.

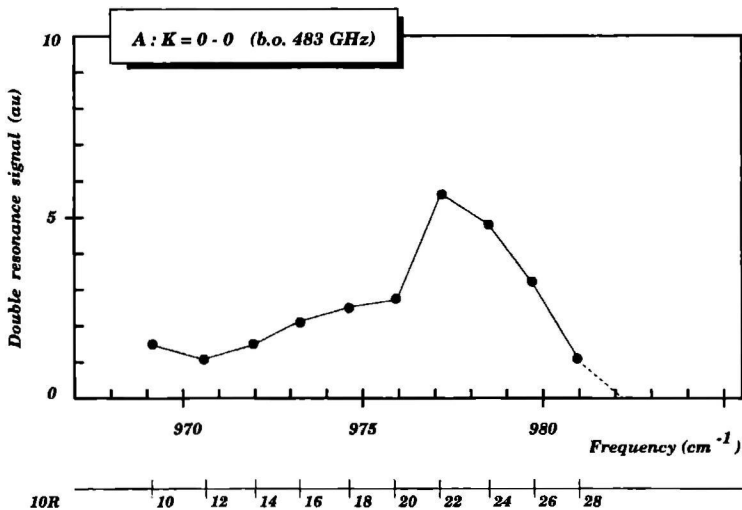


Figure 2.17: The double resonance spectrum for the  $A:K=0-0$  (b.o. 483 GHz). The error is smaller than 10 % of the depletion signal.

between the 10R22 and 10R28 reflects the inversion splitting ( $\approx 3.7 \text{ cm}^{-1}$ ) in states with  $K=0$  G-symmetry, which is about 10% of the splitting in free  $\text{NH}_3$ . Due to collisional relaxations the infrared-far infrared double resonance spectrum shows an overall result, as is explained in [16]. These relaxations only take place for levels involving same K values. Using the results of the infrared-microwave double resonance experiment by Fraser *et al* [18] on the  $K=0$  G ( $G_2^\pm$ ) states, it is clear that the peak at 10R22 is arising from the  $G_2^-$  and the peak at 10R28 from the  $G_2^+$  state. For  $|K|=1$  states of G symmetry two additional inversion components are expected which are situated at the 10R12, between 10R18 and 10R20, 10R22 and 10R28  $\text{CO}_2$  laser line frequencies. Due to collisional relaxations, again, the infrared-far infrared double resonance spectra show the overview of the involved states. The peak found at 10R32 is due to K-type degeneracy. The double resonance spectra of the  $|K|=1$  G-symmetries can be explained by collisional relaxation and transitions between the different G: $|K|=1$  states. If we take the same assumption for the E-states, we have to conclude that the inversion splitting amounts to  $7 \text{ cm}^{-1}$ . This splitting is at first sight surprising, since in the ground state the splitting for the E-states was found to be smaller than for the G-states. The splitting is not clearly reflected in the overall spectrum of Snels (probably because the transitions are too weak to influence the overall spectrum substantially), although there seems to be some structure at 10R18 in case of a heated nozzle and a less diluted mixture [11] which also indicates that this peak arises from a higher K state. The inversion splitting for the  $E_{1,2}$  state therefore provides a sensitive test for ab initio calculations, predicting inversion tunneling splittings.

In the infrared spectrum measured by Snels also a structure around  $988 \text{ cm}^{-1}$ , in between both main bands, can be seen. This could correspond to one of the K-type components of the  $E_{1,2}$  band which is situated about  $12 \text{ cm}^{-1}$  from the other component. Furthermore the infrared spectrum shows a small additional peak at  $961.5 \text{ cm}^{-1}$ , in case of a "warm" beam. This indicates that the peak is arising from a  $K \geq 1$  level or from the upper component of the interchange levels. Since the energy difference is of the order of  $20 \text{ cm}^{-1}$  this could be a plausible explanation.

From the assignment, discussed above, it should be clear that the second band, situated at  $1004 \text{ cm}^{-1}$ , should also show some substructure. In the overall spectrum this can be hardly seen since we were not able to scan in this region, perhaps we may speculate that there is some structure visible in the infrared-infrared double resonance spectra of Heijmen *et al* [13]. This structure should reflect the inversion splittings for  $K=0$  and  $|K|=1$  in the symmetric excited vibration. However, only an infrared-far infrared experiment with a  $^{13}\text{CO}_2$  laser with powers high enough, would give a better insight into this problem.

## Acknowledgment

This work was supported by the European Community under grant (EC 892 001 59/OP1).

## References

- [1] D.D. Nelson Jr., G.T. Fraser and W. Klemperer, *J. Chem. Phys.* 83 (1985) 6201.
- [2] D.D. Nelson Jr., W. Klemperer, G.T. Fraser, F.J. Lovas, and R.D. Suenram, *J. Chem. Phys.* 87 (1987) 6364.
- [3] D.D. Nelson Jr. and W. Klemperer, *J. Chem. Phys.* 87 (1987) 139.
- [4] Z. Latajka and S. Schreiner, *J. Chem. Phys.* 84 (1986) 341.
- [5] S. Liu, C.E. Dykstra, K. Kolenbrander, J.M. Lisy, *J. Chem. Phys.* 85 (1986) 2077.
- [6] M.J. Frisch, J.E. Del Bene, J.S. Binkley, H.F. Schaefer, *J. Chem. Phys.* 84 (1986) 2279.
- [7] D.D. Nelson Jr., G.T. Fraser and W. Klemperer, *Science* 238 (1988) 1670.
- [8] R.J. Saykally and G.A. Blake, *Science* 259 (1993) 1570.
- [9] K.P. Sagarik, R. Ahlrichs, S. Brode, *Mol. Phys.* 57 (1986) 1247.
- [10] J.W.I. van Bladel, A. van der Avoird and P.E.S. Wormer, R.J. Saykally, *J. Chem. Phys.* 97 (1992) 4750.
- [11] M. Snels, R. Fantoni, R. Sanders and W.L. Meerts, *Chem. Phys.* 115 (1987) 79.
- [12] F. Huisken and T. Pertsch, *Chem. Phys.* 126 (1988) 213.
- [13] B. Heijmen, A. Bizzari, S. Stolte and J. Reuss, *Chem. Phys.* 126 (1988) 201.
- [14] M. Havenith, R.C. Cohen, K.L. Busarow, D.H. Gwo, Y.T. Lee and R.J. Saykally, *J. Chem. Phys.* 94 (1991) 4776.
- [15] E. Zwart, Submillimeter spectroscopy of molecular complexes and ions, Ph.D. Thesis Nijmegen (1991) - see also [16].
- [16] M. Havenith, H. Linnartz, E. Zwart, A. Kips, J.J. ter Meulen and W.L. Meerts, *Chem. Phys. Lett.* 193 (1992) 261.
- [17] J. Loeser, C.A. Schmuttenmaer, R.C. Cohen, M.J. Elrod, D.W. Steyert, R.J. Saykally, R.E. Bumgarner and G.A. Blake, *J. Chem. Phys.* 97 (1992) 4727.
- [18] G.T. Fraser, D.D. Nelson Jr., A. Charo and W. Klemperer, *J. Chem. Phys.* 82 (1985) 2535.
- [19] E. Zwart, H. Linnartz, W.L. Meerts, G.T. Fraser, D.D. Nelson, Jr., W. Klemperer, *J. Chem. Phys.* 95 (1990) 793.
- [20] J.W.I. van Bladel, A. van der Avoird, P.E.S. Wormer, *J. Chem. Phys.* 94 (1991) 501; *J. Phys. Chem.* 95 (1991) 5414; *J. Chem. Phys.* 97 (1992) 4750.
- [21] H. Linnartz, A. Kips, W.L. Meerts, M. Havenith, *J. Chem. Phys.* 99 (1993) 2449.
- [22] E.H.T. Olthof, A. van der Avoird and P.E.S. Wormer, *J. Mol. Struct. (Theochem)* 307 (1994) 201.
- [23] A. van der Avoird, E.H.T. Olthof, P.E.S. Wormer, 97<sup>th</sup> Faraday Discussion, "Structure and Dynamics of Van der Waals Complexes", April 1994.

- [24] M. Havenith, H. Linnartz, W.L. Meerts, E.H.T. Olthof, A. van der Avoird, P.E.S. Wormer, N. Heineken and W. Stahl, *Science*, in preparation.
- [25] R.M. Baum, *C&EN*, 19 (octobre 1992), p. 20.
- [26] D.M. Hassett, C.J. Marsden, B.J. Smith, *Chem. Phys. Lett.* 183 (1991) 449.
- [27] F.M. Tao, W. Klemperer, *J. Chem. Phys.* 99 (1993) 5976.
- [28] P.R. Bunker, *Molecular Symmetry and Spectroscopy*, Academic New York (1979).
- [29] A. van der Avoird, P.E.S. Wormer, R. Moszynski, *Chem. Rev.*, submitted.
- [30] H. Linnartz, W.L. Meerts, M. Havenith, *Chem. Phys.*, submitted.
- [31] M. Snels, *Infrared excitation of molecules and clusters*, Ph.D. Thesis, University of Nijmegen (1986).
- [32] Z. Bacic, U. Buck, H. Meyer, R. Schinke, *Chem. Phys. Lett.* 125 (1986) 47.
- [33] P. Verhoeve, E. Zwart, M. Versluis, M. Drabbels, J.J. ter Meulen, W.L. Meerts, A. Dymanus, D.B. McClay, *Rev. Sci. Instr.* 61 (1990) 1612.
- [34] The other bands are discussed later in this thesis.
- [35] J. Schleipen, J.J. ter Meulen, *Chem. Phys.* 156 (1991) 479.
- [36] J.A. Odutola, T.R. Dyke, B.J. Howard, J.S. Muentner, *J. Chem. Phys.* 70 (1979) 4884.
- [37] T.R. Dyke, in: *Structure and dynamics of weakly bound molecular complexes*, ed. A. Weber (1987).
- [38] J.W.I. van Bladel, A. van der Avoird, P.E.S. Wormer, *J. Phys. Chem.* 95 (1991) 5414.
- [39] Z. Latajka and S. Scheiner, *J. Chem. Phys.* 81 (1984) 407.
- [40] D.A. Dahl, J.E. Delmore, Idaho National Engineering Laboratory, EG & G Idaho Inc., Idaho Falls.
- [41] H. Linnartz, M. Havenith, W.L. Meerts, in preparation.
- [42] E.H.T. Olthof, A. van der Avoird, P.E.S. Wormer, *J. Chem. Phys.*, submitted.
- [43] M.J. Howard, S. Burdinski, D.F. Giese, W.R. Gentry, *J. Chem. Phys.* 80 (1986) 47.
- [44] U. Buck, X. Gu, C. Lauenstein, H. Linnartz, A. Rudolph, *J. Chem. Phys.* 94 (1991) 23.

## Infrared Photodissociation of Small Size-selected Neutral Clusters

2

### Abstract

Clusters are unique in providing an intermediate between gas phase molecules on one side and bulk condensed matter on the other side. For this reason clusters are interesting. From a fundamental point of view it is hoped that a detailed study will improve the understanding of the transition from one to the other and from an applied point of view it allows the microscopic investigation of macroscopic properties, such as solvation and adsorption with technological applications to e.g. catalysis and photography. To study these features it is necessary to be size-selective; the ideal experiment would be one in which properties can be studied as function of the cluster size. Such extended size-selective experimental information, however, is difficult to obtain. In particular the application of molecular beams that normally are used to generate free clusters, leads to a distribution over several cluster sizes.

This chapter starts with the description of the method that is applied here to generate size-selected clusters and that is based upon momentum transfer in a scattering experiment. The subsequent infrared photodissociation yields structural information. This is demonstrated in the second and third part of this chapter for  $(\text{CH}_3\text{NH}_2)_n$  and  $(\text{OCS})_n$  clusters with  $n=2-6$ .

---

<sup>2</sup>This chapter is based on the articles:

- \* Infrared photodissociation of size-selected methylamine clusters; U. Buck, X.J. Gu, R. Krohne, Ch. Lauenstein, H. Linnartz, A. Rudolph, J. Chem. Phys. 94 (1991) 23.
- \* Infrared photodissociation of size-selected molecular clusters and their structures; U. Buck, X.J. Gu, M. Hobein, R. Krohne, Ch. Lauenstein, H. Linnartz, A. Rudolph, Z. Phys. D. 20 (1991) 177.
- \* Fragmentation by electron impact ionization and intracuster reactions of size-selected  $(\text{N}_2\text{H}_4)_n$  and  $(\text{OCS})_n$  clusters; U. Buck, M. Hobein, R. Krohne, H. Linnartz, Z. Phys. D. 20 (1991) 181.
- \* Infrarood fotodissociatie van op grootte geselecteerde neutrale clusters; R. Krohne and H. Linnartz, NtvN, 4 (1992) 53.

### 3.1 Introduction

Information on structure and intracluster dynamics forms, among others, a main object in cluster research, since it provides the key to the general understanding of the spectroscopic features of clustered molecules. The most common way to generate small neutral clusters - which will be the topic of this chapter - is supersonic expansion of a cluster gas in a seeding gas into high vacuum. This leads to a distribution over different cluster sizes. In case of seeded beams with very small fractions of the cluster gas, the cluster formation normally is restricted to dimers and trimers. But in less diluted mixtures that are necessary to study higher clusters, a good distinction between different cluster sizes is difficult due to the large variety in cluster size. For this reason there is a need for size-specific detection techniques.

The easiest way in which this can be achieved, is by ionizing the cluster and detecting the cluster ions in a mass spectrometer. However, in case of neutral clusters this mass filtering does not help very much, since during ionization fragmentation occurs and consequently the signal at one mass will also contain contributions from higher clusters that fragment to this mass. The measured cluster ion distributions obtained in the mass spectrometer, therefore, only reflect the distribution of the formed ions which cannot be simply related to the original neutral cluster size distribution [1]. Since different cluster sizes exhibit different spectral features another way to gain size-selective information is the use of pure spectroscopic techniques [2, 3]. But since extension to larger cluster sizes normally leads to spectral congestion, these techniques are restricted to small clusters, typically dimers and trimers.

The problems can be overcome, if experimental methods are used that label the different cluster sizes independent from an ionization process. In the next paragraph such a technique is discussed briefly; the preparation of a size-selected neutral cluster beam in a scattering experiment. It is only meant as an introduction to understand the results of the photodissociation experiments on the  $(\text{CH}_3\text{NH}_2)_n$  and  $(\text{OCS})_n$  clusters. More detailed information can be found in [4, 5, 6, 7, 8, 9, 10, 11].

The experiments described here were performed at the Max Planck Institute für Strömungsforschung in Göttingen in the group of Prof. Dr. U. Buck.

### 3.2 Experimental method

#### 3.2.1 Size-selection

The method of cluster separation in a scattering experiment of a primary cluster beam with a secondary (rare gas) beam under single-collision conditions, is based on the kinematical principle that lighter clusters are scattered into larger angles with larger final velocities than is the case for heavier clusters. This is shown schematically in figure 3.1 in a Newton diagram for  $(\text{CH}_3\text{NH}_2)_n$  clusters that are scattered from a He beam, assuming that the cluster beam (velocity  $\mathbf{v}_n$ , mass  $M_n$ ), is intersected by the rare gas beam ( $\mathbf{v}_{rg}, m_{rg}$ ) at an angle of  $90^\circ$ .

The relative velocity  $\mathbf{q}$  is given by the difference vector  $\mathbf{v}_n - \mathbf{v}_{rg}$ . From this the center-of-mass motion can be calculated by dividing the relative velocity by the mass ratio of the cluster and rare gas particle

$$\mathbf{u}_n = \frac{m_{rg}}{m_n + m_{rg}} \mathbf{q}, \quad (3.1)$$

where  $\mathbf{u}_n$  stands for the initial velocity of the cluster with size  $n$  in the center-of-mass. Consequently, in case of elastic scattering, all final center-of-mass velocities  $\mathbf{u}'_n$  are restricted to end on a sphere around the center of mass with radius  $u_n$ . For increasing cluster size the value for the final center-of-mass velocity drops and so do the radii of the circles in the Newton diagram. For a given lab-angle the amount in which different cluster sizes contribute to the beam signal depends on the intersection of the lab-angle with the spheres of possible final center-of-mass velocities. This is demonstrated in the figure for a lab-angle of  $6^\circ$ . For this angle only contributions from  $n=1-3$  are expected; larger clusters are excluded kinematically.

When this scattering technique is used, two methods can be applied to make a distinction between different cluster sizes. For a fixed lab-angle the clusters are discriminated either using the difference in final velocity, which is selected using pseudo-random choppers, or the difference in mass which is selected by mass spectroscopy. The latter method was used for the  $(\text{CH}_3\text{NH}_2)_n$  and  $(\text{OCS})_n$  measurements, described here. Using this technique larger clusters can be excluded by kinematical constraints, while the mass spectrometer discriminates against smaller masses. This procedure only works if, at least, a small fraction of the cluster  $x_n$  can be detected at the corresponding mass of the ion  $x_n^+$  or at a fragment mass which is larger than the next smaller cluster size  $x_{n-1}^+$ . The latter typically occurs for hydrogen bonded systems that can be detected at the protonated mass  $x_{n-1}\text{H}^+$ . For the investigated  $(\text{CH}_3\text{NH}_2)_n$  clusters it will be shown that this is indeed the case, since it is not very hard to study the fragmentation probability  $f_{nk}$  upon ionization for a cluster of size  $n$  to an ion of mass  $k$ , once a cluster of size  $n$  is selected.

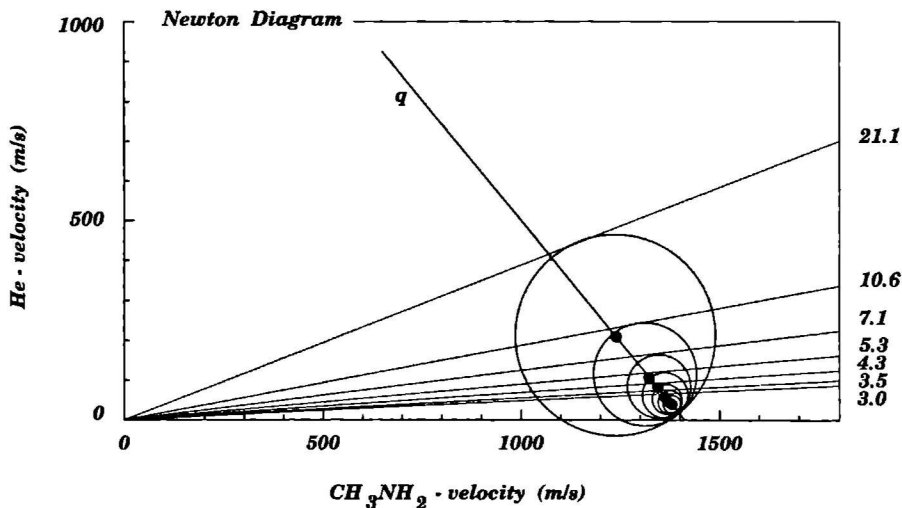
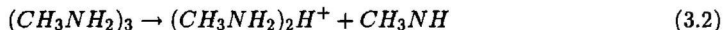


Figure 3.1: The Newton diagram for the scattering of cluster  $n$  (here  $(\text{CH}_3\text{NH}_2)_n$  seeded in He) by a rare gas beam (here He). The positions of the elastically scattered clusters are drawn for  $n=1-7$  together with the limiting angles.  $q$  is the relative velocity. The  $\bullet$  indicates the center of mass for cluster  $n$ .



If we want to select for example  $(\text{CH}_3\text{NH}_2)_3$ , it is possible with the known masses and velocities of the collision partners to calculate the limiting elastic scattering angles. For the  $(\text{CH}_3\text{NH}_2)_n/\text{He} - \text{He}$  experiment this results in the series  $21.1^\circ$  ( $n=1$ ),  $10.6^\circ$  ( $n\leq 2$ ),  $7.1^\circ$  ( $n\leq 3$ ),  $5.3^\circ$  ( $n\leq 4$ ),  $4.3^\circ$  ( $n\leq 5$ ),  $3.5^\circ$  ( $n\leq 6$ ) and  $3.0^\circ$  ( $n\leq 7$ ) which corresponds to a (nearly uniform) cluster velocity of 1404 m/s and rare gas (He) velocity of 1775 m/s. By positioning the detector on a lab-angle of  $6.0^\circ$ , clusters with  $n\geq 4$  are excluded kinematically, because the limiting angle of tetramers is  $5.3^\circ$ . Discrimination against smaller clusters is achieved by tuning the mass filter to a mass larger than the nominal dimer mass. Here the trimer spectrum can be recorded at  $m = 63$  amu, while the dimer mass is 62 amu. This is possible, as will be shown, since the  $(\text{CH}_3\text{NH}_2)_3$  possesses a fragmentation channel to the protonated dimer mass according to



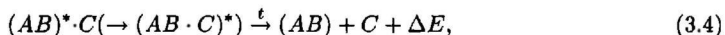
Furthermore it is possible to draw conclusions concerning size dependent fragmentation channels.

### 3.2.2 Infrared photodissociation

In the infrared photodissociation experiments the size-selected clusters are vibrationally excited. If the photon energy is larger than the binding energy of the cluster, energy redistribution normally will induce the predissociation of the complex, i.e. the rupture of the van der Waals bond. Starting from a weakly bound cluster  $(\text{AB})\cdot\text{C}$ , consisting of a molecule (AB) and an atom or molecule C, excitation of the (AB) component results in an excited complex



which by coupling of the molecular vibration directly to the intermolecular motion or indirectly via the intramolecular vibration results in an energy transfer into the complex bond. In case that the amount of transferred energy is larger than the binding energy, dissociation of the complex is induced after a time  $t$



where both dissociation fragments can be excited and where  $\Delta E$  gives the remaining translational energy. A more elaborate treatment of dissociation processes is presented in [10] and [13].

The dissociation is measured by monitoring the depletion of the (size-selected) cluster beam as a function of the laser frequency. This method is, in fact, related to what was described in chapter 2, with the difference that the infrared radiation is used here to obtain information on the same motion for different cluster sizes, whereas in the former chapter it served to yield information on different states for the same cluster size.

From the dissociation pattern three important features can be derived. The lineshift,  $\Delta\nu$ , with respect to the maximum absorption frequency of the monomer. This is determined by the interaction of the excited molecule with the surrounding molecules and as such it provides direct structural information: The full-width-at-half-maximum,  $\Gamma$ . If the lines are homogeneously broadened  $\Gamma$  gives information on the lifetime and thus on the coupling of the originally excited vibrational mode to the internal modes of the complex. And finally, the dissociation cross section,  $\sigma$ , which is related to the absorption strength of the cluster.

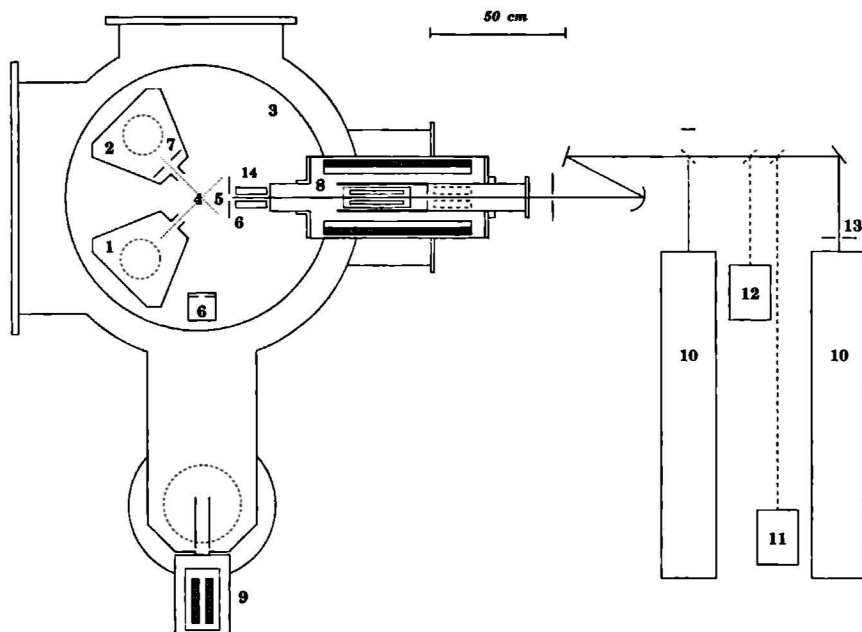


**Figure 3.2:** The scattering machine (P9) at the MPI für Strömungsforschung in Göttingen. The numbers indicate: 1) primary (cluster) beam 2) secondary (rare gas) beam 3) scattering chamber 4) scattering center 5) entrance detector unit 6) time-of-flight choppers 7) lock-in chopper 8) mass spectrometer 9) second detector unit 10) CO<sub>2</sub> lasers 11) spectrum analyser 12) power meter 13) lock-in chopper 14) thermistor. The second CO<sub>2</sub> laser can be used for IR-IR double resonance experiments in order to discriminate against isomeric structures.

### 3.2.3 Experimental setup

In figure 3.2 the complete experimental setup is drawn. The cluster and rare gas beams are generated in two differentially pumped vacuum chambers ( $10^{-4}$  torr during beam operation), intersecting each other at an angle of  $90^\circ$ . This system can be rotated in its entirety around the axis of a cylindrical scattering chamber ( $10^{-7}$  torr) in which both beam chambers are mounted. This axis defines the position of the scattering center. The clusters are formed in the expansion of a gas mixture through a 30 to 100  $\mu\text{m}$  nozzle under high pressure (typically 1 to 20 bar). Both beams are subsequently skimmed and expanded into the scattering chamber. The distance from both nozzles to scattering center amounts to 90.7 mm. The velocities of both beams are measured using a pseudo-random time-of-flight analysis [14].

Both direct and scattered beam are monitored by a fixed detection system consisting of an electron

bombardment ionizer, a quadrupole mass filter and an off-axis particle multiplier. These are mounted in the detector unit that is maintained at ultra high vacuum ( $10^{-9}$  torr). For mass filtering the (size-selected) clusters are first ionized by 70 eV electron impact, subsequently focussed by means of electrical lenses on the entry of the quadrupole mass filter and finally detected by a particle multiplier. The output signal is monitored by a PDP11/23 computer, which also registrates the sequence of primary and/or secondary beam by lock-in detection. In this way angular distributions can be measured rather easily [9].

For the photodissociation experiments [10] the scattered beam interacts collinearly with the radiation of a cw line tunable  $\text{CO}_2$  laser, that typically is operated at powers of about 10 W. Due to dissociation less clusters will reach the detector and consequently the dissociation spectra can be monitored by measuring the depletion in beam signal as function of the laser frequency [10]. The main problem in this setup is the alignment of the  $\text{CO}_2$  laser in order to get maximum overlap with the cluster beam. To overcome this problem a thermistor is mounted in the scattering chamber in such a way that it can be put along the ideal laser beam axis. Besides for optimizing the alignment, the thermistor also yields information that is necessary to correct for  $\text{CO}_2$  laser power variations. The dissociation signal is computer monitored by using a double modulation scheme in which both laser and secondary beam are chopper modulated, the secondary beam twice as fast as the laser beam. This results in four different signals; background signal with and without scattering signal, with and without laser dissociation signal. From this a nearly background free dissociation pattern can be obtained by computer analysis [10].

---

# Infrared Photodissociation of Size-selected Methylamine Clusters

U. Buck <sup>a</sup>, X.J. Gu <sup>b</sup>, R. Krohne <sup>a</sup>, Ch. Lauenstein <sup>a</sup>, H. Linnartz <sup>c</sup>, A. Rudolph <sup>a</sup>.

<sup>a</sup> Max Planck Institut für Strömungsforschung, Bunsenstraße 10, D 3400, Göttingen

<sup>b</sup> Department of Chemistry, University of Toronto, Can M55 1A1, Toronto

<sup>c</sup> Department of Molecular and Laser Physics, University of Nijmegen,  
Toernooiveld, NL 6525 ED, Nijmegen

## Abstract

Infrared photodissociation spectra of  $(\text{CH}_3\text{NH}_2)_n$  clusters are presented for  $n=2$  to  $n=6$  near the absorption frequency of the C-N stretching mode of the monomer at  $1044\text{ cm}^{-1}$ , using a line tunable cw  $\text{CO}_2$  laser. The clusters are size-selected by scattering the clusters from a He beam. The dimer spectrum shows a double peak structure with a red ( $1038\text{ cm}^{-1}$ ) and a blue ( $1048\text{ cm}^{-1}$ ) shifted component which is attributed to the non-equivalent position of the C-N in the open dimer structure. The larger clusters show only one peak between  $1045.4$  and  $1046.0\text{ cm}^{-1}$ , which is caused by the equivalent position of the C-N in the cyclic structures of the larger clusters. Calculations of the minimum energy configurations confirm these results.

### 3.3 Introduction

There are not many methods to get direct information on the structure of molecular clusters. Most of them rely on spectroscopic results either from high resolution vibration-rotation spectroscopy in the microwave, far infrared [3] and infrared region [2] or from electronically excited states [15]. It takes special care to make sure that the correct cluster size is investigated. This is either provided by the spectrum itself or, for certain classes of molecules, by special detection methods, like the two-color two-photon ionization near threshold [7] in order to avoid fragmentation which is present otherwise. A different, more conventional method is the combination of the infrared photodissociation of weakly bound clusters [16] with the size-selective process in a scattering experiment [5, 6]. The clusters that are generated in an adiabatic expansion are first size-selected by scattering them from a rare gas beam and subsequently photodissociated. For that purpose a vibrational mode of one molecular component is excited by infrared radiation. If this energy is larger than the binding energy of the cluster, energy redistribution usually causes the complex to dissociate. The dissociation spectra are measured by the depletion of the beam signal, as a function of the laser frequency. From the measured line shift and linewidth of the excited molecular vibration, detailed structural and dynamical information is obtained [17, 18]. This method has been applied to clusters up to  $n=8$  for the van der Waals systems  $C_2H_4$  [19, 20, 21] and  $SF_6$  [22] and for the stronger bound molecules  $NH_3$  [23] and  $N_2H_4$  [12]. Very recently the typical hydrogen bonded methanol clusters have been investigated [24, 25, 26], where the photodissociation results agree well with an open dimer with a linear hydrogen bond, a cyclic structure for the trimer, tetramer, and pentamer, and from the hexamer onwards with a heavily distorted structure which manifests itself in a spectrum with two splitted lines.

Methylamine has some similarities with methanol with a hydroxyl group being replaced by an amino group. The clusters can also be scattered into a reasonable large angle region for size-selection because of its "light" mass. The C-N stretch band of  $CH_3NH_2$  at  $1044\text{ cm}^{-1}$  is close to the CO stretch band of  $CH_3OH$  at  $1033.5\text{ cm}^{-1}$  and both of them fall within the 9P branch of the  $CO_2$  laser spectrum. The structures of isolated methylamine clusters have been calculated by Brink and Glasser [27] using empirical potentials. They predicted that the most stable form of the dimer has an open structure and that the structure of the trimer and the tetramer has a cyclic structure in agreement with molecular-beam electric deflection experiments [28]. Since there is no infrared information available for methylamine clusters, it is worthwhile to investigate the photodissociation of the size-selected  $CH_3NH_2$ -clusters in order to obtain some structural and energetic information.

In this chapter we report such measurements with size-selected methylamine clusters. The spectral features vary from dimer to hexamer and are attributed to different cluster configurations. Very small spectral shifts were obtained for the trimer and higher clusters, a result which is different from that found for methanol [26].

### 3.4 Experiment

#### 3.4.1 Molecular beam apparatus

The experimental apparatus consists of two crossed molecular beams that as a whole can be rotated with respect to the scattering center and a fixed quadrupole mass spectrometer detector. In this detector the scattered particles are first ionized by electron impact, then mass selected in the

10 % $\text{CH}_3\text{NH}_2$ in He	0.1 % $\text{CH}_3\text{NH}_2$ in Ne	He	
Nozzle diameter ( $\mu\text{m}$ )	80	60	30
Nozzle temperature (K)	300	300	300
Nozzle pressure (bars)	1.4	1.0	20
Peak velocity (m/s)	1404	819.2	1775
Angular divergence (deg)	1.8	1.7	3.2
Collisional energy (meV)	94	...	

**Table 3.1:** Beam data for the mixtures used in the scattering experiment - primary (10 %  $\text{CH}_3\text{NH}_2$  in He) and secondary beam (He) - and direct beam (0.1 %  $\text{CH}_3\text{NH}_2$  in Ne) experiment.

quadrupole mass filter and finally counted by an electron multiplier. The velocity of the direct and scattered beam is measured by time-of-flight (TOF) analysis using a pseudo-random chopper. A detailed description of the apparatus is given in [4] (see also fig. 3.2). In this experimental arrangement angular distributions with high velocity and angular resolution can be measured. The actual beam data are presented in table 3.1. Since the distribution of cluster sizes depends on the concentration of cluster in the seeding gas, two different gas mixtures have been used. The very diluted mixture (0.1 %  $\text{CH}_3\text{NH}_2$  in He) favors the production of small clusters like dimers and trimers, the less diluted mixture (10 %  $\text{CH}_3\text{NH}_2$  in Ne) the production of clusters also larger than dimers and trimers.

### 3.4.2 Laser system

For the photodissociation experiments, the scattered beam interacts collinearly with the radiation of a homebuilt cw  $\text{CO}_2$  laser and the dissociation spectra are obtained by measuring the depletion of the beam signal as function of the laser frequency. A sketch of this arrangement is shown in figure 3.2. A detailed description of the apparatus can be found in [26]. The  $\text{CO}_2$  laser is a line tunable flowing gas laser with typical maximum output powers of about 15 W. For the dissociation of the  $\text{CH}_3\text{NH}_2$ -clusters the laser is operated at 10 W which corresponds to a fluence of  $42 \text{ mJ/cm}^2$ .

## 3.5 Results

### 3.5.1 Size-selection

The size-selection proceeds by the deflection of the cluster beam from the He beam. Figure 3.1 shows the kinematical (Newton) diagram calculated for the beam parameters of table 3.1. The velocities of all clusters are approximately the same as measured by the TOF spectrum. The limiting laboratory angles for the scattering of monomers to heptamers are given by  $21.1^\circ$  (1),  $10.6^\circ$  (2),  $7.1^\circ$  (3),  $5.3^\circ$  (4),  $4.3^\circ$  (5),  $3.5^\circ$  (6) and  $3.0^\circ$  (7). The numbers in parentheses are the corresponding cluster sizes. Each cluster size is confined to a specific angular range. If we set the detector, say, at  $6^\circ$ , clusters larger than  $n=3$  are excluded by these kinematical constraints. In order to exclude the smaller clusters  $n=1$  and  $n=2$  a mass spectrometer is used. This procedure, however,

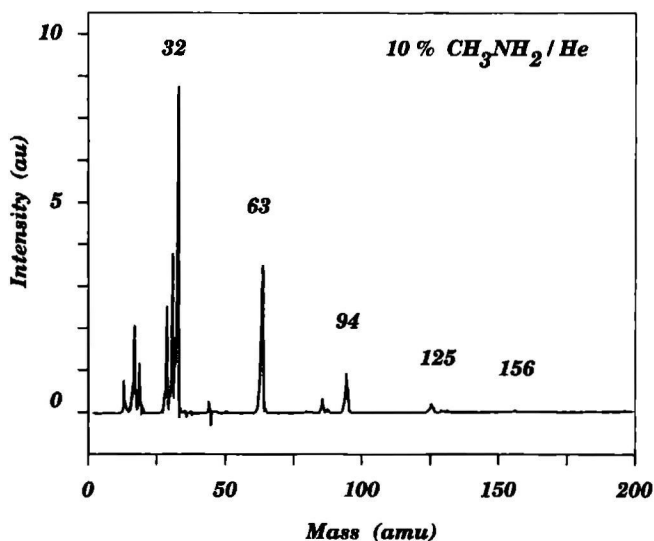
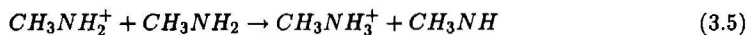


**Figure 3.3:** The mass spectrum of a 10 %  $\text{CH}_3\text{NH}_2/\text{He}$  mixture at a scattering angle of  $3^\circ$  which contains all clusters with  $n < 8$ . The indicated mass peaks correspond to  $(\text{CH}_3\text{NH}_3)^+(\text{CH}_3\text{NH}_2)_{n-2}$  for  $n=2$  to  $n=6$ .

only works if the cluster  $n=3$  does not completely fragment during the ionization process to the next smaller cluster size. The information about this behaviour can be obtained by measuring;

1. the mass spectra with all fragment channels and
2. the angular distributions for these fragment channels.

Figure 3.3 presents the mass spectrum of the  $(\text{CH}_3\text{NH}_2)_n$  clusters taken at  $3^\circ$  for which only clusters with  $n < 8$  contribute to the signals. The spectrum is, aside from the monomer fragments at 31 and 30 amu, completely dominated by the protonated species  $\text{CH}_3\text{NH}_3^+(\text{CH}_3\text{NH}_2)_{n-2}$  at  $m = 32, 63, 94, 125$  and  $156$  amu. The large peak at  $(\text{CH}_3\text{NH}_3)^+$  (32 amu) already indicates that fragmentation is appreciable for clusters with  $n < 8$ . This is confirmed by the measured angular distributions taken at the different fragment ion masses which is shown in figure 3.4. The limiting angles for each cluster size are marked by arrows. A step in the angular distribution appears whenever a new cluster size contributes to the detection signal. At a deflection angle of  $6^\circ$  to which only clusters up to the trimer can contribute, we find signals of about 500 Hz at  $\text{CH}_3\text{NH}_2^+$ , 700 Hz at  $\text{CH}_3\text{NH}_3^+$  and only 120 Hz at  $\text{CH}_3\text{NH}_3^+\text{CH}_3\text{NH}_2$ , the nominal protonated ion mass of the trimer. We conclude that in addition to the intra-cluster reaction



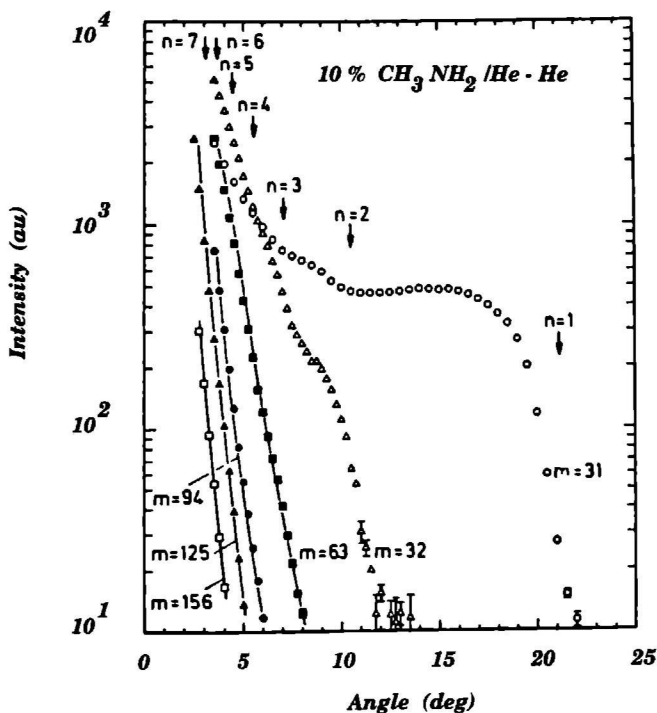
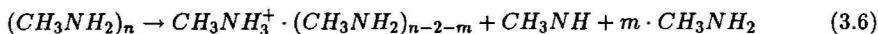


**Figure 3.4:** The measured angular distribution of the scattered  $(\text{CH}_3\text{NH}_2)_n$  clusters seeded in He at different detection masses. The onset of intensity at the limiting angles is marked by arrows.

which leads to the protonated species, also further monomer units are lost, according to the decay process



This reaction occurs, since the interaction of the  $\text{CH}_3\text{NH}_3^+$  ion, formed after the first ionization step with the neutral partner molecule, leads to deeper well depths and smaller minimum distances [29] compared to the neutral system. For this reason the system is internally excited and a final probability exists that a neutral molecule evaporates. Compared with van der Waals complexes or other systems ( $\text{C}_2\text{H}_4$ ,  $\text{NH}_3$ ) [30, 31] the energetic differences are smaller for methylamine and there is always a small probability left to detect a cluster  $(\text{CH}_3\text{NH}_2)_n$  at its protonated ion mass  $\text{CH}_3\text{NH}_3^+(\text{CH}_3\text{NH}_2)_{n-2}$ . Consequently the size-selective process works well.

In contrast to what has been said before, the size-selection is not pure. In all cases except for the dimer spectrum contributions from larger clusters cannot be ruled out, because of the finite angular



No. <sup>a)</sup>	$\Theta$ (deg)	m (amu)	Fraction of cluster size n						
			2	3	4	5	6	7	8
1	8.5	32	1.0	....	....	....	....	....	....
2	6.0	63	...	0.90	0.10	....	....	....	....
3	5.0	94	...	....	0.70	0.25	0.05	....	....
4	4.0	125	...	....	....	0.60	0.30	0.10	....
5	3.0	156	...	....	....	....	0.50	0.30	0.20

<sup>a)</sup> The numbers (no.) correspond to the numbers in table 3.3.

**Table 3.2:** Cluster composition of the different spectra.

resolution of the apparatus and the decreasing spacing of the limiting angles. These contributions are estimated from the measured angular distributions of the larger clusters. The actual data for the photodissociation experiments are listed in table 3.2.

### 3.5.2 Photodissociation

To analyze the measured data we apply a simple model based on one-photon absorption which leads to a dissociated fraction [32]

$$P_{diss} = 1 - e^{-L(\nu)} \quad (3.7)$$

with

$$L(\nu) = \sigma(\nu) \cdot \frac{F}{h\nu} \quad (3.8)$$

in which  $\sigma(\nu)$  is the dissociation cross section, F the laser fluence (energy/area), and  $h\nu$  the photon energy. If it is assumed that a photon is absorbed from the initial state  $i$  to the vibrationally excited state  $f$  and then directly coupled to the continuum state  $\alpha$  with energy E, the cross section is given by [33]

$$\sigma(\nu, i \rightarrow \alpha E) = \frac{8\pi^2}{c} \nu | \langle i | \mu e | f \rangle |^2 \frac{\Gamma}{(h\nu - h\nu_f)^2 + (\frac{\Gamma}{2})^2} \quad (3.9)$$

where  $\mu$  is the transition dipole moment,  $e$  the polarization vector,  $h\nu_f$  the energy of the excited level, and  $\Gamma$  the dissociation rate, given by the golden rule expression

$$\Gamma = \pi | \langle f | V | \alpha E \rangle |^2 \quad (3.10)$$

with the intermolecular potential V for the coupling. Expression 3.7 is still valid, if more than one photon is absorbed, provided the decay process is very fast [26]. Therefore the data are evaluated by fitting equation 3.7 to the spectra. The function  $L(\nu)$  is a Lorentzian profile with three free parameters;  $\nu_0$ , the maximum frequency,  $\Gamma$ , the full width at half maximum (FWHM), and  $L_0$ , the value of the maximum. It is noted that the cross section, integrated over the Lorentzian profile, is

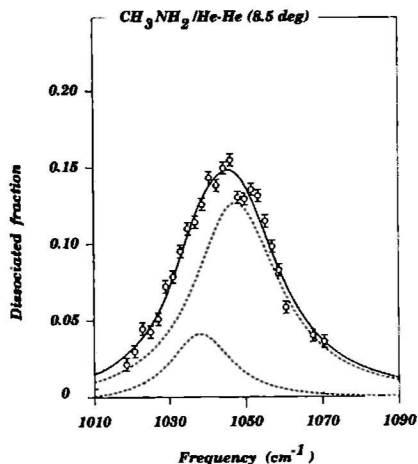


**Figure 3.5:** The measured dimer dissociation spectrum for the 10 %  $\text{CH}_3\text{NH}_2$  mixture in He at a scattering angle of  $8.5^\circ$ . The dashed lines are the results of a fit using the position of the resolved measurement of figure 3.8.

proportional to  $L_0\Gamma$ . If the spectrum for one cluster size is given by two or more profiles a sum of the corresponding Lorentzians is used in equation 3.7.

In the spectral region of the C-N stretching mode ( $\nu_8$ ) of methylamine, the photodissociation spectra are measured by varying the  $\text{CO}_2$  laser lines at constant power for different cluster sizes using the conditions of table 3.1. The results obtained at a laser fluence of  $42 \text{ mJ/cm}^2$  are shown in figure 3.5 and 3.6. The parameters for the Lorentzian line shapes are presented in table 3.3. All the spectra exhibit a large maximum between  $1045.4$  and  $1046.0 \text{ cm}^{-1}$  slightly shifted to the blue from the gas-phase frequency of the C-N stretch at  $1044 \text{ cm}^{-1}$  [34]. The halfwidth decreases dramatically from more than  $20 \text{ cm}^{-1}$  for the dimer and  $11.3 \text{ cm}^{-1}$  for the trimer to about  $6 \text{ cm}^{-1}$  for the larger clusters. From the trimer to the hexamer there also exists a smaller peak at the lower-frequency side around  $1020$ - $1025 \text{ cm}^{-1}$ . The only frequency reported in literature in this frequency range is the  $2\nu_{15}$  overtone excitation of the  $\text{NH}_2$  torsion which has been observed in the spectrum of the solid near  $1005 \text{ cm}^{-1}$  [34].

While the existence of one large peak of the C-N stretch mode is very pronounced for all spectra from the trimer to the hexamer, the same conclusion is somewhat doubtful for the dimer. There seems to be some structure in the spectrum which can be attributed to a peak splitting around  $1042.5$  and  $1054 \text{ cm}^{-1}$ . A better resolution of any line splitting is hindered by the relative large linewidth of the spectrum. Since this is essentially caused by the internal excitation of the dimer during the scattering process with helium, we have repeated the dimer measurement with cold species, without scattering, in a direct beam experiment of  $\text{CH}_3\text{NH}_2$  seeded in Ne. The beam data are given in table 3.1. In order to get size-selectivity very diluted mixtures of  $\text{CH}_3\text{NH}_2$  in Ne were used in this experiment. The results are shown in figures 3.7 and 3.8 for two different masses. If

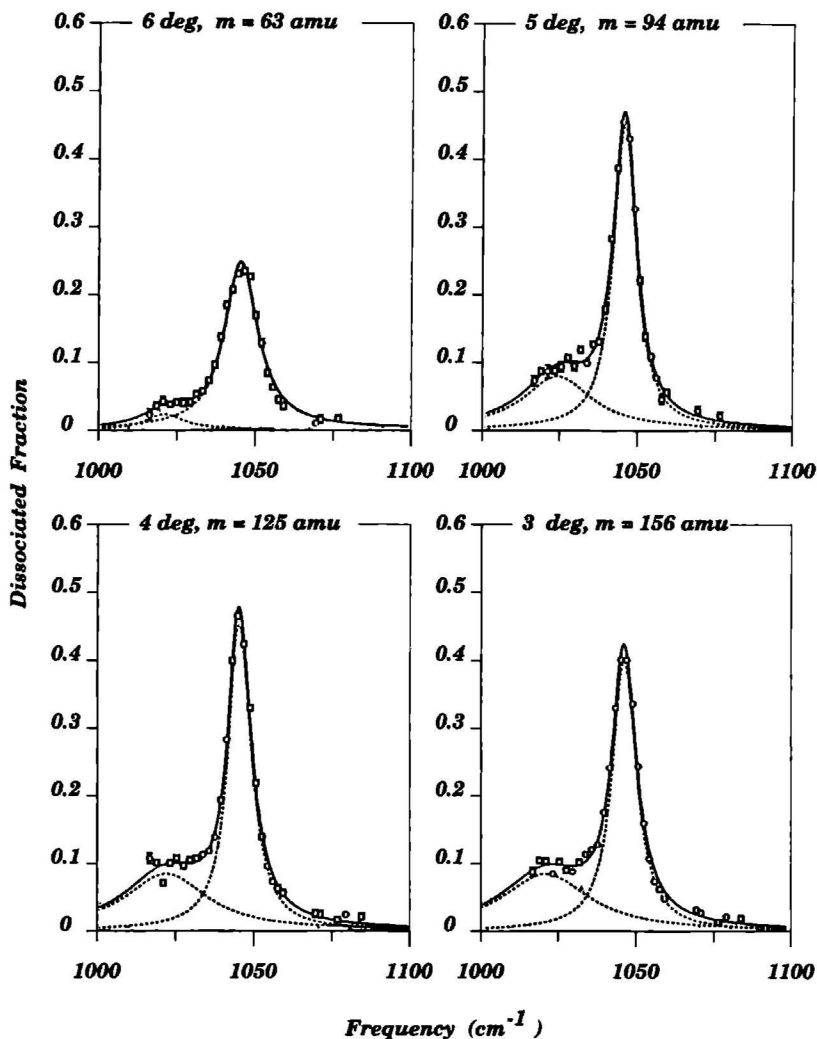


Figure 3.6: The measured dissociation spectra for the clusters with  $n=3$  to  $n=6$  and the cluster composition of table 3.2. (A) is mainly the trimer spectrum at  $6^\circ$  ( $m = 63$  amu), (B) the tetramer spectrum at  $5^\circ$  ( $m = 94$  amu), (C) the pentamer spectrum at  $4^\circ$  ( $m = 125$  amu) and (D) the hexamer spectrum at  $3^\circ$  ( $m = 156$  amu).

the spectrometer is tuned to  $m = 63$  amu, only trimers and heavier clusters are detected. For the

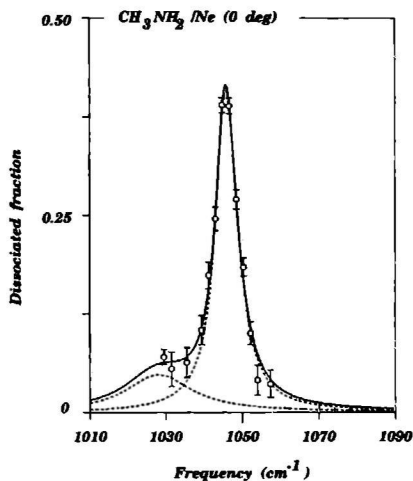


Figure 3.7: The trimer dissociation spectrum for the 0.32 %  $\text{CH}_3\text{NH}_2$  mixture in Ne measured at  $m=63$  amu in the direct beam.

0.32 % mixture one large peak appears, of which the maximum position agrees well with the results of the size-selected experiment (fig. 3.6). For the 0.1 % mixture the peak completely disappears, thus indicating that the beam is free of higher clusters than dimers. For this mixture and a mass of  $m = 33$  amu, the pure dimer spectrum is measured. A clear line splitting is observed with the line positions at  $1038$  and  $1048$   $\text{cm}^{-1}$  (fig. 3.8a). The fits gets even better if a very small peak around  $1030$   $\text{cm}^{-1}$  is added which again is attributed to the overtone excitation of the  $2\nu_{15}$  torsion (fig. 3.8b). If we use the values obtained in the fitting procedure of figure 3.8a for the size-selected internally excited dimer, a satisfactory fit is obtained, as is demonstrated in figure 3.5. Thus we conclude that the dimer displays a line splitting for the excitation of the  $\nu_8$  mode of  $10$   $\text{cm}^{-1}$  between  $1038$  and  $1048$   $\text{cm}^{-1}$ .

## 3.6 Discussion

### 3.6.1 Line shifts and structural implications

One of the first aspects to notice is the complete change of line profile for the transition from the dimer to the trimer spectrum. For the trimer and the larger clusters, there is one dominating maximum at  $1045.5 \pm 0.5$   $\text{cm}^{-1}$  which is caused by the excitation of the C-N stretching mode. The smaller shoulder around  $1020$   $\text{cm}^{-1}$  probably results from the  $2\nu_{15}$   $\text{NH}_2$ -torsion. For the dimer, however, there are two distinct maxima, one (shifted to the red) at  $1038$   $\text{cm}^{-1}$  and one (shifted to the blue) at  $1048$   $\text{cm}^{-1}$ . There is a clear line splitting for the excitation of the  $\nu_8$  mode of about  $10$   $\text{cm}^{-1}$ . Furthermore, it is also possible to fit the contribution of the  $2\nu_{15}$  torsion into the dimer spectrum. Therefore it is very likely that the line splitting of the dimer and the single line of the larger clusters are originating from different cluster structures.

A. Scattered beam: 10 % CH <sub>3</sub> NH <sub>2</sub> in He/He									
No. <sup>a)</sup>	n	Fig.	C-N stretch			Broad peak			
			$\nu_0$ (cm <sup>-1</sup> )	$\Gamma$ (cm <sup>-1</sup> )	$L_0$	$L_0\Gamma$	$\nu_0$ (cm <sup>-1</sup> )	$\Gamma$ (cm <sup>-1</sup> )	$L_0$
1	2	fig. 3.5	1038.3	19.8	0.04	0.87	....	....	....
		fig. 3.5	1047.9	26.3	0.13	3.49			
2	3	fig. 3.6a	1045.8	11.3	0.248	2.8	1020.5	16.3	0.024
3	4	fig. 3.6b	1045.5	6.3	0.456	2.9	1024.5	25.2	0.082
4	5	fig. 3.6c	1045.4	6.2	0.459	2.9	1022.1	30.1	0.085
5	6	fig. 3.6d	1046.0	7.1	0.403	2.9	1021.0	32.0	0.085

B. Direct beam: 0.1 % CH <sub>3</sub> NH <sub>2</sub> in Ne									
n	Fig.	C-N stretch			Broad peak				
		$\nu_0$ (cm <sup>-1</sup> )	$\Gamma$ (cm <sup>-1</sup> )	$L_0$	$L_0\Gamma$	$\nu_0$ (cm <sup>-1</sup> )	$\Gamma$ (cm <sup>-1</sup> )	$L_0$	
2	fig. 3.8a	1038.3	8.5	0.030	0.26	....	....	....	
		1047.9	8.1	0.050	0.42				
2	fig. 3.8b	1038.8	4.7	0.029	0.14	1032.0	15.0	0.15	
		1047.9	8.0	0.057	0.45				
3	fig. 3.7	1046.1	6.1	0.520	3.19	1028.0	20.9	0.048	

<sup>a)</sup> The numbers (no.) correspond to the numbers in table 3.2.

**Table 3.3:** Parameters of the fitted Lorentzian curves for the different clusters, both for the scattered and direct beam.

A more detailed understanding of the observed dissociation spectra can be achieved, if one looks at the calculated minimum configurations for the methylamine clusters. The configurations are calculated by the EPEN/2 (empirical potential of electrons and nuclei) model [35]. To find the most likely configuration one molecule is fixed and the coordinates of the other molecules are varied to find a configuration with minimum energy. The results for the total binding energies and the energy  $\Delta E$  which is necessary to remove one monomer are given in table 3.4. The results agree very well with similar calculations carried out up to the tetramer [27]. The dimer prefers an open configuration, while greater clusters have cyclic structures which start to get distorted for  $n=6$ . If one regards the influence of the cluster bond on the excited C-N stretch, it becomes clear that there are two different possibilities within the dimer. In one molecule the nitrogen atom is bound within the cluster, while in the other molecule the N-atom just sees a slightly different bond with respect to a hydrogen atom, but does not participate in the cluster bond. In the cyclic configurations of the greater clusters all C-N bonds are disturbed in the same way. In these configurations all N-atoms contribute to the cluster bond and at the same time all of them have an H-atom bond which is changed by the cluster bond in the same way.

The absorption frequencies for the C-N stretching mode of gaseous (1044 cm<sup>-1</sup>) and solid (1048

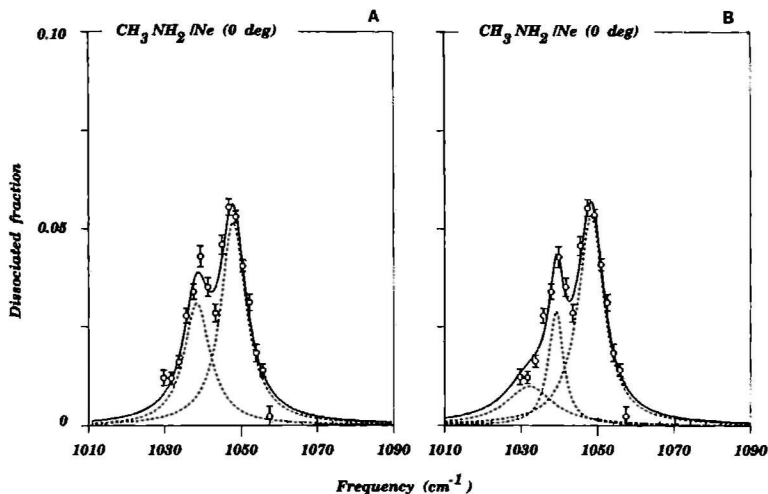


**Figure 3.8:** The dimer dissociation spectrum for the diluted 0.1 %  $\text{CH}_3\text{NH}_2$  mixture in Ne, measured in a direct beam experiment. A clear double-peak structure is found (A). In (B) a small contribution around  $1030\text{ cm}^{-1}$  is added in the fit which is also seen for the larger clusters.

$\text{cm}^{-1}$ ) methylamine are very close together. The maxima of the greater clusters lie exactly between these two values. The measured absorption of isolated molecules in a matrix also shows an interesting splitting in the stretching mode of  $1041$  and  $1051\text{ cm}^{-1}$ . In [36] this is explained by the different positions, which the molecules have in the matrix or by polymerized molecule bonds. Compared with the positions found for the dimer splitting, these matrix values are just  $3\text{ cm}^{-1}$  shifted to the blue which supports the idea of two differently bound N-atoms in the methylamine dimer.

If we compare these measurements with the results for methanol [26] we see that both dimers exhibit a similar splitting due to the same effect. The splitting, however, is smaller in the present case. For the higher clusters the similarity continues concerning the one-peak structure, but for  $\text{CH}_3\text{NH}_2$  the maximum does not shift with increasing cluster size and the shift with respect to the gas absorption frequency is much less. Furthermore, we see no line splitting for the methylamine hexamer, as was found for the methanol hexamer. However, the linewidth is slightly broader than in the case of the smaller cyclic clusters. Since for  $(\text{CH}_3\text{NH}_2)_n$  clusters line shifts are generally smaller than for  $\text{CH}_3\text{OH}$ , it can be assumed that a small line splitting is present which is not resolved in the present experiment. The alternative explanation that  $(\text{CH}_3\text{NH}_2)_6$  exhibits a well-behaved cyclic structure which, in contrast to  $(\text{CH}_3\text{OH})_6$ , is not very much distorted is less probable. Such a structure is not found in the calculations.

Cluster size	This work	Ref. [18]	$\Delta E$ <sup>a)</sup>	Configuration
n=2	-13.38	-13.64	13.4	open
n=3	-37.24	-37.55	23.9	cyclic
n=4	-60.10	-59.97	22.9	cyclic
n=5	-89.80	....	29.7	cyclic
n=6	-117.81	....	28.0	cyclic, distorted

<sup>a)</sup> Energy necessary to remove one monomer.

**Table 3.4:** Total energy of the most stable cluster configuration in kJ/mol.

### 3.6.2 Linewidth

The linewidth is strongly influenced by the amount of energy transferred into the cluster by the scattering process. This is clearly seen for the dimer, if we compare the results for the scattered and the direct beam. The  $\Gamma$  values are 19.8 and 26.3  $\text{cm}^{-1}$  for the internally excited dimers and 8.5 and 8.1  $\text{cm}^{-1}$  for the cold dimers. The effect for the trimer is smaller (11.3  $\text{cm}^{-1}$  vs. 6.1  $\text{cm}^{-1}$ ). With increasing cluster size the broadening effects decrease, probably because the transferred energy can be better distributed among the higher degree of freedom.

While the differences in the linewidth between the scattered and the direct beam can be traced back to the internal excitation in the scattering process, we are left with the intrinsic linewidth of about 8  $\text{cm}^{-1}$  for the cold dimer. The interpretation of this number is difficult. The line tunability of the laser and the resulting low resolution does not allow the interpretation of the linewidth as homogeneously broadened; probably a contour of an unresolved band is measured which contains contributions of rotation and internal rotation as well as the predissociation lifetime. It is interesting to note that the value found here for  $\text{CH}_3\text{NH}_2$  dimers is larger than the result for  $\text{CH}_3\text{OH}$  dimers under similar experimental conditions, for which values smaller than 3  $\text{cm}^{-1}$  have been reported [37]. The reason is probably the additional internal rotation of the  $\text{NH}_2$  group in combination with a faster decay caused by the additionally accessible vibrational band of the  $\text{NH}_2$  wagging mode at 780  $\text{cm}^{-1}$ . This band is relatively close to the originally excited band and should according to the momentum gap law enhance the predissociation rate [16].

### 3.6.3 Cross sections

The  $L_0$  values listed in table 3.3 are directly proportional to the cross sections at the maximum  $\sigma_0$ . The calibration constant is according to equation 3.7 and the known values of the fluence and frequency 0.5 $\cdot 10^{-18}$   $\text{cm}^2$ . These values increase with increasing cluster size up to n=4 and then level off. What, however, is really important for the absorption process is the average transition dipole moment which according to equation 3.9 is proportional to  $\Gamma L_0$ . These values are also listed in table 3.3. For the dimer we find, if the two components are added, a large difference between the values of the internally excited (4.36) and the cold (0.68) species. For the larger clusters a nearly constant value of 2.9 is found. Both results are at variance with what would be expected for the absorption cross sections. For one cluster species, the dimer, it should be constant, and for larger clusters it should increase linearly with the number of absorbers, a result which is indeed found for

$(\text{C}_2\text{H}_4)_n$  clusters [38]. The reason for the deviations from the expected behaviour can be found, if we look at the binding energies and the number of absorbed photons. For the dimer a binding energy of 13.4 kJ/mol is calculated, while the infrared radiation corresponds to 12.5 kJ/mol. Even if a certain amount of zero-point energy is accounted for in addition to the uncertainty of the calculated numbers, it is obvious that a cold cluster can be dissociated only by two photons, while an internally excited cluster with an additional energy of about 3 kJ/mol is dissociated by one photon. This result probably explains the large difference in the absorption cross section.

Similar considerations hold for the larger clusters. There are two contradicting influences for these species. The cross section should increase with an increasing number of absorbers, and it should decrease with an increasing binding energy and the increasing number of photons necessary to break these bonds. This is clearly seen in the results of table 3.4 which require, at least, two photons for  $n=3$  and  $n=4$  and three photons for  $n=5$  and  $n=6$ . These arguments explain the nearly constant behaviour of the cross section.

### **Acknowledgment**

We gratefully acknowledge financial support from the Deutsche Forschungsgemeinschaft (SFB93). We thank B. Schmidt for carrying out the calculation of the minimum-energy configurations of the  $(\text{CH}_3\text{NH}_2)_n$  clusters for  $n=5$  and  $n=6$ .





---

# Infrared Photodissociation of Size-selected Carbonyl Sulphide Clusters

3

*U. Buck, R. Krohne*

*Max Planck Institut für Strömungsforschung, Bunsenstraße 10, D 3400, Göttingen*

*H. Linnartz*

*Department of Molecular and Laser Physics, University of Nijmegen,  
Toernooiveld, NL 6525 ED, Nijmegen*

## Abstract

Infrared photodissociation spectra of  $(\text{OCS})_n$  clusters are presented for  $n=2$  to  $n=6$ . A line tunable cw  $\text{CO}_2$  laser is used to excite the first overtone of the  $\nu_2$  bending vibration around  $1045 \text{ cm}^{-1}$ . The size-selected cluster beam is generated by scattering the  $(\text{OCS})_n$  clusters from a He or Ne beam. The general feature is that all clusters exhibit one clear peak between  $1045.9$  and  $1044.1 \text{ cm}^{-1}$ , indicating that a cyclic structure is most likely. For dimers and trimers the results are compared with the non size-selected results of Hoffbauer *et al* (J. Phys. Chem. 87 (1983) 2096).

---

<sup>3</sup>Unpublished results.

### 3.7 Introduction

Weakly bound molecular clusters are known to fragment significantly when they are ionized by electron bombardment [7]. The reason is, generally, a structural change going from the neutral to the ionized configuration which is often accompanied with large excess energy and which, in turn, leads to the partial evaporation of the cluster. For this reason it is hard to obtain size-selective information for neutral clusters; simple mass filtering does not help, since the signal on one mass also contains contributions from higher clusters that also fragment to this ion mass. The measured cluster ion distribution obtained in the mass spectrometer therefore only reflects the distribution of the formed ions, which cannot simply be related to the original cluster size distribution. Therefore the size-selective process should be independent of the ionization step.

One method to achieve this is by high resolution vibration-rotation spectroscopy, which is based on the phenomenon that different cluster sizes have different spectroscopic features and consequently can be distinguished because of their spectra [2]. This method works well for small clusters but for larger clusters the spectra become too congested to analyze. Furthermore only small clusters can be generated more or less controlled in molecular beams by using diluted mixtures of the cluster gas in the seeding gas. For less diluted mixtures that are necessary to generate also higher clusters, the size distribution is to a certain extent arbitrary. For this reason the  $(\text{OCS})_n$  clusters are studied using another method that was discussed in detail before [5, 6, 7]; the scattering of the cluster beam from a rare gas beam. Structural information is obtained by subsequent infrared photodissociation of the size-selected beam [10, 18]. To do so, a vibrational mode of one molecular component is excited and in case the photon energy is larger than the binding energy of the complex, energy redistribution normally causes the complex to dissociate. From the measured line shift and linewidth structural and dynamical information is obtained, as was shown in former experiments on  $\text{C}_2\text{H}_4$  [21],  $\text{NH}_3$  [23],  $\text{N}_2\text{H}_4$  [12],  $\text{CH}_3\text{OH}$  [12, 24, 25],  $\text{CH}_3\text{NH}_2$  [39] and  $\text{CH}_3\text{CN}$  [40] clusters.

In this paragraph infrared photodissociation spectra for OCS clusters, from dimer to hexamer are presented. These spectra are compared to the results of Hoffbauer *et al* [41] for dimers and trimers. The result found for the dimer agrees with our observation, but the splitting that was found for  $(\text{OCS})_3$  probably is due to clusters larger than trimers.

### 3.8 Experimental

The experimental apparatus, that was described in detail previously [4], consists of two molecular beams which intersect each other at an angle of  $90^\circ$ . The beams are together rotatable with respect to the scattering center, while the detector unit is fixed. The detector consists of an electron bombardment ionizer, a quadrupole mass filter and an off-axis mounted particle multiplier. Furthermore a time-of-flight spectrometer is used to measure the velocities of the scattered clusters. The clusters are generated in a molecular beam expansion of a 10 % mixture of OCS in He or Ne through a  $60 \mu\text{m}$  nozzle at a source pressure of 1.3 bar.

The size-selection after scattering is achieved by positioning the detector in such a way that larger clusters are excluded kinematically. The limiting elastic scattering angles depend on the momentum transfer. This is shown in table 3.5 for two mixtures with different collision partners.

As can be seen from table 3.5 the seeding gas and scattering partner are important in determining the angular distributions. Taking into account the decreasing spacing of the limiting angles and

Mixture	Scattered from	Cluster size								
		1	2	3	4	5	6	7	8	9
OCS/He (1300 m/s)	He (1775 m/s)	13.0°	6.5°	4.4°	3.3°	2.6°	2.2°	1.9°	1.6°	1.5°
OCS/Ne (770 m/s)	He (1775 m/s)	18.6°	9.4°	6.2°	4.7°	3.7°	3.1°	2.7°	2.3°	2.1°
OCS/Ne (770 m/s)	Ne (800 m/s)	46.3°	23.6°	15.8°	11.9°	9.5°	7.9°	6.8°	5.9°	5.3°

**Table 3.5:** The limiting elastic scattering angles for different mixtures and different collision partners, for clusters  $n=1$  to  $n=9$ .

the finite angular resolution of the beam machine larger clusters can be studied better for large momentum transfers, whereas for smaller clusters the opposite is true. In the latter case the clusters are scattered over smaller angles, but since the angular resolution is still more than sufficient, additional signal strength is gained because of the higher angular cluster density.

Clusters smaller than the desired size subsequently can be excluded by tuning the mass spectrometer to the corresponding ion mass or to a mass that is larger than the mass of the next smaller cluster. The latter method is especially applicable for hydrogen bonded systems but not for  $(\text{OCS})_n$  clusters. Therefore, the clusters are detected on the masses  $(\text{OCS})_n^+$ ; 60, 120, 180 and 240 amu.

In principle it is possible to obtain pure cluster beams in this way. However, due to the finite angular resolution of the apparatus - also in case of more suitable collision partners - only for the dimer spectrum contributions from larger clusters can be ruled out. In table 3.6 the actual cluster compositions are listed as obtained from the angular distributions.

No. <sup>a)</sup>	Scattering Angle			Fraction of cluster size n				
	OCS/He-He	OCS/Ne-He	m (amu)	2	3	4	5	6
1	5.50°	8.00°	120	1.00	....	....	....	....
2	4.25°	5.75°	120	0.25	0.75	....	....	....
3	3.00°	4.25°	180	....	0.35	0.65	....	....
4		3.50°	180	....	≈ 0	0.30	0.70	....
5		3.00°	240	....	....	0.10	0.30	0.60

<sup>a)</sup> The numbers (no.) correspond to the numbers in table 3.7.

**Table 3.6:** Cluster composition of the different spectra.

For the photodissociation experiments the size-selected beam is irradiated collinearly with infrared photons supplied by a line tunable cw  $\text{CO}_2$  laser. The typical power operation amounts to 10 W. The dissociation spectra are obtained by measuring the depletion of the cluster signal as function

of the laser frequency. A detailed description can be found in [26].

### 3.9 Results and discussion

In table 3.7 the photodissociation results are listed for  $(\text{OCS})_n$  clusters with  $n=2$  to  $n=6$  and for mixtures containing clusters with sizes  $n=3$  to  $9$  and  $n=3$  to  $14$ . The parameters are calculated according to equations 3.7 to 3.10 and from the cluster composition - obtained from angular distributions - as listed in table 3.6. For the dimers and trimers the values found by Hoffbauer *et al* [41] are listed too.

No. <sup>a)</sup>	n	Size selected results		Hoffbauer <i>et al</i>	
		$\nu_0$ (cm <sup>-1</sup> )	$\Gamma$ (cm <sup>-1</sup> )	$\nu_0$ (cm <sup>-1</sup> )	$\Gamma$ (cm <sup>-1</sup> )
1	2	1045.9 ± 0.4	8.71	1044.7 ± 0.1	5.0
2	3	1045.0 ± 0.3	7.35	1044.0 ± 0.2	6.0
	3	.....	.....	1035.8 ± 0.5	8.0
3	4	1044.7 ± 0.2	5.60		
	4	1036.0 ± 0.5	6.00		
4	5	1044.3 ± 0.2	4.92		
5	6	1044.2 ± 0.2	5.46		
-	3-9	1044.3 ± 0.2	6.20		
-	3-14	1044.1 ± 0.2	6.39		

<sup>a)</sup> The numbers (no.) correspond to the numbers in table 3.6.

**Table 3.7:** Parameters for the fitted Lorentzian curves for the different clusters, including the dimer and trimer results of Hoffbauer *et al*.

#### 3.9.1 Structural implications

OCS is a linear triatomic molecule, i.e. it has three vibrational modes; the  $\nu_1$  "symmetric" stretch around 859 cm<sup>-1</sup>, the  $\nu_3$  "asymmetric" stretch at 2062 cm<sup>-1</sup>, that was studied for non size-selected  $(\text{OCS})_n$  clusters in [42] and the double degenerate  $\nu_2$  bend at 527 cm<sup>-1</sup> of which the first overtone is used in this experiment.

The size-selected dissociation patterns show one clear peak that gradually shifts from 1045.9 cm<sup>-1</sup> to 1044.1 cm<sup>-1</sup> going from smaller to larger clusters. This is in agreement with the expectation that a progressive shift is induced and consequently the absorption bands should lie in between the frequency range of the gas phase frequency (1047.04 cm<sup>-1</sup> [43]) and the frequency in the solid phase (1042.7 cm<sup>-1</sup> [44]). With exception of Ar-OCS, that has a T-shaped structure [45], little information is available for OCS clusters. In [41] it was concluded from the observed infrared dissociation pattern that the  $(\text{OCS})_2$  has a staggered anti-parallel structure. The T-shaped structure is not expected, since in that case the bending frequencies of the two OCS monomers must be significantly different, yielding line splittings as were found previously for  $\text{CH}_3\text{OH}$  [12] and  $\text{CH}_3\text{NH}_2$  [39] clusters. This is confirmed in our experiment; although the  $\nu_0$ -frequency is found

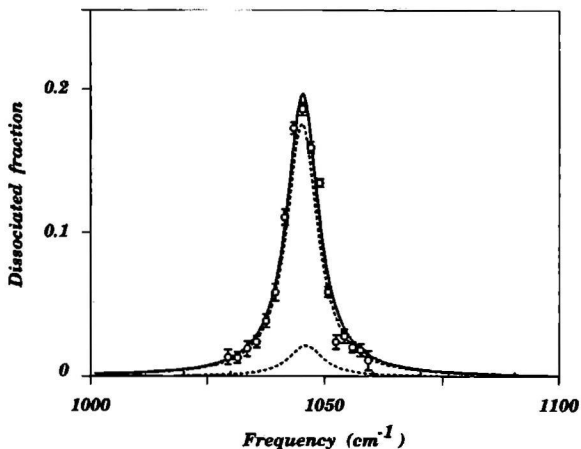


**Figure 3.9:** The infrared photodissociation signal for  $(\text{OCS})_3$ . The dotted lines indicate the dimer and trimer contributions to the overall infrared signal.

to be slightly shifted to the blue compared to the result found in [41], one clear peak is observed. Based on similar arguments, the same conclusion was reached in [42] for dissociation experiments using the  $\nu_3$  vibration.

Hoffbauer and coworkers considered the OCS trimer as an extension of the OCS dimer, in which all three OCS molecules are essentially parallel and the molecule as a whole is linear. For  $(\text{OCS})_3$  they found two lines, positioned at  $1044.0$  and  $1035.8 \text{ cm}^{-1}$  with an intensity ratio of about 2:1, whereas in this experiment only one peak is found (fig. 3.9). This suggests that the peak at  $1035.8 \text{ cm}^{-1}$  is not due to an absorption of the central OCS molecule in an out-of-plane bend, which indeed would be the logical explanation for a spectrum as observed in [41]. On the contrary the three molecules must have equivalent positions relative to each other which suggests a cyclic like structure. The band around  $1036 \text{ cm}^{-1}$  originates from contributions of higher clusters, against which could not be discriminated in the experiment of Hoffbauer and coworkers. This seems to be confirmed by pressure dependent measurements on the  $\nu_3$  absorption band [42], in which increasing pressure, yielding the formation of larger clusters, results in more and more red shifted contributions to the dissociation signal. However, this experiment is not size-selective either and the obtained results only reflect a size dependency in a qualitative way. To obtain detailed information a size-selective experiment is necessary.

In figure 3.10 the infrared photodissociation signal for the  $(\text{OCS})_4$  is shown. It turns out that this is the only cluster size which shows a small shoulder at the place where the second peak in [41]

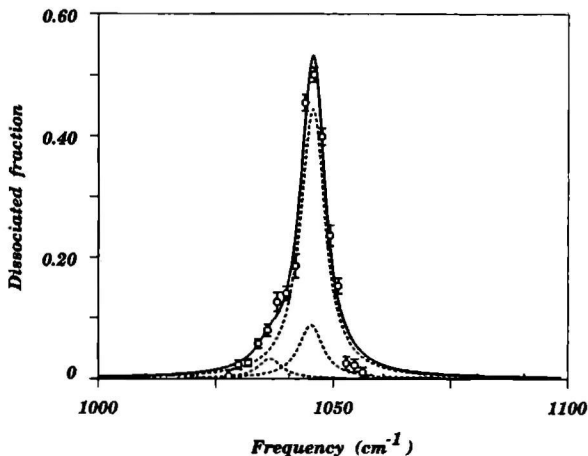


**Figure 3.10:** The infrared photodissociation signal for  $(\text{OCS})_4$ . The dotted lines indicate the separated Lorentz fits for tetramer, trimer and possible tetramer contribution around  $1036 \text{ cm}^{-1}$ .

is observed. The dissociation pattern can be fitted by assuming an absorption band around  $1036 \text{ cm}^{-1}$ . The ratio between this and the main band is much smaller (1:10) as it was observed in [41]. A reasonable explanation for this would be, that in [41] the trimer signal also includes contributions from the tetramer. In figure 3.10 this is visualized by the ratio (1:3) of the signal at  $1036 \text{ cm}^{-1}$  arising from tetramers and the signal around  $1045 \text{ cm}^{-1}$  arising from trimers in a beam that for 0.35 % exists of trimers and 0.65 % of tetramers. It is not very hard to imagine that in a slightly different composition the result of Hoffbauer can be obtained.

The contribution around  $1036 \text{ cm}^{-1}$  is only found for the tetramer, indicating that besides a cyclic structure, probably a structure exist in which at least one of the OCS monomers is non-equivalent in the bond compared to the other monomers. A possible explanation for this could be a structure which is alike the structure proposed by Hoffbauer *et al* for the trimer and in which both inner OCS monomers see two bonds instead of the one of the monomers that are located at the ends. For clusters larger than tetramers no contributions around  $1036 \text{ cm}^{-1}$  are found. The dissociation pattern consists of one clear peak, suggesting that the structure for these clusters is cyclic.

### 3.9.2 Linewidths

The linewidth is strongly influenced by the amount of energy transferred into the cluster by the scattering process. This is clearly seen for the dimer, if the results without scattering [41] and

the size-selected results with scattering are compared (table 3.7). With increasing cluster size the broadening effect decreases, probably because the transferred energy can be better distributed among more degrees of freedom. This can be seen from the values in table 3.7. Furthermore, the determination of the exact linewidth is not allowed, due to the limited tunability of the laser. For these reasons the interpretation of the linewidth as homogeneous broadened is not possible. Consequently it is very hard to draw conclusions concerning the life time and intracluster energy redistribution schemes.



### References

- [1] U. Buck, R. Krohne, H. Linnartz, *J. Chem. Phys.* 93 (1990) 3726.
- [2] R.E. Miller, *Science* 240 (1988) 447.
- [3] See chapter 2 of this thesis and the references therein.
- [4] U. Buck, F. Huisken, J. Schleusener, J. Schäfer, *J. Chem. Phys.* 72 (1980) 1512.
- [5] U. Buck, H. Meyer, *Phys. Rev. Lett.* 52 (1984) 109.
- [6] U. Buck, H. Meyer, *J. Chem. Phys.* 84 (1986) 4854.
- [7] U. Buck, *J. Phys. Chem.* 92 (1988) 1023.
- [8] U. Buck, in *Atomic and Molecular Beam Methods*; edited by G. Scoles; Oxford, New York (1988).
- [9] Ch. Lauenstein, *Zerfallsprozesse stoßselektierten Molekülcluster*, Ph.D. Thesis, MPI für Strömungsforschung, Göttingen (1989).
- [10] A. Rudolph, *Infrarot Photodissoziation von Stoßselektierter Molekülcluster*, Ph.D. Thesis, MPI für Strömungsforschung, Göttingen (1989).
- [11] R. Krohne, *He-Atom-Streuung zur Größenbestimmung und Schwingungsanregung großer Cluster*, MPI für Strömungsforschung, Göttingen (1989).
- [12] U. Buck, X.J. Gu, M. Hobein, Ch. Lauenstein, *Chem. Phys. Lett.* 163 (1989) 455.
- [13] B. Heijmen, *Photo-excitation and dissociation of small molecular clusters*, Ph.D. Thesis, University of Nijmegen (1987).
- [14] G.E. Ewing, *J. Phys. Chem.* 91 (1987) 4662.
- [15] S. Leutwyler, J. Jortner, *J. Phys. Chem.* 91 (1987) 5558.
- [16] R.E. Miller, *J. Phys. Chem.* 90 (1986) 330.
- [17] U. Buck, in *Enrico Fermi School on the Chemical Physics of Atomic and Molecular Clusters*, edited by G. Scoles (Il Nuovo Cimento, Bologna, 1990).
- [18] U. Buck, X.J. Gu, M. Hobein, Ch. Lauenstein, A. Rudolph, *J. Chem. Soc. Faraday Trans. 11* (1990) 1923.
- [19] F. Huisken, H. Meyer, Ch. Lauenstein, R. Sroka, U. Buck, *J. Chem. Phys.* 84 (1986) 1042.
- [20] F. Huisken, T. Pertsch, *J. Chem. Phys.* 86 (1987) 106.
- [21] U. Buck, F. Huisken, Ch. Lauenstein, H. Meyer, R. Sroka, *J. Chem. Phys.* 87 (1987) 6276.
- [22] F. Huisken, M. Stemmler, *Chem. Phys.* 132 (1989) 351.
- [23] F. Huisken, T. Pertsch, *Chem. Phys.* 126 (1988) 213.
- [24] U. Buck, X.J. Gu, Ch. Lauenstein, A. Rudolph, *J. Phys. Chem.* 92 (1988) 5561.
- [25] F. Huisken, M. Stemmler, *Chem. Phys. Lett.* 144 (1988) 391.
- [26] U. Buck, X.J. Gu, Ch. Lauenstein, A. Rudolph, *J. Chem. Phys.* 92 (1990) 6017.

- [27] G. Brink, L. Glasser, *J. Mol. Struct.* 85 (1981) 317.
- [28] J.A. Odutola, R. Viswanathan, T.R. Dyke, *J. Am. Chem. Soc.* 101 (1979) 4787.
- [29] S.S. Wee, S. Kim, M.S. Ihon, H.A. Scheraga, *J. Phys. Chem.* 94 (1990) 1656.
- [30] U. Buck, Ch. Lauenstein, H. Meyer, R. Sroka, *J. Phys. Chem.* 92 (1988) 1916.
- [31] U. Buck, Ch. Lauenstein, *J. Chem. Phys.* 92 (1990) 4250.
- [32] M.P. Cassasa, D.S. Bomse, K.C. Janda, *J. Chem. Phys.* 74 (1981) 5044; M.A. Hoffbauer, K. Liu, C.F. Giese, W.R. Gentry, *ibid.* 78 (1983) 5567.
- [33] J.A. Beswick, in *Structure and Dynamics of Weakly Bound Molecular Complexes*, edited by A. Weber (Reidel, Dordrecht, 1987), p. 563.
- [34] J.R. Durig, S.F. Bush, F.G. Baglin, *J. Chem. Phys.* 49 (1968) 2106.
- [35] J. Snir, R.A. Nemenoff, H.A. Scheraga, *J. Chem. Phys.* 82 (1978) 2497; L.L. Shipman, A.W. Burgess, H.A. Scheraga, *Proc. Natl. Acad. Sci. U.S.A.* 72 (1975) 543.
- [36] G.C. Pimentel, M.O. Bulanin, M. van Theil, *J. Chem. Phys.* 36 (1965) 500.
- [37] J.P. LaCrosse, J.M. Lisy, *J. Phys. Chem.* 94 (1990) 4398.
- [38] R. Ahlrichs, S. Brode, U. Buck, M. De Kieviet, Ch. Lauenstein, A. Rudolph, B. Schmidt, *Z. Phys. D.* 15 (1990) 341.
- [39] U. Buck, X.J. Gu, R. Krohne, Ch. Lauenstein, H. Linnartz, A. Rudolph, *J. Chem. Phys.* 94 (1991) 23.
- [40] U. Buck, X.J. Gu, R. Krohne, Ch. Lauenstein, *Chem. Phys. Lett.* 174 (1990) 247.
- [41] M.A. Hoffbauer, K. Liu, C.F. Giese, W.R. Gentry, *J. Phys. Chem.* 87 (1983) 2096.
- [42] G. Hillrichs, *Molekularstrahlexperimente zur Infrarot Photodissoziation von van der Waals Komplexen*, Ph.D. Thesis, MPI für Strömungsforschung, Göttingen (1989).
- [43] J.S. Wells, F.R. Petterson, A.G. Maxi, *Appl. Opt.* 18 (1979) 3567.
- [44] F.D. Verderame, E.R. Nixon, *J. Chem. Phys.* 44 (1966) 43.
- [45] S.J. Harris, K.L. Janda, S.E. Novick, W. Klemperer, *J. Chem. Phys.* 63 (1973) 88.



## Determination of the electric dipole moment of $\text{KrH}^+$ <sup>4</sup>

*H. Linnartz*

*Department of Molecular and Laser Physics, University of Nijmegen  
Toernooiveld, NL 6525 ED, Nijmegen*

*M. Havenith*

*Institut für Angewandte Physik, Wegelerstraße 8, D 53115 Bonn*

*E. Zwart, W.L. Meerts, J.J. ter Meulen*

*Department of Molecular and Laser Physics, University of Nijmegen  
Toernooiveld, NL 6525 ED, Nijmegen*

### Abstract

By measuring the isotope shift of the rotational  $g_R$ -factors for two different isotopic species, the electric dipole moment of the molecular ion  $\text{KrH}^+$  is determined. For this purpose the Zeeman effect is studied for the  $J=1 \leftarrow 0$  transition of  $\text{KrH}^+$  at 494.5 GHz and the  $J=2 \leftarrow 1$  transition of  $\text{KrD}^+$  at 503 GHz. In a magnetic field of 4.950 T the rotational transition splits into two  $\Delta M = \pm 1$  components, resulting in splittings of approximately 41.8 MHz ( $\text{KrH}^+$ ) and 21.1 MHz ( $\text{KrD}^+$ ). From the analysis it turns out that there is a major influence of the zero point vibrations. This results in an uncertainty of the interpretation of the experimental data and, consequently, the determination of the electric dipole moment is difficult.

The ions are generated in a modified anomalous discharge placed in a superconducting magnet. The transitions are observed by direct absorption of the harmonics of a 70 GHz klystron, using the tunable far infrared sideband spectrometer at the University of Nijmegen.

---

<sup>4</sup>This chapter is based on the article:  
Determination of the electric dipole moment of  $\text{KrH}^+$ ; H. Linnartz, M. Havenith, E. Zwart, J.J. ter Meulen, W.L. Meerts, *J. Molec. Spectrosc.* 153 (1992) 710.

## 4.1 Introduction

Determination of the electric dipole moment by conventional Stark spectroscopy, as is usual for neutral molecules (see chapter 2), is not possible for molecular ions, since the electric field accelerates the ions towards the wall of the discharge tube. However, the electric dipole moment of molecular ions in a  $^1\Sigma$  state can be determined by measuring the Zeeman splitting for several isotopes and by determining the isotope shift of the rotational  $g$ -factors. The idea of this method is based on the following (see also [1]).

If we consider the case of a diatomic ion for which the complete net charge is located on one nucleus, the overall magnetic moment consists of contributions from nuclei and electrons and can be described as

$$\mu_{mag} = \frac{\mu_n M_p}{I} z^2 J \quad (4.1)$$

Here  $\mu_n$ ,  $M_p$ ,  $I$  and  $z$  stand for the nuclear magneton, the proton mass, the moment of inertia and the distance of the charge from the center-of-mass, respectively. For  $^1\Sigma$  molecules is  $J$ , the overall angular momentum, in first approximation equal to  $R$ , the rotational angular momentum, which describes the rotation of the molecule around its center-of-mass. The rotational  $g_R$ -factor is defined by

$$E_{Zeeman} = \mu_{mag} H = \mu_n g_R J H, \quad (4.2)$$

where  $H$  stands for the applied magnetic field. Consequently,  $g_R$  can be written as

$$g_R = \frac{M_p}{I} Q z^2, \quad (4.3)$$

where  $Q$  is the effective net charge in units of  $e$  ( $Q=1$  in this example). For the same ion the electric dipole moment in the center-of-mass is given as

$$\mu = e Q z. \quad (4.4)$$

Consequently in a  $^1\Sigma$  molecule there exists a direct relation between the resulting  $g_R$ -factor and the electric dipole moment with respect to the center-of-mass. It is worthwhile to note here that, in contrast to the electric dipole moment of a neutral molecule, the dipole moment of an ion depends on the coordinate system to which it is referred. In this chapter the dipole moment is always defined relative to the center-of-mass.

In order to obtain an expression for the electric dipole moment, it is necessary to know  $g_R$  and the moment of inertia - i.e. the rotational constant - for two isotopic species. Upon substitution the distance of each charge to the center-of-mass is shifted from  $z$  to  $z+\Delta z$ . Under the assumption that the total intermolecular distance is not affected, this corresponds to the shift of the center-of-mass. Consequently, by taking the difference ( $g'_R I' - g_R I$ ), where the primes indicate the isotopic species, an expression is obtained from which  $\mu$  can be derived;

$$g'_R I' - g_R I = C M_p \left( 2\mu \frac{\Delta z}{e} + Q \Delta z^2 \right) \quad (4.5)$$

This picture is of course a highly simplified one, but it helps to understand the main physical ideas upon which a more rigorous treatment is based. The factor  $C$  therefore should be regarded as a

"simple picture correction factor". In an exact quantum mechanical derivation with the effect of zero point motion being neglected, Townes *et al* [2] showed that  $\mu$  is given by

$$\boldsymbol{\mu} \cdot \boldsymbol{d} = -\frac{eh}{16\pi^2 M_p} \left( \frac{g'_R}{B'} - \frac{g_R}{B} \right) + \frac{1}{2} Qe|\boldsymbol{d}|^2 \quad (4.6)$$

Here,  $\boldsymbol{\mu}$  is the electric dipole moment,  $\boldsymbol{d}$  the displacement vector ( $\Delta z$ ) of the center-of-mass of the primed isotopic species referred to the center-of-mass of the non-primed isotopic species,  $g_R$  the rotational  $g$ -factor,  $B$  the rotational constant and  $Q$  the net charge of the ion.

Because  $\frac{g'_R}{B'}$  and  $\frac{g_R}{B}$  represent two nearly equal quantities it is necessary to measure these ratios with very high precision in order to obtain an acceptable error for  $\mu$ . The result yields both the value and the sign of the electric dipole moment.

Up to now there are only two experimentally determined electric dipole moments for molecular ions. This lack of experimental data contrasts a large number of theoretical results obtained by *ab initio* calculations. The first direct measurement of an electric dipole moment for a molecular ion was carried out by Laughlin *et al* for  $\text{ArH}^+$  ( $\text{ArD}^+$ ). In subsequent experiments the dipole moment was determined as  $(1.4 \pm 0.4)$  D [3],  $(1.6 \pm 0.4)$  D [4] and  $(3.0 \pm 0.6)$  D [5], whereas a theoretical value of 2.2 D was obtained by Rosmus [7]. The second measurement was performed by Havenith *et al* for the astrophysically important ion  $^{14}\text{N}^{14}\text{NH}^+$  ( $^{14}\text{N}^{15}\text{NH}^+$ ,  $^{15}\text{N}^{14}\text{NH}^+$ ) [6]. The dipole moment of  $\text{N}_2^+\text{H}$  was determined as  $(3.4 \pm 0.2)$  D which agreed very well with the theoretical value obtained by Botschwina [8], 3.37 D.

From the results of both determinations it was concluded [6] (see also [9]) that as long as vibrational corrections for the  $g$ -factors are lacking, it is important to restrict the isotopic substitution to the heavy nucleus. This could explain the discrepancy with theory for the  $\text{ArH}^+$  measurements, whereas the  $\text{N}_2\text{H}^+$  measurement agreed very well with the theoretical value. However, because in the  $\text{N}_2\text{H}^+$  experiment several improvements were introduced - among others a superconducting magnet, providing high and highly stable magnetic fields - we decided to choose a second rare gas hydride ion,  $\text{KrH}^+$ , for a further test. For this ion high precision *ab initio* calculations performed by Rosmus *et al* [10] predict an electric dipole moment of 1.944 D. Zero point vibrations should have a similar impact on the result for this ion as for  $\text{ArH}^+$ .

In this work we present far infrared measurements on  $\text{KrH}^+$  and  $\text{KrD}^+$  transitions which agree very well with the predictions based upon the Dunham coefficients of Johns [11] and Warner *et al* [12]. In spite of experimental improvements the vibrational effects influencing the method mentioned above are not yet understood well enough to permit the determination of  $\mu$ . Several approaches to deal with this problem will be discussed.

## 4.2 Experimental

In order to keep the error in  $g_R$  as small as possible the Zeeman splittings of pure rotational transitions are measured in high (4.950 T) and highly stable (fluctuations less than 0.05 %) magnetic fields. The lines are recorded in the submillimeter region where the linewidth, determined by Doppler and pressure broadening, is sufficiently small. For this purpose the tunable far infrared sideband spectrometer in Nijmegen is used which was described in detail elsewhere [13] (see fig. 1.1). The radiation that is used for the dipole measurements, is generated with the seventh harmonic of a 70 GHz klystron in a Schottky barrier diode and selected using a monochromator with

a grating of 0.8 grooves/mm. The radiation passes the discharge cell and is focussed onto an InSb hot-electron bolometer. The radiation is frequency modulated at 5 kHz and the detector output is monitored at twice this frequency with a PDP11/23+ computer using a phase sensitive detector.

The ions are generated in a liquid nitrogen cooled discharge cell using a mixture of Kr and H<sub>2</sub> (D<sub>2</sub>). In order to increase the signal strength at low pressures (typically less than 50 mTorr) a magnetically enhanced anomalous glow discharge is used, as was described by de Lucia *et al* [14]. In order to allow measurements at a high magnetic field, which is used both for the extension of the negative glow and for the Zeeman field, a modified cathode design has to be used. In [14] a magnetic field of 300 to 400 G is used to extend the negative glow over the entire length of the discharge tube. However, it was found that the ion signal strength decreased for higher magnetic fields. Furthermore, it was found that the decrease of the signal is accompanied by a decrease of the discharge voltage. For sufficiently high magnetic fields the discharge voltage became too low to maintain a negative glow. Since for an anomalous discharge the current is proportional to the voltage, the maximum current for which an anomalous discharge could be observed, decreased with increasing magnetic field. In order to allow also measurements at high magnetic fields a modified cathode design is used. The principal setup was described in [6]. In this setup an adjustable stainless steel cathode surface was used to keep the discharge voltage sufficiently high. To achieve this the cathode surface can be altered by sliding a glass tube inside the cathode. Maximum signal to noise ratios are achieved with an uncovered cathode length of about 2 cm, yielding a discharge current of 5 mA at a voltage of 1.6 kV. However, after half an hour of operation the discharge became instable, which turned out to be the result of the sputtering of the stainless steel on the glass tube. The resulting metal layer on the inner side increased the cathode surface, thereby changing the discharge conditions substantially. Therefore, we tried a 1 cm long stainless steel cathode, without glass tube, which turned out to be a good alternative (fig. 4.1). Normal discharge conditions are 4 mA at 1 kV. Signals of the isotopic species KrH<sup>+</sup> and KrD<sup>+</sup> are generated with a mixture of Kr and H<sub>2</sub> or D<sub>2</sub> in a ratio of about 1:4.

### 4.3 Results

Direct absorption spectroscopy of molecular ions in the far infrared frequency range is usually performed with the use of a hollow cathode discharge cell [15] or a cell with a magnetically extended negative glow [14]. To determine the production efficiency we first tried to detect KrH<sup>+</sup> and KrD<sup>+</sup> in a hollow cathode discharge. A typical result is shown in figure 4.2. The transition frequencies can be calculated very accurately with the Dunham coefficients obtained from infrared emission [11] and microwave work [12]. We have detected several transitions and the measured frequencies agree within 1 or 2 MHz with the calculated ones.

The transitions of KrH<sup>+</sup> (J=1←0) and KrD<sup>+</sup> (J=2←1) around 500 GHz are detected, using the harmonics of a 70 GHz klystron. The frequencies around 1500 GHz are generated, using the first sideband of a 80 GHz klystron and the 9R(34) CO<sub>2</sub> laser pumped CH<sub>2</sub>F<sub>2</sub> far infrared line at 1 397 118.6 MHz. Unfortunately it is not possible to measure the J= 3←2 of KrD<sup>+</sup> at 754 GHz, due to strong H<sub>2</sub>O absorption centered at 752 GHz. The same holds for the J= 2←1 of KrH<sup>+</sup> at 988.8 GHz, due to strong absorption around 987.8 GHz [16]. The KrH<sup>+</sup> J= 3←2 transition at 1482 GHz is very strong, even stronger than transitions of the well known "strong absorbers" N<sub>2</sub>H<sup>+</sup> and HCO<sup>+</sup>. The KrH<sup>+</sup> J= 1←0 transition is weaker. Assuming Doppler broadening and a rotational temperature of 150 K, the calculated ratio of the peak absorptions at 1500 and 500 GHz, amounts

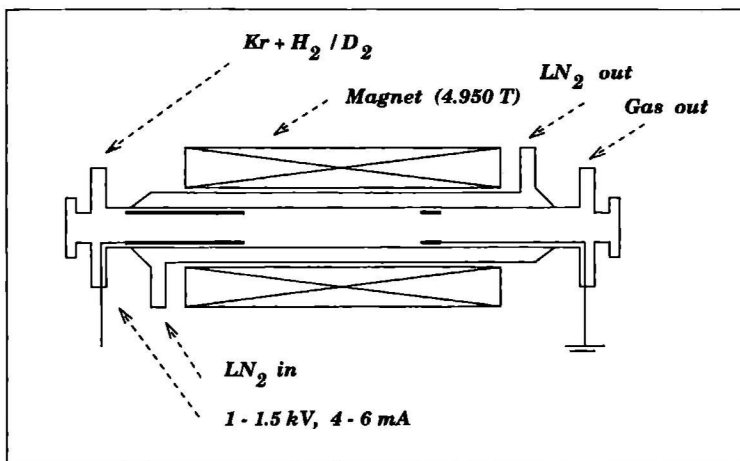


**Figure 4.1:** The modified magnetically extended negative glow discharge for measurements in high magnetic fields with a small fixed cathode surface in order to circumvent sputtering problems.

to approximately 5. However, from an experimental point of view it is easier to perform the dipole measurements on the 500 GHz transitions, because the frequencies of both  $\text{KrH}^+$  and  $\text{KrD}^+$  can be generated with the harmonics of one single klystron. This has the advantage that the frequency can be determined more precisely, since no far infrared laser is involved. Furthermore, Doppler broadening is increased by a factor of three at 1500 GHz, which increases the error in determining the frequency.

The Zeeman splittings of the  $J=1 \leftarrow 0$  transition of  $^{84}\text{KrH}^+$  and the  $J=2 \leftarrow 1$  transition of  $^{84}\text{KrD}^+$  are recorded in a magnetic field of 4.950 T, using a superconducting magnet (BOC, 7T) in the modified discharge. The measured transitions are shown in figure 4.3 and 4.4. The spectra are computer recorded and a curve fitting with 500 points per line is carried out. Each Zeeman component is fitted with a Gaussian profile determined by three parameters: the height, the transition frequency and the width of the line. The result of the curve fits is also shown in these figures. The SNR of the  $\text{KrH}^+$  lines turns out to be an order of magnitude smaller than that of the  $\text{KrD}^+$ . This is probably due to a worsening of the discharge conditions during the measurements. The results from two successive scans of the same isotopic species deviated by less than 25 kHz for the  $\text{KrD}^+$  and by less than 100 kHz for the  $\text{KrH}^+$ . The results are listed in table 4.1.

#### 4.4 Theory

The Zeeman energy for a linear  $^1\Sigma$  molecule is given by  $E = g_R \beta_I M_J H$  ( $H$  magnetic field,  $\beta_I$  nuclear magneton). In a magnetic field perpendicular to the polarization of the laser, pure rotational transitions split as  $\nu = \nu_0 \pm \beta_I g_R H$  where  $\nu_0$  is the zero field transition and the  $\pm$  corresponds to allowed  $\Delta M = \pm 1$  transitions. This means that two separate transitions can be observed, split by  $\Delta\nu = 2g_R \beta_I H$ .



If the same magnetic field is used for measurements on two isotopically substituted species, equation 4.6 can be modified to

$$\mu = -\frac{eh}{16\pi^2 M_p \Delta z} \frac{1}{2\beta_I H} \left( \frac{\Delta\nu'}{B'} - \frac{\Delta\nu}{B} \right) + \frac{1}{2} Qe \Delta z \quad (4.7)$$

with  $\Delta z$  being the shift in the center-of-mass upon isotopic substitution ( $z' = z - \Delta z$ ) and with  $\Delta\nu$  and  $\Delta\nu'$  the Zeeman splittings for the two species. In this way  $\mu$  is directly related to the experimentally determinable parameters  $\Delta\nu$ ,  $B$  and  $H$ .

The application of equation 4.7 is based on the assumption that the structure of the molecule remains constant upon isotopic substitution. This implies that only the center-of-mass is shifted, while the distance between the atoms is kept constant. An internuclear distance  $r_{KrH^+} = 1.42 \text{ \AA}$  [10, 12] leads for the substitution  $^{84}\text{KrH}^+ \leftrightarrow ^{84}\text{KrD}^+$  to a value for  $\Delta z$  of  $0.0163 \text{ \AA}$ . This is in the same order of magnitude as for the  $^{14}\text{N} \leftrightarrow ^{15}\text{N}$  substitution in  $\text{N}_2\text{H}^+$ . However, in case of  $\text{KrH}^+$  also the effect of zero point vibrations has to be taken into account.

The zero point vibration causes the vibrationally averaged  $r$ -value ( $r_0$ ), being the distance between the atoms, to deviate from  $r_e$ , the common equilibrium value for all isotopic species. This was discussed in detail in [5]. The experimentally determined Zeeman splitting will yield  $g(r_0)$  rather than  $g(r_e)$ . It was therefore tried in the  $\text{ArH}^+$  measurements [5] to extrapolate the  $g_R$ -factor for both isotopes to  $r_e$  and by subsequently use of equation 4.7 to determine  $\mu(r_e)$ . In the  $\text{N}_2\text{H}^+$  experiment [6] this procedure was not necessary, because the "heavy" N-atom was substituted so

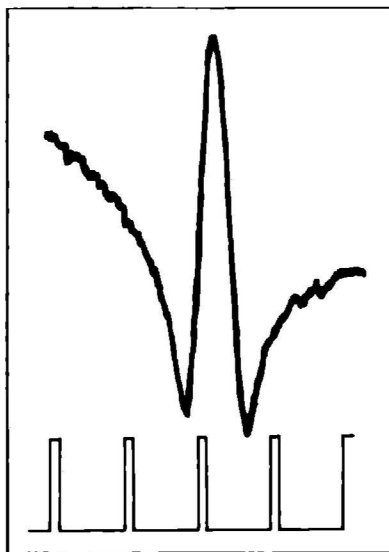


**Figure 4.2:** Recording of the  $J=1 \leftarrow 0$  transition of  $^{84}\text{KrH}^+$  in the hollow cathode discharge. The distance between two markers amounts to 5 MHz.

Ion	Component	Frequency	Splitting	$g_R$
$^{84}\text{KrD}^+$	Low	503010.7580	→ 21.064	- 0.279113
	High	503031.8215		
$^{84}\text{KrH}^+$	Low	494494.452	→ 41.846	- 0.554489
	High	494536.298		

**Table 4.1:** The Zeeman splitting for  $^{84}\text{KrH}^+$  and  $^{84}\text{KrD}^+$  in a magnetic field of 4.950 T with resulting  $g_R$ -factors.

that the influence of zero point vibrations for different isotopic species is neglectable indeed. For  $\text{KrH}^+/\text{KrD}^+$  as well as for  $\text{ArH}^+/\text{ArD}^+$  this is not the case.

A natural way to circumvent this problem is by measuring the splitting for  $^{86}\text{KrD}^+$  relative to the value found for  $^{84}\text{KrD}^+$ . But the accuracy that could be achieved in determining the line positions together with the very small value of  $\Delta z$  for  $^{84}\text{KrD}^+ \leftrightarrow ^{86}\text{KrD}^+$  substitution, was not sufficient to yield a significant value for  $\mu$ . For this reason an alternative approach to deduce the vibrational equations is followed.

The rotational  $g$ -factor can be expressed as a sum of nuclear and electronic contributions [17].

$$g_R(r) = g_{nuc} + g_{el} = \frac{M_p}{I(r)} \sum_k Z_k z_k^2 - \frac{2M_p}{mI(r)} \sum_{n \neq 0} \frac{|\langle n | L_x | 0 \rangle|^2}{E_n - E_0} \quad (4.8)$$

where  $M_p$  is the proton mass,  $m$  the electron mass,  $Z_k$  the charge and  $z_k$  the coordinate of nucleus  $k$ .  $L_x$  is the electronic angular momentum about the  $x$ -axis,  $E_n$  and  $E_0$  are the energy of the electronically excited state  $n$  and ground state  $0$  and  $I(r)$  is the moment of inertia ( $m_{red}r^2$ ). From here on we will use unprimed quantities for  $\text{KrH}^+$  and primed quantities for  $\text{KrD}^+$ .

While  $g_{nuc}$  can be shown to be independent of  $r$ , this is not the case for  $g_{el}$ . If we assume that  $\sum_{n \neq 0} \frac{|\langle n | L_x | 0 \rangle|^2}{E_n - E_0}$  is independent of  $r$ ,  $g_{el}$  would vary as  $I^{-1}$ , according to the equation above. This assumption seems reasonable for well separated electronic states, like in  $\text{KrH}^+$ , where the sum should be nearly constant for small variations of  $r$ . Therefore we would expect an  $r$ -dependence of  $g_{el}$  as  $r^{-2}$ . We then can obtain the dipole moment in two simple cases:

1.  $g_R$  dominated by  $|g_{nuc}|$

In this case  $g_R = g_{nuc}$  is independent of  $r$ . This implies that  $g_R(r_e) = g_R(r_0)$ , where  $g_R(r_0)$  corresponds to the measured quantities. Using this we can determine  $\mu(r_e)$  according to:

$$\mu(r_e) = -\frac{eh}{16\pi^2 M_p \Delta z} \left( \frac{g'_R(r_e)}{B'_e} - \frac{g_R(r_e)}{B_e} \right) + \frac{1}{2} Q_e \Delta z \quad (4.9)$$

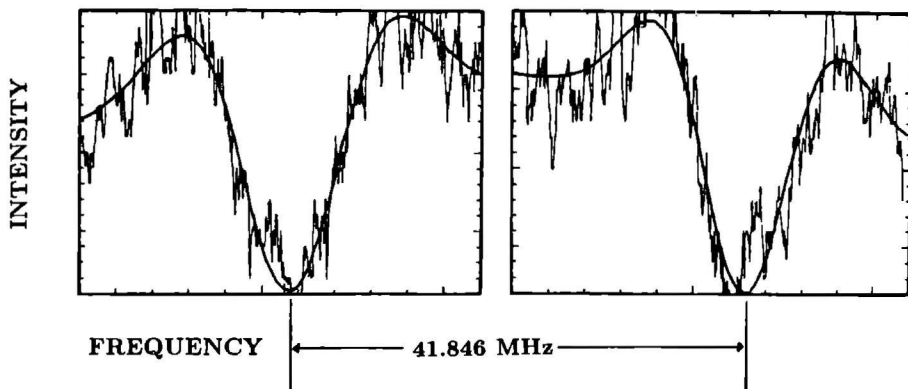
SPLITTING OF  $\text{KrH}^+$ 

Figure 4.3: The experimental and fitted line splittings for the  $^{84}\text{KrH}^+$  ( $J=1\leftarrow 0$ ) transition in a magnetic field of 4.950 T.

## 2. $g_R$ dominated by $g_{el}$

We now have to extrapolate the  $g_R (= g_{el})$  values to a *common*  $r$  value which not necessarily has to coincide with the equilibrium distance  $r_e$  and for convenience we have extrapolated  $g'_R$  and  $g_R$  to  $r_0$ , the mean  $r$  value of  $\text{KrH}^+$  at  $v=0$ . Therefore the measured  $g'_R$  value,  $g'_R(r'_0)$ , where  $r'_0$  is the mean  $r$  value of  $\text{KrD}^+$  at  $v=0$  ( $r_0 \neq r'_0$ ), has to be extrapolated to  $g'_R(r_0)$ . If we assume that  $g_{el} \propto r^{-2}$ , then

$$g'_R(r_0) = g'_R(r'_0) \left( \frac{r'_0}{r_0} \right)^2 \quad (4.10)$$

$$B'(r_0) = B'(r'_0) \left( \frac{r'_0}{r_0} \right)^2 \quad (4.11)$$

This results in:

$$\mu(r_0) = -\frac{eh}{16\pi^2 M_p \Delta z} \left( \frac{g'_R(r'_0)}{B'(r'_0)} - \frac{g_R(r_0)}{B(r_0)} \right) + \frac{1}{2} Qe \Delta z \quad (4.12)$$

where  $\frac{g'_R(r'_0)}{B'(r'_0)} = \frac{g'_R(r_0)}{B'(r_0)}$ , as can be seen from equations 4.10 and 4.11.

Ion	$g_R$	$g_{nuc}$	$g_{el}$
$\text{KrD}^+$	-0.279113	0.494917	-0.77403
$\text{KrH}^+$	-0.554489	0.985555	-1.54004

**Table 4.2:** The nuclear and electronic contribution to the  $g_R$ -factor.

If we apply these equations to our data, we obtain in the first case an electric dipole moment of  $\mu(r_e) = 1.0$  D. In the second case we find an absolute value for  $g'_R(r_0) = g'_R(r'_0) \left(\frac{r'_0}{r_0}\right)^2 = 0.2777829$ , resulting in a value of  $\mu(r_0) = 1.8$  D.

We will now describe the case where neither of the two limiting cases is applicable. From equation 4.8 we find that  $g_{nuc}^{\text{KrH}^+} = 0.985555$  and that  $g_{nuc}^{\text{KrD}^+} = 0.494917$ . Before we can calculate  $g_{el}$  according to  $g_{el} = g_R - g_{nuc}$ , we have to know the sign of  $g_R$ .

Since  $\mathbf{d}$  is pointing in the direction from the hydrogen atom towards the Kr atom, a negative difference of  $\left(\frac{g'_R}{B} - \frac{g_R}{B}\right)$  implies that  $\mu$  is pointing from H towards Kr (polarity  $^+\text{Kr-H}^-$ ). A positive difference means that  $\mu$  is pointing from Kr in the direction of H (polarity  $^-\text{Kr-H}^+$ ). *Ab initio* calculations clearly predict the polarity  $^-\text{Kr-H}^+$ . By putting in the measured  $g_R$  and B values, we see that in this case  $g_R$  and  $g'_R$  have to be negative, assuming that they have the same sign. From the calculated values for  $g_{nuc}$  we then find the values listed in table 4.2.

### SPLITTING OF $\text{KRD}^+$

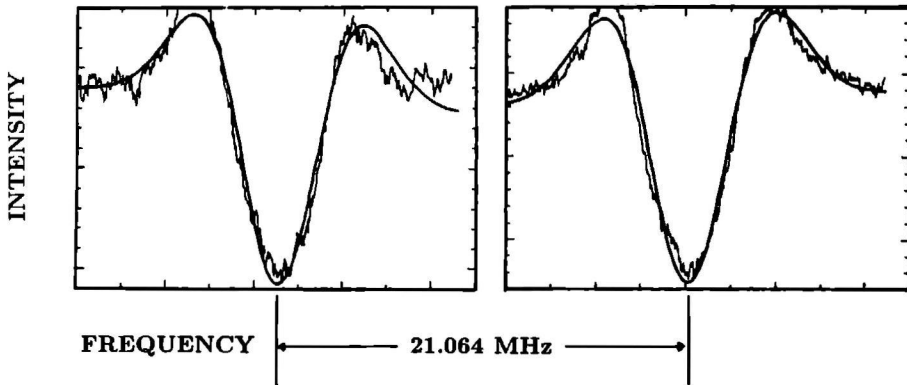


**Figure 4.4:** The experimental and fitted line splittings for the  $^{84}\text{KrD}^+$  ( $J=2-1$ ) transition in a magnetic field of 4.950 T.

Now  $g_R$  can be extrapolated by

$$g'_R(r_0) = g'_{nuc} + g'_{el}(r'_0) \left(\frac{r'_0}{r_0}\right)^2 \quad (4.13)$$

if we assume that  $\sum_{n \neq 0} \frac{|\langle n | L_z | 0 \rangle|^2}{E_n - E_0}$  is really independent of  $r$ .  $r_0$  and  $r'_0$  are calculated according to the formula  $r^2 = \frac{505379}{Bm_{red}}$  (MHz  $\text{\AA}^2$  amu) using the results of Johns *et al* [11]. This can also be considered as an approximation. We then obtain a dipole moment of  $\mu = 3.0$  D.

## 4.5 Summary

Summarizing it can be concluded that different methods of extrapolating the *same* experimental data result in different values for the electric dipole moment which do not agree within their experimental uncertainty (about 0.3 D). From this we can state that although the experimental accuracy is very good we are not able to obtain a final value for the dipole moment without more information on the  $r$ -dependence of  $g_{el}(r)$ .

Whereas in the paper of Laughlin *et al* [5] the correction of  $\mu$  by extrapolating  $r$  is estimated smaller than 0.6 D, we find a much bigger influence on the final value of the dipole moment. It is also intriguing to note that the  $g_R$  for  $\text{KrH}^+$  was found to be negative. We should therefore expect to find also a negative  $g_R$  value for  $\text{ArH}^+$ , but according to [18], the sign was determined to be positive by comparing  $\text{ArH}^+$  with CO which was found to have opposite sign for  $g_R$  and by using the result that CO has a negative  $g$ -factor [4]. So far we have no explanation for this discrepancy.

We found evidence for a major influence of the zero point vibrations on the experimentally determined dipole moment using the method of Townes *et al* [2] and substituting  $\text{H} \leftrightarrow \text{D}$  for  $^{84}\text{KrH}^+$ . This influence does not allow to obtain a proper result for the experimental value of the dipole moment as long as the  $r$ -dependence of  $g_{el}$  is not exactly known. This problem can be overcome, in principle, by substituting the heavy Kr component. However, under the experimental conditions used the results were too inaccurate to yield a final value and to be able to make a quantitative comparison of heavy vs. light partner substitution.

## Acknowledgment

We want to thank Eugène van Leeuwen and John Holtkamp for indispensable technical assistance. This work was supported by the European Community under grant (EC 892 001 59 / OP1).

## References

- [1] M. Havenith, Infrared spectroscopy of van der Waals complexes and ions, Ph.D. Thesis, Institut für Angewandte Physik der Universität Bonn (1990).
- [2] C.H. Townes, G.C. Dousmanis, R.L. White and R.F. Schwarz, *Discuss. Faraday Soc.* 19 (1955) 56.
- [3] K.B. Laughlin, G.A. Blake, R.C. Cohen, D.C. Hovde, R.J. Saykally, *Phys. Rev. Lett.* 58 (1987) 996.

- [4] K.B. Laughlin, G.A. Blake, R.C. Cohen, D.C. Hovde and R.J. Saykally, *Phil. Trans. R. Soc. Lond. A*, 324 (1988) 109.
- [5] K.B. Laughlin, G.A. Blake, R.C. Cohen and R.J. Saykally, *J. Chem. Phys.* 90 (1989) 1358.
- [6] M. Havenith, E. Zwart, W. Leo Meerts and J.J. ter Meulen, *J. Chem. Phys.* 93 (1990) 8446.
- [7] P. Rosmus, *Theor. Chim. Acta* 51 (1979) 359.
- [8] P. Botschwina, *Chem. Phys. Lett.* 107 (1984) 535.
- [9] M. Gruebele, E. Keim, A. Stein and R.J. Saykally, *J. Mol. Spectrosc.* 131 (1988) 343.
- [10] P. Rosmus and E.A. Reinsch, *Z. Naturforsch. Teil A* 35 (1980) 1066.
- [11] J.W.C. Johns, *J. Mol. Spectrosc.* 106 (1984) 124.
- [12] H.E. Warner, W.T. Connor and R.C. Woods, *J. Chem. Phys.* 81 (1984) 5413.
- [13] P. Verhoeve, E. Zwart, M. Versluis, M. Drabbels, J.J. ter Meulen, W.L. Meerts, A. Dymanus and D.B. McLay, *Rev. Sci. Instrum.* 61 (1990) 1612.
- [14] F.C. de Lucia, E. Herbst, G.M. Plummer and G.A. Blake, *J. Chem. Phys.* 78 (1983) 2312.
- [15] F.C. van den Heuvel and A. Dymanus, *Chem. Phys. Lett.* 92 (1982) 219.
- [16] R.T. Hall and J.M. Dowling, *J. Chem. Phys.* 47 (1967) 2454.
- [17] W. Gordy and R.L. Cook, *Microwave Molecular Spectra*, Interscience Publishers, N.Y. 1970.
- [18] B. Rosenblum, A.H. Nethercot and C.H. Townes, *Phys. Rev.* 109(2) (1958) 400.



# Tunable Infrared and Far Infrared Direct Absorption Spectroscopy of Molecular Ions in a Supersonic Jet Expansion <sup>5</sup>

G. Hilpert<sup>a</sup>, H. Linnartz<sup>b</sup>, M. Havenith<sup>a</sup>, J.J. ter Meulen<sup>b</sup>, W.L. Meerts<sup>b</sup>

<sup>a</sup> *Institut für Angewandte Physik, Wegelerstraße 8, D 53115 Bonn*

<sup>b</sup> *Department of Molecular and Laser Physics, University of Nijmegen, Toernooiveld, NL 6525 ED, Nijmegen*

### Abstract

A newly designed two dimensional corona excited slit nozzle discharge is described and its first applications for direct absorption spectroscopy of molecular ions in a supersonic expansion in the infrared ( $\text{NO}^+$ ) and far infrared ( $\text{N}_2\text{H}^+$ ). The results are discussed and it will be shown that under the conditions described, for  $\text{N}_2\text{H}^+$  linewidths of 750 kHz and rotational temperatures of 12 K can be achieved.

---

<sup>5</sup>This chapter is based on the article:  
Tunable infrared and far infrared direct absorption spectroscopy of molecular ions in a supersonic jet expansion; G. Hilpert, H. Linnartz, M. Havenith, J.J. ter Meulen, W.L. Meerts, *Chem. Phys. Lett.* 219 (1994) 384.



## 5.1 Introduction

Direct absorption spectroscopy of ions in the far infrared is usually performed with the use of hollow cathode or magnetically extended negative glow discharges (see e.g. [1, 2]). In both cases, the larger part of the discharge consists of a negative glow, which is an ion-rich discharge region. Although these glass tube discharges form very effective methods for the production of ions, they have the disadvantage of bad rotational cooling. Even with liquid nitrogen cooling, rotational temperatures are of the order of 100 K. Furthermore, number densities are low, since high pressures will make the discharge unstable and in the far infrared pressure broadening will become a serious problem. As a consequence complex formation will hardly take place. It is for this reason that until now just one ion complex, the  $\text{ArH}_3^+$  [3, 4], was found.

In infrared experiments ions are also generated in normal discharges. In this type of discharge the positive column is observed, where the ion density is lower as in the negative glow region. But normal discharges can be operated at much higher pressures and as long as pressure broadening is negligible, for this disadvantage can be made up. Moreover spectroscopy in the positive column allowed the introduction of velocity modulation, a sensitive ion-selective detection scheme [5] that initiated a great activity in the field of infrared ion spectroscopy. The cooling properties, however, are still very poor and although complex formation could take place, due to the higher pressures, no ion complexes have been observed until now. The reason is, that with the higher degree of freedom the number of states increases, which implies that the population density in each state is expected to be too small to be detected. For this reason cooling of ion complexes is highly desirable, since it should restrict the population to the lowest states. This can be achieved by combining expansion and discharge techniques.

In 1983 a realization of a corona excited supersonic expansion through a circular nozzle was reported by Droege and Engelking [6]. This technique turned out to be a very effective way to study radicals with LIF spectroscopy [7], but since the absorption length is small it is not a good alternative to direct absorption spectroscopy. Only  $\text{SH}^+$  was measured in a free expansion by Hovde and Saykally [8], using a setup similar to the one used by Droege and Engelking in combination with LMR techniques. In this case the detection was only possible since the sensitivity of the LMR setup was increased, compared to ordinary absorption spectroscopy. Another way to use expansions for direct absorption ion spectroscopy was reported by Coe *et al* [9], using fast ion beams. This complicated technique, that allows for mass selective detection at the same time, looked very promising, but the rotational temperatures achieved are still high (420-600 K) [10].

In general the absorption length in a point nozzle expansion is not sufficient. For this reason much work on expansion cooled radicals was performed using (pulsed) slit jets - where absorption lengths are longer - either combining it with excimer laser photolysis [11] or corona excitation [12]. Recently Comer and Foster [12] reported the use of a continuous corona excited supersonic slit nozzle expansion for the detection of CS and  $\text{NH}_2$ . Slit nozzles are more difficult to handle, but offer some advantages. The smaller Doppler widths associated with the planar expansion increase resolution and peak intensity. Furthermore the absorption length between molecular and laser beam is increased, yielding larger absorption signals. However, until now these techniques were not used for the detection of ions.

In this chapter the first direct absorption signals of ions in the infrared and far infrared are presented, with a continuous high voltage high pressure slit nozzle discharge. This type of discharge

has several advantages, compared to the bulk discharges, mentioned before:

- Small Doppler width, yielding narrow linewidths.
- Expansion cooled, yielding low rotational temperatures, which will simplify the analysis of complex spectra. But it also is a necessary condition for complex formation.
- A relatively simple setup, with small absorption lengths (typically 5 cm) but high molecular densities.

The slit nozzle discharge has also a major disadvantage in that a stable continuous expansion from a 5 cm x 150  $\mu\text{m}$  slit has to be maintained, which necessitate the use of very large pumps (3000-4000  $\text{m}^3/\text{hr}$ ). As a consequence the gas consumption is very large.

Here we report the first results on rovibrational transitions of  $\text{NO}^+$  (see also [13]) and rotational transitions of  $\text{N}_2\text{H}^+$  using a cw slit nozzle discharge. The nitrosyl ion is assumed to play an important role in atmospherical chemistry [14] and may exist in interstellar space [15]. Until now in the infrared only six rovibrational transitions in the  $X^1\Sigma^+$  ground state were measured [16]. From these transitions the band origin could be determined as well as the molecular parameters for the excited vibrational level, using the (sub)millimeter data found by Bowman *et al* [17].

$\text{N}_2\text{H}^+$  is a well known linear ion [1, 18], that is regarded to be of interstellar interest. In 1990 the electric dipole moment was determined experimentally by Havenith *et al* [19]. In this work we present several rotational transitions from which the rotational temperature can be determined. Furthermore it will be shown that with the new technique narrow linewidths for ions can be achieved.

## 5.2 Experimental

One of the problems in obtaining a stable discharge in a slit nozzle, is to extend the discharge over the whole length of the slit (5 cm). Since a discharge normally will run on a single point - from which the Droege-Engelking discharge benefits - it is necessary to use several independent electrodes, that are isolated from each other by resistances (100 k $\Omega$ ) and that are connected to the same high voltage power supply (figure 5.1). When the discharge does not run at one electrode, there will be no voltage drop over its resistor. The voltage at that specific electrode will become higher than the starting voltage of the discharge and a restart of the discharge at that point will be induced. In this way a quasi continuous discharge is created over the whole length of the slit. This is shown in the photograph.

It is important to choose the resistances in such a way that a restart of the discharge at one of the electrodes does not cause a voltage drop at its resistance below the burning value. This value is approximately two times smaller than the starting voltage.

In the experiments described, we have used slit nozzles of (5 cm x 150  $\mu\text{m}$ ) in which five to seven electrodes are mounted. Typical discharge conditions are 2 kV in front of the resistances, 50-80 mA, backing pressures of about 300 Torr and a pressure of 200 mTorr in the vacuum chamber during jet operation. The voltage across the discharge is typically around 500 V.

In the infrared experiment (Bonn) we have combined the computer controlled diode laser spectrometer [20] with a crossed molecular jet setup. As was reported by Huber and Vervloet [21]  $\text{NO}^+$  can be produced efficiently by diffusing NO on a beam of metastable He. This is expected

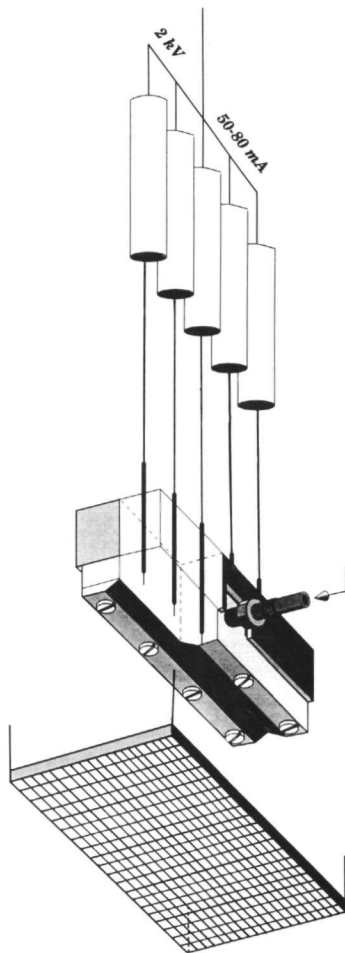


**Figure 5.1:** Experimental setup for a high voltage high pressure slit nozzle discharge for direct absorption spectroscopy of jet cooled molecular ions.

to be the best way to populate the excited  $^3\Sigma$  state, which is the future goal of our setup. In the experiment, described here, we have used the slit nozzle discharge to produce a stable source of  $\text{He}^*$ . The second slit nozzle (5 cm x 50  $\mu\text{m}$ ) - without discharge - is positioned perpendicular to the  $\text{He}^*$  jet, about 1.5 cm from the reaction centre. The infrared beam multipasses the reaction zone four times and the absorption signal can be detected both by frequency modulation, high voltage (HV) and double modulation [22]. The best results were obtained using HV modulation.

In the far infrared setup (Nijmegen) we have used the tunable sideband spectrometer, that was described in detail before [23]. The  $\text{N}_2\text{H}^+$  ions are generated in the expansion of a gas mixture of  $\text{N}_2$  and  $\text{H}_2$  flowed in a ratio of approximately 10:1 through the slit nozzle discharge. For the measurements on  $\text{N}_2\text{H}^+$  we have used higher harmonics of klystron radiation in the 60-80 GHz range, that are generated in a Schottky barrier diode. The radiation passes the discharge expansion about 1 to 1.5 cm under the slit and is focussed onto an InSb hot electron bolometer. The radiation is frequency modulated and detected at 2f by lock-in amplification. About 2.5 cm under the slit nozzle a fine wire grid is mounted (see also figure 5.1), which only slightly affects the expansion. This grid is connected to ground. The presence of the grid made the discharge much more stable. Since the discharge produces much electronic noise, the best way to overcome interferences with laboratory equipment is to let vacuum machinery and HV supply share the same ground. This has to be isolated from the laboratory ground circuit.



**Figure 5.2:** A photograph of the high voltage high pressure slit nozzle discharge, expanding a  $\text{N}_2/\text{H}_2$  mixture. On top the five electrodes can be seen. The discharge starts at the nozzle and ends on the grid. The far infrared beam is guided in between.

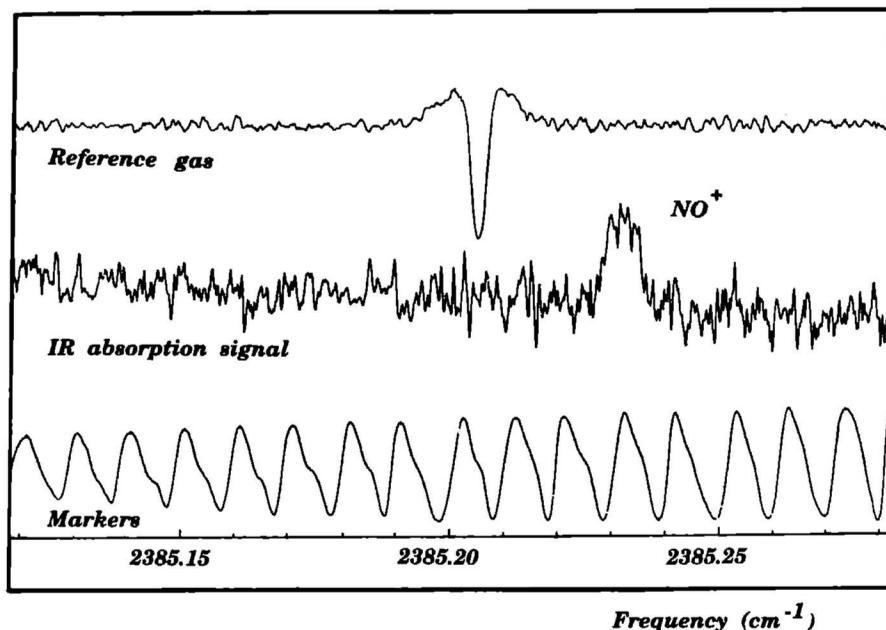


Figure 5.3: The  $P(10)$  transition for  $\text{NO}^+$  measured in a crossed jet setup. The upper line shows the reference gas ( $\text{H}_2\text{O}$ ), the lower line the marker etalons.

## 5.3 Results and discussion

### 5.3.1 $\text{NO}^+$

We have measured the R(8) and R(10) transition in the ground state of  $\text{NO}^+$  at  $2378.089\text{ cm}^{-1}$  and  $2385.2328\text{ cm}^{-1}$ , respectively. Using the constants derived by Ho *et al* [16] these observed values coincide within the experimental uncertainty with the calculated values. In figure 5.3 the R(10) transition is shown, measured with 8 kHz high voltage modulation. Since diode laser spectroscopy is limited by its mode scanning range of approximately 1 to  $1.5\text{ cm}^{-1}$  it is usually impossible to measure subsequent rovibrational transitions for molecules with large rotational constants. Furthermore different modes show different intensity characteristics. For these reasons it was not possible to determine a rotational temperature for the ions produced in this way. However, we expect the ions to be rotationally excited due to collisions. The rather large linewidth (200 MHz) is caused by the poor quality of the laser mode in this range, but we expect the lines to be collisionally broadened as well. Linewidths of the order of 30 MHz, as could be achieved for complexes formed in a slit expansion ( $\text{Ar-CO}$  [22] and  $(\text{CO})_2$  [24]), probably cannot be achieved in this way. On the contrary this method, using two crossed jets, should be the best way to tackle

Transition	FM Modulation (MHz)	Linestrengths (a.u.)
J: 2 → 3 (279 511.7 MHz)	0.85	11.8
	1.10	16.6
J: 3 → 4 (372 672.5 MHz)	0.85	9.75
	1.10	13.45

**Table 5.1:** Line intensities for J for J:3←2 and J:4←3 for different modulations.

the excited metastable electronic  $^3\Sigma$  state as is described in [21].

### 5.3.2 $N_2H^+$

We have studied the J:3←2 and 4←3 rotational transitions of  $N_2H^+$  at 279 511.7 and 372 672.5 MHz. A typical result is shown in figure 5.4.

By reducing the frequency modulation it is possible to obtain a minimal linewidth of  $(750\pm 50)$  kHz. This is not as small as is found for neutral expansions (typically 200 kHz) (see e.g. [25]). Probably this is due to the higher expansion velocity of the ions, caused by the potential difference between slit and fine metal wire grid and the temperature rise, induced by the discharge.

By comparing the linestrengths of several transitions, it is possible, to derive a rotational temperature for the  $N_2H^+$ . Starting from a Boltzmann distribution the relative line intensities for two J-levels (here J=2 and 3) is given by

$$T = \frac{E_{J_2} - E_{J_1}}{k \ln\left(\frac{2J_2+1}{2J_1+1} \frac{I_{J_2}}{I_{J_1}} \left(\frac{\nu_{J_2}}{\nu_{J_1}}\right)^2\right)} \quad (5.1)$$

where  $E_{J_2} - E_{J_1}$  gives the energy difference between the energy levels,  $k$  is the Boltzmann constant,  $I_J$  gives the line intensity and  $\nu$  the frequency for the labeled J level. In table 5.1 the linestrengths are shown for different frequency modulations and normalized for power deviations. From the results listed we calculate a rotational temperature of 12 K.

## 5.4 Conclusions

From the first measurements with the high voltage high pressure slit nozzle discharge we conclude that it is possible to generate rotationally cold ions. In case of a crossed jet setup both linewidth and rotational temperature are influenced by the collisional process. From the results of the far infrared experiment we expect smaller linewidths and substantially lower temperatures. However, to investigate the metastable  $^3\Sigma$  state of  $NO^+$ , this technique is probably the best way to follow, since no  $^3\Pi \rightarrow ^3\Sigma$  emission was found in an expansion where the NO is seeded in the He directly. The diffusion process seems to be essential [26].

In case of the  $N_2H^+$  formation in a discharge nozzle directly, low rotational temperatures can be achieved. Furthermore, since the expansion has a small Doppler width, narrow linewidths can be obtained. Both characteristics are important for a more accurate analysis of spectra. Since slit nozzle expansions form ideal sources for Van der Waals complexes [27] the combination with a

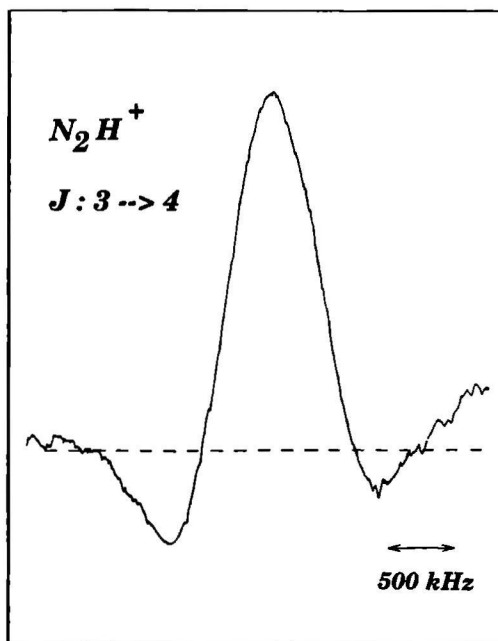


Figure 5.4: The  $J:3 \rightarrow 4$  transition for  $N_2H^+$  measured in the slit nozzle discharge ( $RC=10s$ ).

discharge will form an effective way for the investigation of weakly bond radicals (like Ar-OH or Ar-NH) or ion complexes, which until now have not been investigated successfully with infrared and far infrared techniques. Furthermore it turns out that the discharge can be operated relatively easily and that it is stable during long periods ( $> 10$  hours). The discharge sometimes shows dark regions between the electrodes, but this can be improved by using more independent electrodes.

We conclude, that the high voltage high pressure continuous slit nozzle discharge offers a good alternative to the conventional discharge techniques. It has several advantages, that will simplify spectroscopic studies. But the main point of interest is, that it probably offers the possibility to investigate a class of molecules, that could not be studied until now by direct absorption techniques: the radical and ion complexes.

### Acknowledgment

We want to thank Mr. Frans van Rijn (Nijmegen), D. Rossrucker and F. Wenisch (Bonn) for excellent technical assistance. This work was supported by the European Community under grant EC 892 001 59/OP1.

### References

- [1] F.C. van den Heuvel and A. Dymanus, Chem. Phys. Lett. 92 (1982) 219.

- [2] F.C. de Lucia, E. Herbst, G.M. Plummer and G.A. Blake, *J. Chem. Phys.* 78 (1983) 2312.
- [3] M. Bogey, H. Bolvin, C. Demuyne, J.L. Destombes, *Phys. Rev. Lett.* 58 (1987) 988.
- [4] M. Bogey, H. Bolvin, C. Demuyne, J.L. Destombes, B.P. van Eijck, *J. Chem. Phys.* 88 (1988) 4120.
- [5] C.S. Gudeman, M.H. Begemann, J. Pfaff and R.J. Saykally, *Phys. Rev. Lett.* 50 (1983) 727; C.S. Gudeman, R.J. Saykally, *Ann. Rev. Phys. Chem.* 35, (1984) 387.
- [6] A.T. Droege and P.C. Engelking, *Chem. Phys. Lett.* 96 (1983) 316.
- [7] P.G. Carrick and P.C. Engelking, *J. Chem. Phys.* 81, (1984) 1661; S.D. Brossard, P.G. Carrick, E.L. Chappell, S.C. Hulegard and P.C. Engelking, *J. Chem. Phys.* 84, (1986) 2459; E.L. Chappell and P.C. Engelking, *J. Chem. Phys.* 89 (1988) 6007.
- [8] D.C. Hovde and R.J. Saykally, *J. Chem. Phys.* 87, (1987) 4332.
- [9] J.V. Coe, J.C. Owrutsky, E.R. Keim, N.V. Agman, D.C. Hovde, R.J. Saykally, *J. Chem. Phys.* 90 (1988) 3893.
- [10] E.R. Keim, M.L. Polack, J.C. Owrutsky, J.V. Coe and R.J. Saykally, *J. Chem. Phys.* 93 (1990) 3111.
- [11] R.F. Curl, K.K. Murray, M. Petri, M.L. Richnow and F.K. Tittle, *Chem. Phys. Lett.* 161 (1989) 98; R.C. Cohen, K.L. Busarow, C.A. Schuttenmaer, Y.T. Lee and R.J. Saykally, *Chem. Phys. Lett.* 164 (1989) 321.
- [12] K.R. Comer and S.C. Foster, *Chem. Phys. Lett.* 202 (1993) 216.
- [13] M. Havenith, G. Hilpert, H. Linnartz, W. Urban, Book of abstracts, p B9, 22<sup>nd</sup> international symposium on free radicals (6-10 september 1993), Doorwerth, The Netherlands
- [14] A.T. Stair and H.P. Gauvin, *Aurora and Airglow*, 365 (1967) - (Reinhold, New York).
- [15] E. Herbst and W. Klemperer, *Astrophys. J.* 185, (1973) 505.
- [16] W.C. Ho, I. Ozier, D.T. Cramb, M.C.L. Gerry, *J. Mol. Spectr.* 149 (1991) 559.
- [17] W.C. Bowman, E. Herbst, F.C. De Lucia, *J. Chem. Phys.* 77 (1982) 4261.
- [18] J.P. Bekooy, P. Verhoeve, W.L. Meerts and A. Dymanus, *J. Chem. Phys.* 82 (1985) 3868.
- [19] M. Havenith, E. Zwart, W.L. Meerts and J.J. ter Meulen *J. Chem. Phys.* 93 (1990) 8446.
- [20] R. Brügemann, M. Petri, H. Fischer, D. Mauer, D. Reinert, W. Urban, *Appl. Phys. B.* 48 (1989) 105.
- [21] K.P. Huber and M. Vervloet, *J. Mol. Spectr.* 146, (1991) 188.
- [22] M. Havenith, G. Hilpert, M. Petri, W. Urban, *Mol. Phys.* 81 (1994) 1003.
- [23] P. Verhoeve, E. Zwart, M. Versluis, M. Drabbels, J.J. ter Meulen, W.L. Meerts, A. Dymanus and D.B. McLay, *Rev. Sci. Instrum.* 61 (1990) 1612.
- [24] M. Havenith, M. Petri, C. Lubina, G. Hilpert, W. Urban, *J. Mol. Spectrosc.*, accepted.
- [25] H. Linnartz, A. Kips, W.L. Meerts, M. Havenith, *J. Chem. Phys.* 99 (1993) 2449.



[26] M. Vervloet, private communication.

[27] D. Perry in "Laser Techniques in Chemistry", ed. T. Rizzo and A. Myers (Wiley, expected 1994).

## Infrared and Far Infrared Spectroscopy on Transient Molecules

Each molecule reacts different when it is irradiated with light. It has, so to say, its own spectroscopic fingerprint; the molecule spectrum. This spectrum is unique. It is the reflection of all possible energy levels in the molecule and as such of the motions that can occur within the molecule. A good comprehension of the spectrum therefore makes it possible to understand matter at the very fundamental level of molecular motions. This is the guiding principle for the chapters described here.

In this thesis experiments are described on complexes and ions, molecules that are transient under normal conditions. Complexes are the topic of the first part and ions of the second part. The investigated frequency range covers the infrared and far infrared part of the electromagnetic spectrum. These frequencies typically correspond to low energetic motions and it pre-eminently can be used to study weakly bound complexes. The infrared radiation is generated with CO<sub>2</sub> or diode lasers and the far infrared radiation with the Nijmegen tunable far infrared sideband spectrometer. The experimental setup for the latter one is described in chapter 1. The applied technique is direct absorption spectroscopy.

In the second chapter the "ammonia dimer riddle" is point of discussion. In the last years a large number of weakly bound molecular complexes has been investigated in order to gain a better insight in the complex dynamics of weak intermolecular interactions. The (NH<sub>3</sub>)<sub>2</sub> turned out to be of special interest in providing unsolvable problems, both from a structural and dynamical point of view. This is described in the introduction of chapter 2. These problems were caused partly due to the wrong assumptions that the NH<sub>3</sub> monomer umbrella inversion is completely quenched and that the complex as a whole is rigid. In the second part of this chapter an infrared - far infrared double resonance experiment is described. From this it is concluded that the ammonia monomer inversion, actually, contributes to the internal dynamics and that the ammonia dimer is not a rigid complex. Remains the structural problem. This is point of discussion in the third part of chapter 2. By studying the Stark shifts and splittings of the vibration-rotation-tunneling states in a homogeneous electric field, explicitly taking into account the monomer inversion, the electric dipole moment for one of the tunneling states can be determined, yielding structural information.

Furthermore it confirms once again that the ammonia dimer is a very floppy molecule. In the last part of chapter 2 an additional infrared - far infrared double resonance experiment is described in order to obtain a state selective assignment of the infrared spectrum.

In the case of dimers, recently also trimers, a lot of molecule specific information can be obtained from high resolution spectroscopy. However, experimental investigations on weakly bound complexes consisting of more than two or three molecules are difficult since the conventional techniques (molecular beams) are not size selective. In case of high resolution techniques it is not necessary, in principle, to be size selective, but since the spectral information in most cases is very congested and since it is not clear *a priori* which transitions belong to which cluster sizes, a detailed analysis normally is an endless job. For these reasons spectroscopic information has to be obtained in another way. In the introduction of chapter 3 a method is described in which the combination of a kinematical process - scattering of a cluster beam from a rare gas beam - and mass spectrometry allows for size selective detection. The subsequent infrared excitation of the size selected cluster beam can cause photodissociation. If the photon energy is larger than the binding energy of the cluster, energy redistribution induces the predissociation of the complex, i.e. the rupture of the van der Waals bond. By determining the dissociation signal as function of the infrared frequency structural information can be obtained. This is demonstrated in the second and third part of chapter 3 by measurements on  $(\text{CH}_3\text{NH}_2)_n$  and  $(\text{OCS})_n$  clusters for  $n=2$  to 6.

In the second part of this thesis, chapters 4 and 5, experiments are described on charged molecules, ions. Experimental data allow for a verification of *ab initio* calculations that for many ions are known to be very precise. Furthermore, ions are assumed to play an important role in interstellar chemistry. By comparing the frequencies of the radiation received from outer space with laboratory data a picture can be formed of what is going on outside Earth's atmosphere. To be able to do so it is necessary that ions can be produced in densities high enough to be detectable by direct absorption. In chapter 4, in which measurements on  $\text{KrH}^+$  and  $\text{KrD}^+$  are described, this is achieved with the use of a hollow cathode discharge and a magnetically extended negative glow discharge. The magnetic field in the latter one is further used to determine the Zeeman splittings for different isotopes. From the difference in splittings the permanent electric dipole moment can be calculated, although this is complicated by non-negligible vibrational effects. In chapter 5 a new production source for molecular ions is used; a high voltage high pressure slit nozzle discharge. This technique has several advantages compared to the conventional discharge techniques that are used in direct absorption spectroscopy; the linewidths can be reduced by more than a factor of two and the ions can be produced rotationally cold. This is demonstrated by measurements in the infrared for  $\text{NO}^+$  and in the far infrared for  $\text{N}_2\text{H}^+$ .

## Infrarode en Ver Infrarode Spectroscopie aan Kort Levende Moleculen

Wanneer een molecuul met licht wordt beschonen reageert het slechts op een aantal welbepaalde kleuren. Het heeft als het ware zijn eigen spectroscopische vingerafdruk; het molecuulspectrum. Dit spectrum is voor ieder molecuul uniek. Het is de weerspiegeling van de mogelijke energie toestanden van het molecuul en daarmee van de mogelijke bewegingen zoals die zich afspelen in het molecuul zelf of van het molecuul als geheel. Een goed begrip van het spectrum maakt het derhalve mogelijk om op het niveau van vrije moleculen te begrijpen wat er met de materie aan de hand is. Dit is het doel dat als een (infra)rode draad door de diverse hoofdstukken loopt.

In dit proefschrift wordt het onderzoek beschreven naar complexen en ionen, moleculen die onder normale omstandigheden kort levend zijn. Complexen vormen het onderwerp van het eerste deel en ionen van het tweede deel van dit proefschrift. Het onderzochte frequentie bereik is het infrarode en ver infrarode deel van van het elektromagnetische spectrum. Deze straling correspondeert typisch met laag energetische bewegingen en kan bij uitstek worden gebruikt voor de bestudering van zwak gebonden complexen. De infrarode straling wordt gegenereerd met  $\text{CO}_2$  of diode lasers en de ver infrarode straling met de Nijmeegse ver infrarode zijband spectrometer. Deze opstelling wordt kort in het eerste hoofdstuk beschreven, evenals de techniek van directe absorptie spectroscopie.

In het tweede hoofdstuk wordt ingegaan op het "Ammoniak dimeer probleem". In de afgelopen jaren is een groot aantal zwak gebonden moleculaire complexen onderzocht met het doel een beter inzicht te krijgen in de complexe dynamica van zwakke intermoleculaire interacties. Het  $(\text{NH}_3)_2$  bleek daarbij voor zowel structureel als dynamisch onoplosbare problemen te zorgen. Dit staat beschreven in het inleidende stuk van hoofdstuk 2. Deze problemen ontstonden mede door de niet correcte aannamen dat de  $\text{NH}_3$  monomeer inversie geheel onderdrukt is in het complex en dat het complex als zodanig star is. In het tweede deel van dit hoofdstuk wordt een infrarood - ver infrarood twee kleuren experiment beschreven. Hiermee wordt aangetoond, dat de ammoniak monomeer inversie wel degelijk een belangrijke bijdrage levert aan de intermoleculaire dynamica en dat het ammoniak dimeer niet als een star complex mag worden beschouwd. Resteert het structurele probleem. Hierop wordt in het derde deel van hoofdstuk 2 ingegaan. Door de verschuivingen en opsplitsingen van de vibratie-rotatie-tunnel niveaus in een elektrisch veld te bestuderen, is met de

wetenschap dat de  $\text{NH}_3$  inversie slechts deels is onderdrukt, het elektrisch dipoolmoment voor een van de tunneltoestanden bepaald met behulp van het Stark effect. Behalve in structurele informatie resulteert dit wederom in de bevestiging dat het ammoniak dimeer een "floppy" karakter heeft. In het laatste deel van hoofdstuk 2 wordt nogmaals een infrarood - ver infrarood twee kleuren experiment beschreven, nu met het doel een toestandsselectieve toekenning van het infrarode spectrum te verkrijgen.

In het geval van dimeren, recentelijk ook trimeren, kan met behulp van hoge resolutie spectroscopie veel molecuul specifieke informatie worden verkregen. Echter het experimentele onderzoek naar vrije complexen bestaande uit meer dan twee of drie moleculen wordt vooral bemoeilijkt door de gebrekkige grootte selectiviteit van de gangbare technieken. Wanneer gebruik wordt gemaakt van hoge resolutie technieken is het in principe weliswaar niet noodzakelijk om clusters op grootte te selecteren, maar omdat de spectrale informatie in het algemeen zeer overvloedig is en het *a priori* niet duidelijk is welke overgangen bij welke cluster grootte horen, is een uitvoerige analyse veelal onbegonnen werk. Spectroscopische informatie moet daarom op een andere manier worden verkregen. In de inleiding van het derde hoofdstuk wordt een techniek beschreven waarmee door middel van een kinematisch proces - de verstrooiing van een clusterbundel aan een edelgasbundel - en de daarop volgende massaspectrometrie, grootte gevoelige detectie mogelijk is. De simultane infrarood excitatie van de geselecteerde bundel induceert fotodissociatie. Door de mate van dissociatie te bepalen als functie van de infrarood frequentie kan vervolgens structurele informatie worden verkregen. In het tweede en derde deel van hoofdstuk 3 wordt dat geïllustreerd met metingen verricht aan  $(\text{CH}_3\text{NH}_2)_n$  en  $(\text{OCS})_n$  clusters met  $n=2-6$ .

In het tweede deel van dit proefschrift, de hoofdstukken 4 en 5, worden experimenten beschreven aan geladen moleculen, ionen. Experimentele data maken een verificatie mogelijk van de in het algemeen zeer nauwkeurige *ab initio* berekeningen voor ionen. Verder spelen ionen een belangrijke rol in de interstellaire chemie. Door de straling zoals die uit het heelal wordt ontvangen te vergelijken met de spectroscopische vingerafdruk die in het laboratorium wordt gemeten, kan er een beeld worden gevormd van wat er buiten onze dampkring gaande is. Een belangrijke voorwaarde daarvoor is, dat ionen met voldoende dichtheid worden geproduceerd om (in directe absorptie) waargenomen te kunnen worden. In hoofdstuk 4, waarin metingen aan  $\text{KrH}^+$  en  $\text{KrD}^+$  worden beschreven, wordt dat bewerkstelligd met behulp van een holle cathode ontlading en een magnetisch uitgerekte anomale glim ontlading. Het magneetveld wordt verder gebruikt om de Zeeman opsplitsing voor verschillende isotopen te meten. Uit het verschil in opsplitsing kan het permanente dipoolmoment worden bepaald, zijhet dat vibrationele effecten de interpretatie van de meetdata moeilijk maken. Het dipoolmoment bepaalt mede de intensiteit van de straling die op Aarde wordt opgevangen. In hoofdstuk 5 wordt een nieuwe techniek beschreven om ionen in directe absorptie te kunnen meten. Deze techniek, de hoge spanning hoge druk supersone spleetnozzle ontlading, heeft een aantal voordelen vergeleken met de conventionele ontladings technieken. Lijnbreedten kunnen tot de helft worden gereduceerd en ionen kunnen rotationeel koud geproduceerd worden. Dit wordt gedemonstreerd aan de hand van metingen in het infrarood aan  $\text{NO}^+$  en in het ver infrarood aan  $\text{N}_2\text{H}^+$ .

---

## Curriculum Vitae

I was born on October 16<sup>th</sup> 1965 in Heerlen, on the margin of the hills of Southern Limburg. After my primary education at the "Anselschool" in Eygelshoven I visited from 1978 to 1984 the grammar school "Rolduc" in Kerkrade where I got my Gymnasium  $\beta$  diploma in 1984. In the same year I started in Nijmegen to study physics at the Catholic University with specializations in the field of astrophysics and experimental physics. In 1989 I graduated at the Department of Molecular and Laser Physics under direction of Prof. J. Reuss with an investigation on state resolved collisionally induced excitations of  $\text{NH}_3$  with  $\text{H}_2$  and on the possibility of producing Ar-OH in a continuous point nozzle discharge. During the same time I performed photometric measurements on double star systems at the Dutch observatory in Auserbinn (Ch). In August 1989 I received my Master's in Physics. From September 1989 to May 1990 I worked as guest scientist at the Max Planck Institut für Strömungsforschung in Göttingen in the group of Prof. U. Buck, investigating the infrared photodissociation of size selected neutral clusters. In June 1990 I returned to Nijmegen to start with my Ph.D. (AIO) study. Within the framework of the EC Network "Structure and Dynamics of Molecular Ions" I investigated transient molecules in the far infrared under supervision of Dr. W.L. Meerts and Dr. J.J. ter Meulen. During this time I worked closely together with Dr. M. Havenith of the Department Molekülspektroskopie under direction of Prof. W. Urban at the Institut für Angewandte Physik in Bonn. I visited this institute several times as "Sommergast" and participated in the work on the ion jet. The results of the work performed in Göttingen, Nijmegen and Bonn are described in this thesis.

During my Ph.D. time I gave tutorials in astrophysics and set up two astrophysical experiments for the primary and research practical in physics. Since 1984 I am a member of the astronomical society of Nijmegen, the last five years in the function of secretary. In June 1994 I hope to obtain my doctorate in physics with this thesis. In July 1994 I will start in the group of Prof. W. Urban at the Institut für Angewandte Physik in Bonn investigating the infrared absorption of weakly bound complexes containing open shell molecules.

Nijmegen, May 1994  
Harold Linnartz



---

## List of Publications

- Reply to the comment on "Electron bombardment fragmentation of size selected  $\text{NH}_3$  clusters."  
U. Buck, R. Krohne, H. Linnartz, *J. Chem. Phys.* 93 (1990) 3726.
- Infrared photodissociation of size-selected methylamine clusters.  
U. Buck, X.J. Gu, R. Krohne, Ch. Lauenstein, H. Linnartz, A. Rudolph, *J. Chem. Phys.* 94 (1991) 23.
- Infrared photodissociation of size-selected molecular clusters and their structures.  
U. Buck, X.J. Gu, M. Hobein, R. Krohne, Ch. Lauenstein, H. Linnartz, A. Rudolph, *Z. Phys. D.* 20 (1991) 177.
- Fragmentation by electron impact ionization and intra-cluster reactions of size-selected  $(\text{N}_2\text{H}_4)_n$  and  $(\text{OCS})_n$  clusters.  
U. Buck, M. Hobein, R. Krohne, H. Linnartz, *Z. Phys. D.* 20 (1991) 181.
- Microwave and submillimeter spectroscopy of  $\text{Ar-NH}_3$  states correlating with  $\text{Ar} + \text{NH}_3$  ( $j=1, |K|=1$ ).  
E. Zwart, H. Linnartz, W.L. Meerts, G.T. Fraser, D.D. Nelson, Jr., W. Klemperer, *J. Chem. Phys.* 95 (1991) 793.
- Werken met licht  
H. Linnartz, *J. Schleipen*, *N&T* 11 (1991) 856.
- Infrarood fotodissociatie van op grootte geselecteerde neutrale clusters.  
R. Krohne and H. Linnartz, *NtvN*, 4 (1992) 53.
- Determination of the electric dipole moment of  $\text{KrH}^+$ .  
H. Linnartz, M. Havenith, E. Zwart, J.J. ter Meulen, W.L. Meerts, *J. Molec. Spectrosc.* 153 (1992) 710.
- An infrared - far infrared double resonance study on  $(\text{NH}_3)_2$  in a jet.  
M. Havenith, H. Linnartz, E. Zwart, A. Kips, J.J. ter Meulen, W.L. Meerts, *Chem. Phys. Lett.* 193 (1992) 261.
- The electric dipole moment of  $(\text{NH}_3)_2$  for  $G:|K|=1$ .  
H. Linnartz, A. Kips, W.L. Meerts, M. Havenith, *J. Chem. Phys.* 99 (1993) 2449.



- Het Ammoniak dimeer, complexe dynamica met een dynamisch complex.  
H. Linnartz, A. Kips, W.L. Meerts, M. Havenith, *A&Q* 5 (1993) 20.
- Tunable infrared and far infrared direct absorption spectroscopy of molecular ions in a supersonic jet expansion.  
G. Hilpert, H. Linnartz, M. Havenith, J.J. ter Meulen, W.L. Meerts, *Chem. Phys. Lett.* 219 (1994) 384.
- The ammonia dimer; complex dynamics with a dynamical complex.  
H. Linnartz, M. Havenith, *CAMP*, accepted (may 1994).
- The ammonia dimer, new infrared - far infrared double resonance results.  
H. Linnartz, W.L. Meerts, M. Havenith, *Chem. Phys.*, submitted (april 1994).
- The ammonia dimer; to be or not to be hydrogen bonded.  
M. Havenith, H. Linnartz, W.L. Meerts, E.H.T. Olthof, A. van der Avoird, P.E.S. Wormer, N. Heineking, W. Stahl, *Science*, in preparation.
- The electric dipole moment of  $(\text{NH}_3)_2$  for  $G:|K|=1$  (b.o. 747 GHz).  
H. Linnartz, M. Havenith, W.L. Meerts, in preparation.





# STELLINGEN

## I

Het verdient aanbeveling proefschriften te citeren onder vermelding van auteur, jaartal, universiteit en titel.

Dit proefschrift

## II

De moeilijkheden die zijn opgetreden bij de bepaling van het elektrisch dipoolmoment van  $\text{ArH}^+$  kunnen slechts ten dele worden teruggevoerd op de theoretische interpretatie van de meetdata.

K.B. Laughlin *et al*, Phys. Rev. Lett. 58 (1987) 996, Phil. Trans. R. Soc. Lond. A, 324 (1988) 109, J. Chem. Phys. 90 (1989) 1358.

## III

De conclusie dat het afwijkende ionisatie patroon voor  $(\text{NH}_3)_n$  clusters, zoals gevonden door U. Buck en Ch. Lauenstein (J. Chem. Phys. 92 (1990) 4250) het gevolg is van een koudere expansie (M.T. Coolbaugh *et al*, J. Chem. Phys. 93 (1990) 3725), is onjuist.

U. Buck *et al*, J. Chem. Phys. 93 (1990) 3726

## IV

De discussie met betrekking tot het al dan niet waterstof gebonden zijn van  $(\text{NH}_3)_2$  als functie van de tijd kan grafisch zeer goed tot uitdrukking worden gebracht met een sinus.

## V

De toekenning van de opsplitsingen in het overall infrarood spectrum van  $(\text{NH}_3)_2$  als excitatie van ongelijke N-H bindingen in het complex en interchange beweging, staat gelijk aan de aanname dat een molecuul gelijktijdig star en niet star kan zijn.

M. Snels *et al*, Chem. Phys. 115 (1987) 79

## VI

Een eenvoudige manier om meer aan lichaamsbeweging te doen, kan worden verkregen door het persoonlijke arsenaal aan afstandsbedieningen het raam uit te gooien.

## VII

Het infrarood photodissociatie spectrum voor OCS trimeren zoals gevonden door M.A. Hoffbauer *et al* (J. Phys. Chem. 87 (1983) 2096) bestaat gedeeltelijk uit bijdragen van clusters groter dan trimeren.

Dit proefschrift

## VIII

Het verdient aanbeveling naast het Holwerdapad een fietspad aan te leggen.

## IX

Gezien het volhardende karakter van de Rheinländer is het niet onwaarschijnlijk dat de Bonner Donnerstagabend Demo ook dan nog plaats zal vinden, wanneer het complete Bundeshaus al in Berlijn is gestationeerd.

## X

Het feit dat semi-wetenschappelijk taalgebruik in reclamespotjes succesvol blijkt, toont aan dat het met het kritisch bewustzijn van de Nederlandse consument triest is gesteld.

Nijmegen, 5 mei 1994  
Harold Linnartz



